

→ RESEARCH LIBRARY

1401

key words -
1 - connections
2 - gusset plates



STRESS, STRAIN AND FORCE DISTRIBUTIONS IN GUSSET PLATE CONNECTIONS

Prepared for
American Institute of Steel Construction
400 North Michigan Avenue
Chicago, Illinois 60611

by
Donald A. Rabern
George C. Williams
and Ralph M. Richard

main author

of
The Department of Civil Engineering
and Engineering Mechanics
THE UNIVERSITY OF ARIZONA
Tucson, Arizona 85721



March, 1983

7545



AMERICAN INSTITUTE OF STEEL CONSTRUCTION, INC.

The Wrigley Building / 400 North Michigan Avenue / Chicago, Illinois 60611-4185 / 312 • 670-2400

February 28, 1983

Dear Employee:

Enclosed is a draft of the Summary Plan Description for the AISC Employees Pension Plan. You will receive the same information in a printed booklet from Massachusetts Mutual next month. At the same time you will receive a statement from Massachusetts Mutual for the year ended December 31, 1982. This statement will reflect not only the transfer of funds from your account in the old defined benefit plan, but also all contributions in your name in the new account during 1982.

If you have any questions after you have reviewed the Summary Plan Description please feel free to contact me. I'd suggest you wait until you receive your 1982 statement and ask any questions you may have at one time.

Sincerely,

Richard F. Fox

Richard F. Fox
Plan Administrator



AMERICAN INSTITUTE OF STEEL CONSTRUCTION, INC.

The Wrigley Building / 400 North Michigan Avenue / Chicago, Illinois 60611-4185 / 312 • 670-2400



ACKNOWLEDGMENTS

This research was funded by a grant from The American Institute of Steel Construction, and the authors wish to express their gratitude for this financial support. Additionally the authors wish to express their appreciation to the members of the AISC Committee on Large Framing Connections for their advice and guidance.

TABLE OF CONTENTS

	Page
LIST OF ILLUSTRATIONS	v
LIST OF TABLES	vii
ABSTRACT	ix
1. INTRODUCTION	1
2. TESTING	4
University of Alberta	4
University of Illinois	6
3. CONNECTOR SIMULATION	11
4. ANALYSIS OF DIAGONAL BRACING CONNECTIONS	28
5. ANALYTICAL VERSUS TEST RESULTS	56
6. CURRENT DESIGN CONCEPTS	63
7. BLOCK SHEAR	67
8. SUMMARY	74
APPENDIX	75
REFERENCES	144

LIST OF ILLUSTRATIONS

Figure		Page
1.	University of Alberta Test Specimen	2
2.	Gusset Plate Geometries	5
3.	Typical Failure Pattern University of Alberta Testing	8
4.	Framing Angle Behavior in Tension and Compression	9
5.	Single Shear Bolt-Plate Deformation Curve	12
6.	Weld Force Deformation Curve	15
7.	Double Framing Angles	16
8.	Force Deformation of Framing Angles, Richard Curve versus Test Results	17
9.	Orthotropic Element Yield Surface	19
10.	Tensile Force-Deformation Curve for 5 x 5 x 3/8" Framing Angles, 3/4" Diameter Bolt and 1/2" Plate	20
11.	Compressive Force-Deformation Curve for 5 x 5 x 3/8" Framing Angles, 3/4" Bolt and 1/2" Plate	21
12.	Plotted Yield Surface	22
13.	Framing Angle Bar Material Property Formulation . .	24
14.	Angle Performance for Stiffness	25
15.	Cantilever Beam Analytical versus Test Results . .	27
16.	Diagonal Bracing Connection	29

LIST OF ILLUSTRATIONS (Cont.)

Figure		Page
17.	INELAS Finite Element Model of Diagonal Bracing Connection	30
18.	Connection Locations for the 30° Gusset and Beam	33
19.	45°, 1/8" Gusset Undistorted and Distorted Geometry	36
20.	45°, 1/8" Gusset, Effective von Mises Stress Contour and Surface Plots, 75 kip load	37
21.	45°, 1/8" Gusset, Effective von Mises Stress Contour and Surface Plots, 150 kip load	38
22.	45°, 1/8" Gusset, Maximum Shear Stress Contour and Surface Plots, 150 kip load	40
23.	45°, 1/8" Beam-Gusset Undistorted and Distorted Geometry	41
24.	45°, 1/8" Beam-Gusset Effective von Mises Stress Contour and Surface Plots, 150 kip load	42
25.	45°, 3/8" Beam-Gusset Undistorted and Distorted Geometry	44
26.	60°, 1/8" Gusset Undistorted and Distorted Geometry	45
27.	60°, 1/8" Gusset Effective von Mises Stress Contour Plot, 140 kip load	46
28.	60°, 1/8" Gusset Force and Deflection Distributions, 140 kip load	47
29.	60°, 1/8" Gusset Splice Plate Connection Force and Deflection Distributions	49
30.	60°, 1/8" Gusset Splice Plate Connection Force and Deflection Resultants Plotted Vertically	50

LIST OF ILLUSTRATIONS (Cont.)

Figure		Page
31.	60 ^o , 1/8" Gusset Total Force Distribution	51
32.	60 ^o , 1/8" Beam-Gusset Undistorted and Distorted Geometry	52
33.	60 ^o , 1/8" Beam-Gusset Force Distribution, 140 kip load	53
34.	30 ^o , 1/8" Gusset Undistorted and Distorted Geometries	54
35.	30 ^o , 1/8" Beam-Gusset Undistorted and Distorted Geometries	55
36.	45 ^o Gusset, Analytical versus Test Results	57
37.	45 ^o Beam-Gusset, Analytical versus Test Results . . .	58
38.	60 ^o Gusset, Analytical versus Test Results	59
39.	60 ^o Beam-Gusset Analytical versus Test Results . . .	60
40.	30 ^o Gusset, Analytical versus Test Results	61
41.	30 ^o Beam-Gusset, Analytical versus Test Results . . .	62
42.	Whitmore Gusset Plate and Stress Distributions . . .	64
43.	Whitmore Criterion for Effective Area	65
44.	Block Shear Failure Mode for Coped Beams	68
45.	Constant and Linear Stress Distributions in Block Shear	70
46.	Gusset Plate Block Shear Failure	72

LIST OF TABLES

Table		Page
1.	University of Alberta Test Summary	7
2.	Single Bolt Single Shear Force Deformation Curve Parameter Summary	13
3.	Beam End Moments in the Bracing Connection with Uniform Loading	31
4.	Schedule of Finite Element Models	35

ABSTRACT

Results of physical testing and analytical studies are presented for typical column beam gusset connections. Force and displacement distributions are reported for 45°, 60° and 30° diagonal bracing connections. A comparison of analytical versus test results from the connections are found to be similar verifying the methodology in developing the finite element models.

Connector simulation for the finite element models is discussed noting the material property formulation for the orthotropic behavior of double framing angle bolted connections. Weldment, single and double shear connector formulation is also discussed.

Review of previous work and design concepts for gusseted connections are included. The block shear concept is reviewed for possible application in the analysis and design of gusset plate connections.

It is concluded that nonlinear finite element software with orthotropic connector capability can realistically simulate the structural action of gusset connections. Additionally, the block shear criteria may have application as an analysis and design aid.

CHAPTER 1

INTRODUCTION

The design of steel connections that are adequate for strength and economical to fabricate is one of the most challenging problems for structural engineers. The large number of variables, including configurations, types of connectors, load intensities, and load combinations involved makes it difficult to establish standard connection designs. This paper addresses analysis methods developed to better understand the structural action of these connections. Full scale testing of gusseted connections at the University of Alberta (8) provided a basis to compare analytical predictions with test results.

Tests at the University of Alberta involved full scale testing of typical beam, column, gusset bolted connections. Figure 1 illustrates the 45° configuration tested. Six tests were conducted with $1/8''$ and $3/8''$ gussets in 45° , 30° , and 60° connections. Each connection tested was modeled with the nonlinear finite element routine INELAS (1). The program was utilized to simulate nonlinear behavior in material and connectors. Properties for connectors were obtained from tests conducted at the University of Arizona (4) and the University of Illinois (3) on double framing angles, single and double shear. Properties for connectors were input from force deformation curves plotted from physical test data. When this procedure is used, it is possible to include both geometric and material nonlinearity in the

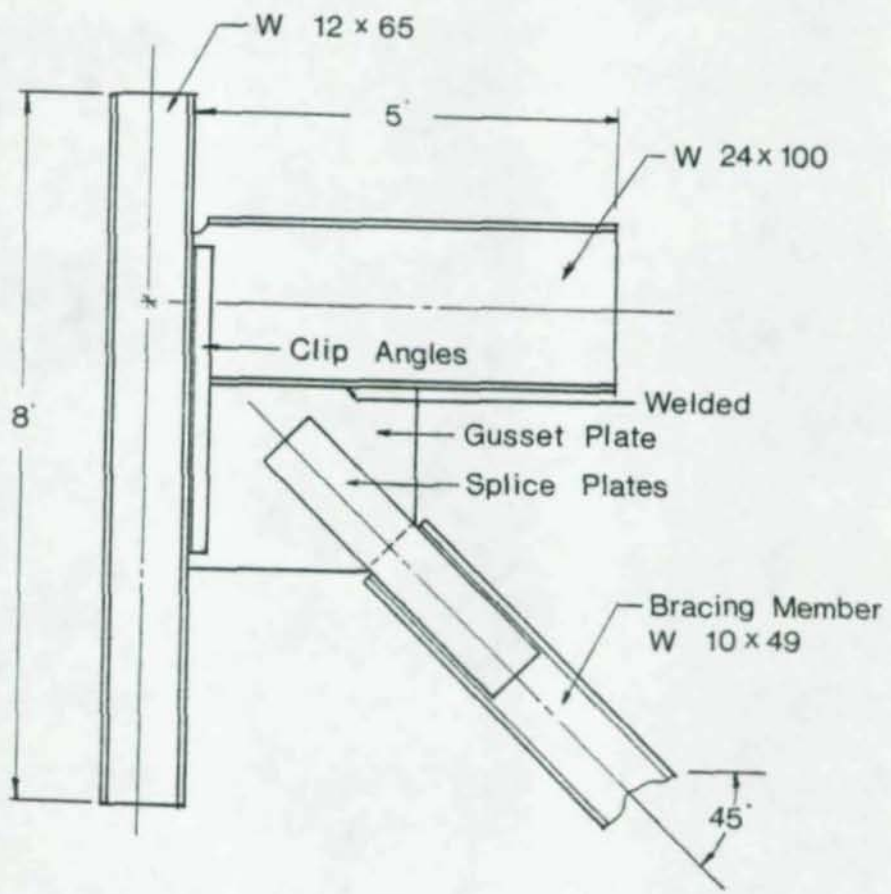


Figure 1. University of Alberta Test Specimen.

analysis in an accurate and numerically efficient way. This methodology was used to assess the moment generated by double angle framed connections (2, 3) and also was used to develop the design procedure for single plate framing connections currently being used by the design profession (4). Additionally, the strength of eccentrically loaded bolt and weldment groups in the current American Institute of Steel Construction Manual is based upon force deformation curves derived from physical tests (5, 6, 7). This method of analysis produced results that compared well with results from full scale testing leading to a clearer understanding of the structural action of the connections.

The following discusses the methodology and results of the research efforts and their significance in the structural integrity of bolted connections.

CHAPTER 2

TESTING

University of Alberta

Six full scale tests were conducted at the University of Alberta. These six connections were designed for 45° , 30° and 60° diagonal bracing systems. Each connection was tested with both $1/8$ " and $3/8$ " gusset plates. Figure 1 illustrates the 45° connection.

The gusset plate was welded to a five foot W24x100 beam with a $1/8$ " fillet on both sides of the plate using E7018 electrodes. The beam to column and gusset to column connection utilized two $3\frac{1}{2}$ " x $3\frac{1}{2}$ " x $3/8$ " framing angles. Three-quarter A325 bolts were used in the connection, seven in the beam and six in gusset. All bolts were three inches on center with a $2\frac{1}{2}$ " edge distance. The column was a standard eight foot W12x65 section with a W10x49 bracing member. Two $7\frac{1}{2}$ " x $3/8$ " splice plates were welded to the bracing member and bolted to the gusset plate with 18 A325 $3/4$ " diameter bolts on $2\frac{1}{2}$ " centers. The steel grade in the specimens were CSA 44W, $F_y = 42.7$ ksi actual. Physical dimensions of the gusset plates are shown in Figure 2.

Load was applied in tension to the bracing member with load actuators and strain recorded at several locations on the gussets for all load increments. Strain was monitored on both sides of the plate. Due to slight eccentricities, strains on opposite sides of

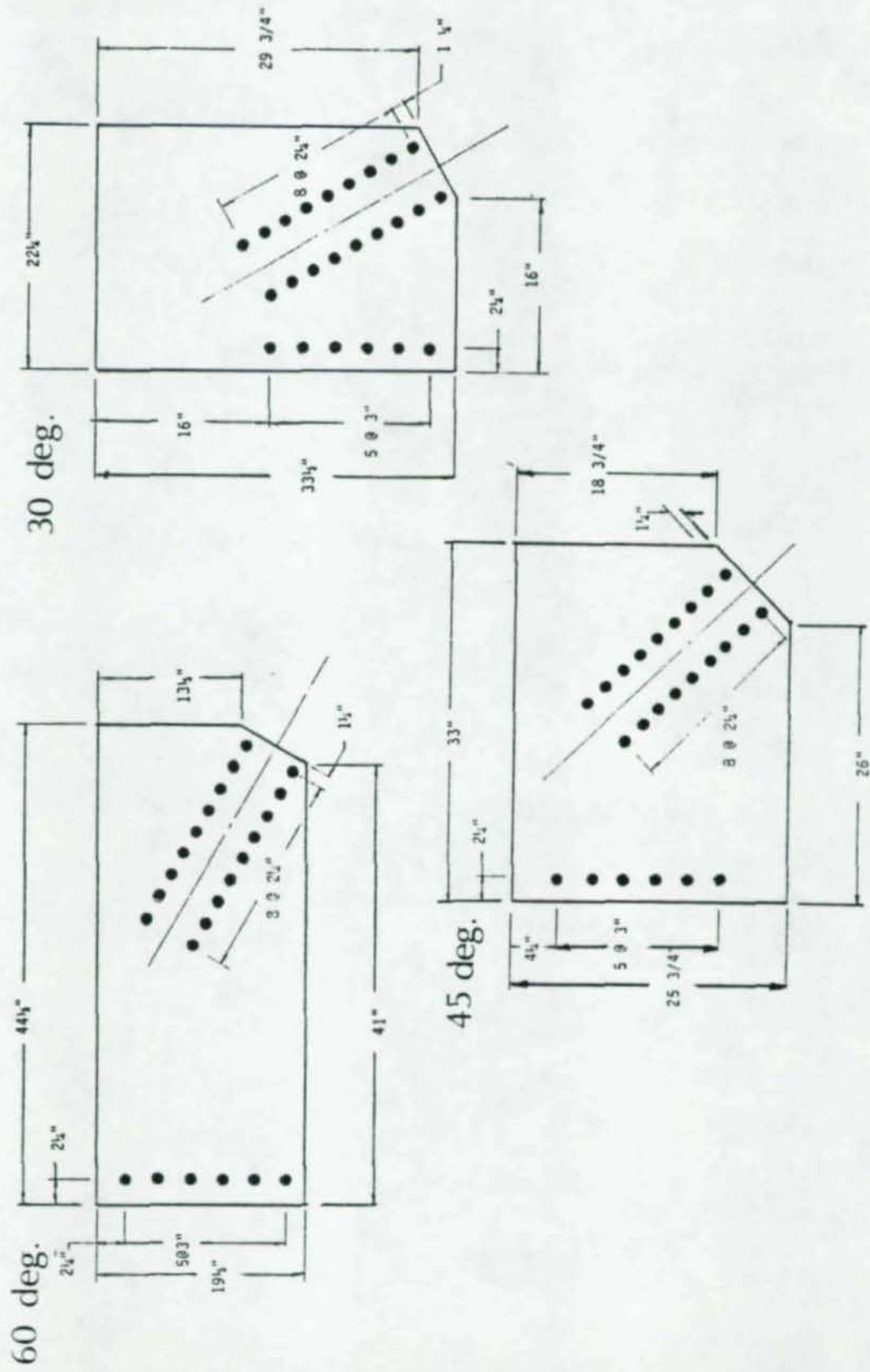


Figure 2. Gusset Plate Geometries.

the plates were not equal, indicating bending in the plates. When comparing analytical results to the test results, gages were averaged to eliminate out of plane bending effects. Table 1 summarizes the tests performed. Figure 3 shows a typical failure that occurred during the testing.

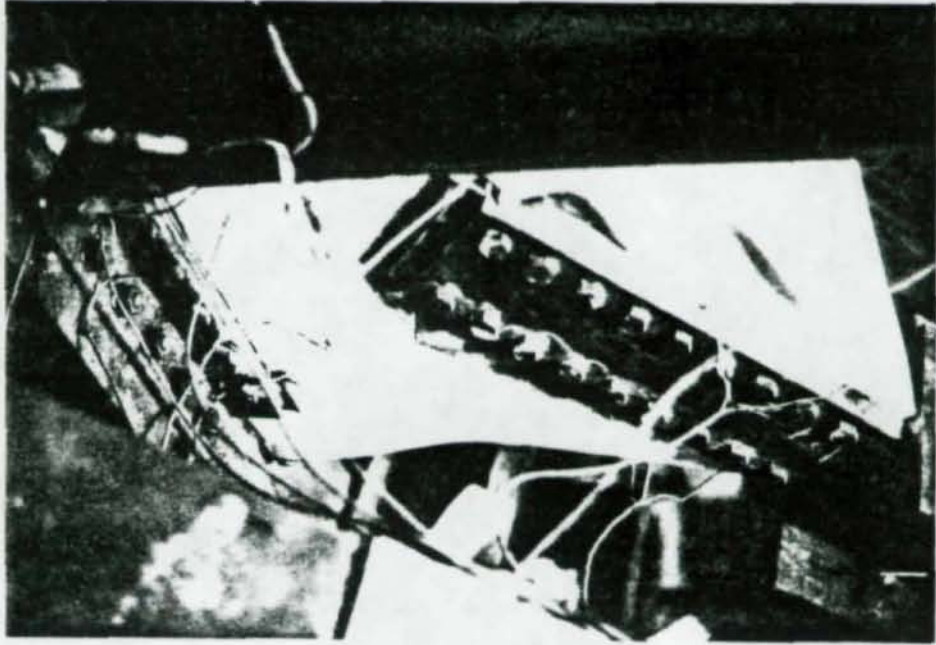
University of Illinois

Research conducted at the University of Illinois was done to determine moment rotation characteristics of beam to column double angle connections. One of the major points of the research was centered around the properties of framing angles in tension and compression and determining what percent of the fixed end beam moment was transmitted by the double angle framing connection. Results from these tests were used to simulate the nonlinear behavior of the framing angles in program INELAS.

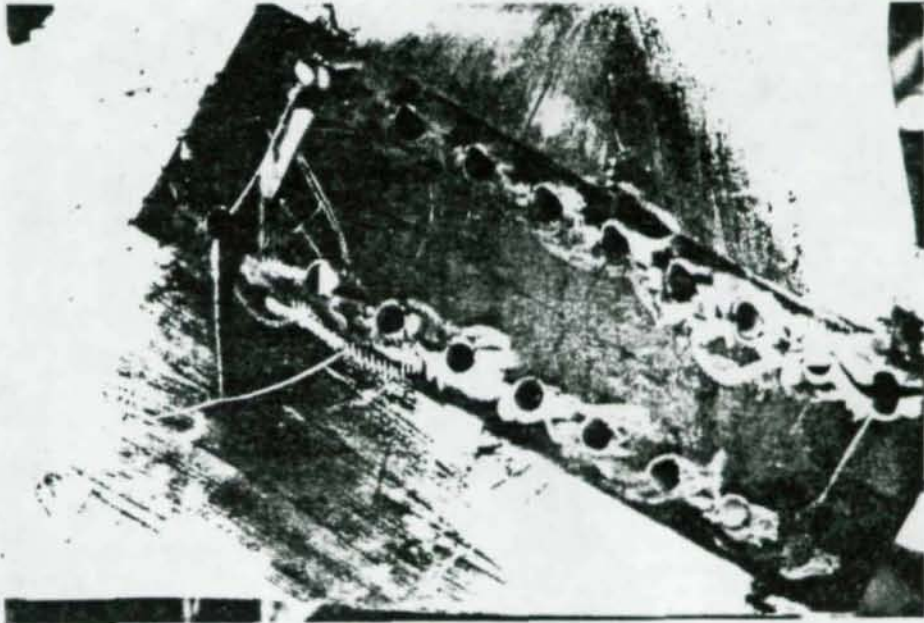
The testing resulted in load-displacement curves for double angles in tension and compression. Figure 4 shows how the angles deflect in compression and tension and their corresponding load deformation curves. It can be seen that the angle allows considerable deformation when loaded in tension. The deformation in the angle legs is similar to the structural action of a fixed beam with one end displaced relative to the other. In compression the angles bear on the bolted surface and what deformation that is seen is due to hole elongation, bolt shear and flexure. It is apparent that the angles are considerably more flexible in tension in compression. How the properties were

Table 1. University of Alberta Test Summary.

Test	Max Load (kips)	Failure Location in Gusset	Comments
1/8" 45 ⁰	150	At last two bolt holes in splice plate bolt pattern	<ul style="list-style-type: none"> i) A tear occurred at the gusset splice plate connection at the end of the bolt pattern. ii) Slight hole elongation in framing angle connection.
3/8" 45 ⁰	324	Did not fail	<ul style="list-style-type: none"> i) Small amount of yielding at same location as the 1/8" test failure.
1/8" 60 ⁰	143	At holes connecting to column framing angles	<ul style="list-style-type: none"> i) Gusset plate column connection holes elongated finally failing with secondary gusset plate failure at beam weld. ii) Slight hole elongation in splice plate bolt pattern
3/8" 60 ⁰	320	Did not fail	<ul style="list-style-type: none"> i) Slight yielding and hole elongation in some areas of 1/8" test.
1/8" 30 ⁰	158	At last two bolt holes in splice plate bolt pattern	<ul style="list-style-type: none"> i) Tearing of the gusset plate through the bottom row of bolts. ii) Slight elongation of bolt-holes for column connection.
1/8" 30 ⁰	399	Did not fail	<ul style="list-style-type: none"> i) Slight yielding and hole elongation in same areas of 1/8" tests.

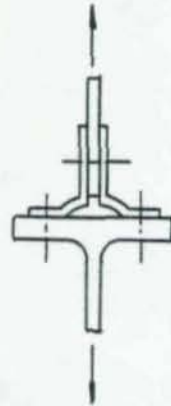


Tested 60° Gusset

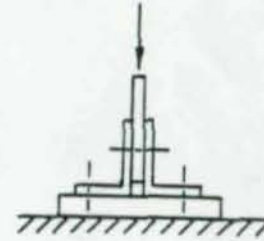


60° Gusset Fracture Pattern

Figure 3. Typical Failure Pattern University of Alberta Testing.



Tension



Compression

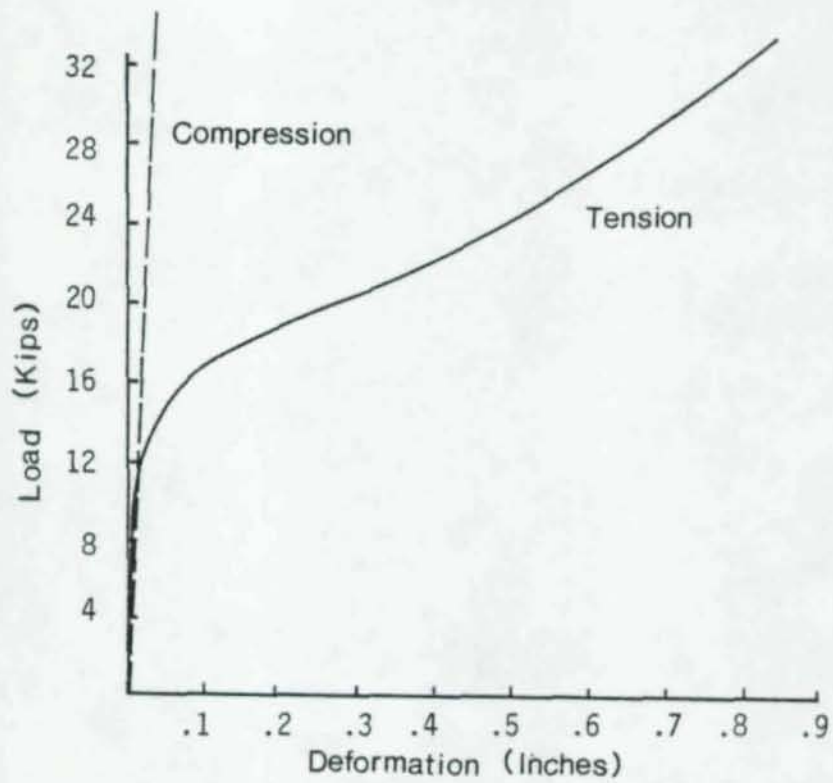


Figure 4. Framing Angle Behavior in Tension and Compression.

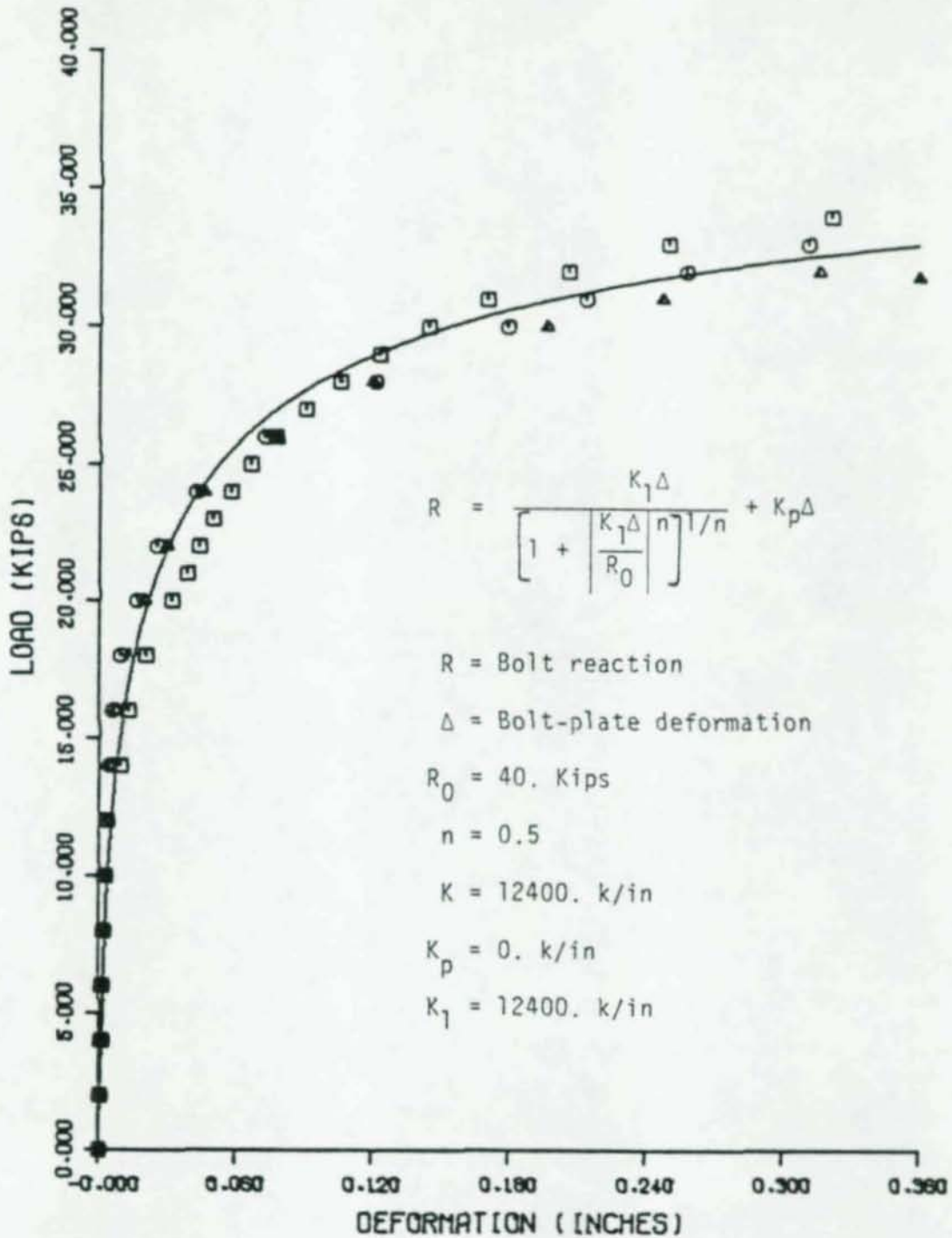
developed for the analytical studies will be discussed later in this report. Similar testing is being done at the University of Arizona (20) to investigate framing angle properties of several other configurations.

CHAPTER 3

CONNECTOR SIMULATION

The analysis of bolted and welded fasteners utilizing the finite element method requires the properties of the fasteners be adequately described. Stiffness, strength and orthotropic behavior should be taken into account to simulate the structural action of the connector. As shown in Figure 4, the double angle connector behaves differently in compression than in tension. Capabilities to simulate the fastener behavior is available in program INELAS (1). This program was written to analyze plates stressed into the inelastic range. The nonlinear structural response is calculated by a numerical algorithm that uses the von Mises yield criteria and the associated flow rule.

Properties of fastener elements are derived from force deformation curves obtained from physical tests. Experimentally determined force deformation curves for high strength bolts are presented in Reference (4). These tests were made to develop design procedure for the single plate framing connection. Figure 5 illustrates a typical plot for two 3/8" (A36) plates connected by a 3/4" A325 high strength bolt along with the analytical formula (9). Table 2 summarizes the force deformation curve parameters for the single bolt single shear tests made for this study. Similar force deformation curves for bolts in double shear may be found in Reference 6.



3/4 A325 BOLTS - A36 PLATES 3/8 AND 3/8

Figure 5. Single Shear Bolt-Plate Deformation Curve.

Table 2. Single Bolt-Single Shear Force-Deformation Curve Parameter Summary.

Bolt	Plates	K	K_D	R_D	n
3/4" A325	1/4 - 1/4 A36	7250.	0.	20.	.3
"	5/16 - 5/16 A36	9063.	0.	24.	.9
"	3/8 - 3/8 A36	10875.	0.	40.	.5
"	7/16 - 7/16 A36	12700.	10.	40.	.5
"	1/2 - 1/2 A36	14500.	20.	30.	.7
"	1/4 - 3/8 A36	3700.	-30.	30.	.6
"	1/4 - 1/2 A36	9667.	-30.	30.	.6
"	3/8 - 1/2 A36	12400.	0.	40.	.5
"	3/8 - 3/8 A572 Gr 50	10875.	20.	30.	.7
7/8" A325	5/16 - 5/16 A36	9063.	0.	30.	.7
"	3/8 - 3/8 A36	10875.	20.	40.	.5
"	7/16 - 7/16 A36	12700.	0.	50.	.5
"	1/2 - 1/2 A36	14500.	10.	40.	.7
"	1/4 - 3/8 A36	3700.	20.	30.	.8
"	1/4 - 1/2 A36	9667.	20.	30.	1.1
"	3/8 - 1/2 A36	12400.	10.	40.	.5
"	3/8 - 3/8 A572 Gr 50	10875.	10.	40.	.9
1" A325	1/2 - 1/2 A36	14500.	20.	30.	.5
"	5/8 - 5/8	18125.	40.	30.	.8
3/4" A490	1/2 - 1/2 A36	14500.	10.	40.	.3
"	5/8 - 5/8 A36	18125.	10.	50.	.4
7/8" A490	1/2 - 1/2 A36	14500.	0.	30.	.3
"	5/8 - 5/8 A36	18125.	40.	30.	.5
"	1/2 - 1/2 A572 Gr 50	14500.	40.	30.	.6
1" A490	1/2 - 1/2 A36	14500.	30.	40.	.7
"	5/8 - 5/8 A36	18125.	20.	50.	.9

The force deformation curves for (E60, 1/4") weldments were presented in Reference 5. Figure 6 is a typical plot of the test data along with its analytical formula. The parameters of this formula for other electrode strengths, weld sizes, and tributary lengths may be computed by direct ratios.

Force deformation (compression and tension) curves for double framing angles were presented in Reference 3. It is apparent from these tests that the double framing angles are orthotropic in both strength and stiffness. To extend these force deformation relationships to the more general case, shear tests were made to determine the shear force deformation curves (R 's versus Δ 's). Figure 7 shows the double framing angles.

In all cases the force deformation characteristics of the fasteners are described analytically by the Richard Equation (9). The equation describes curve shapes from input quantities of elastic stiffness, plastic stiffness, reference load, and the Richard parameter. Figure 8 illustrates possible curve shapes the equation describes and a comparison of a Richard curve fit to a double angle tension test.

Describing the orthotropic behavior of double framing angles requires a yield surface which accounts for the response of angles in tension, compression and shear. This surface can be generated with a combination of a bar and an isotropic fastener element. The bar element increases the shear component of force with the isotropic

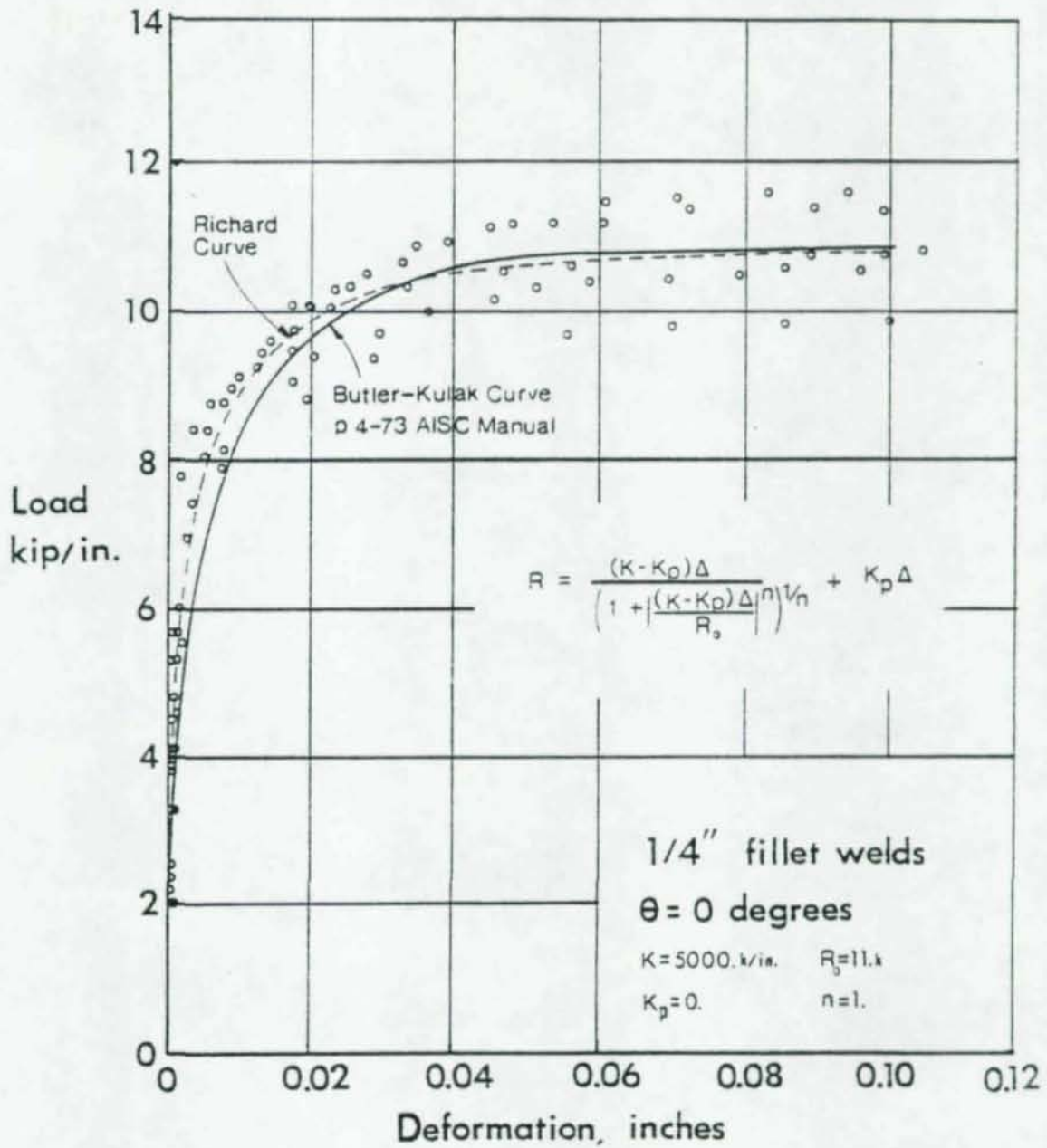


Figure 6. Weld Force Deformation Curve.

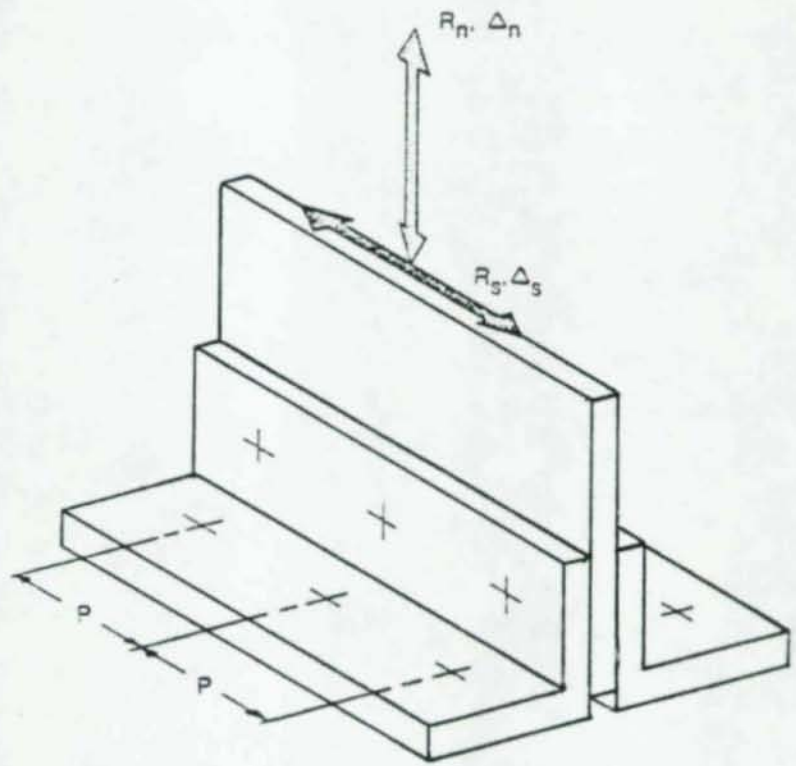
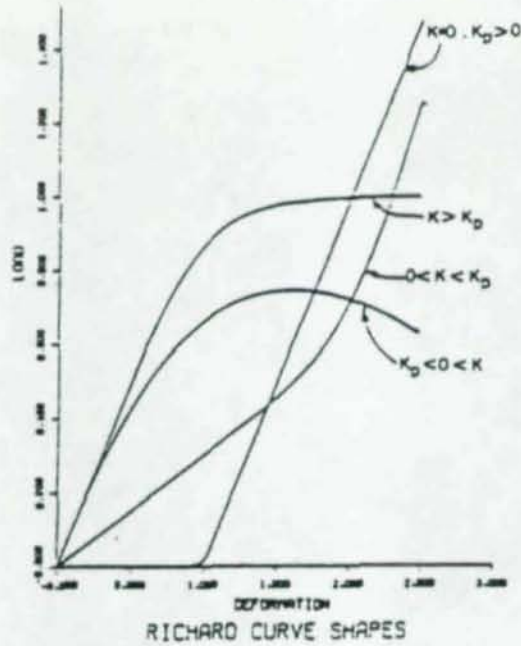


Figure 7. Double-Framing Angles.



$$R = \frac{(K - K_p) \Delta}{\left[1 + \left| \frac{(K - K_p) \Delta}{R_0} \right|^{1/n} \right]^{1/n}} + K_p \Delta$$

- K = Elastic Stiffness
- K_p = Plastic Stiffness
- R_0 = Reference Load
- Δ = Deformation
- R = Load
- n = Richard Parameter

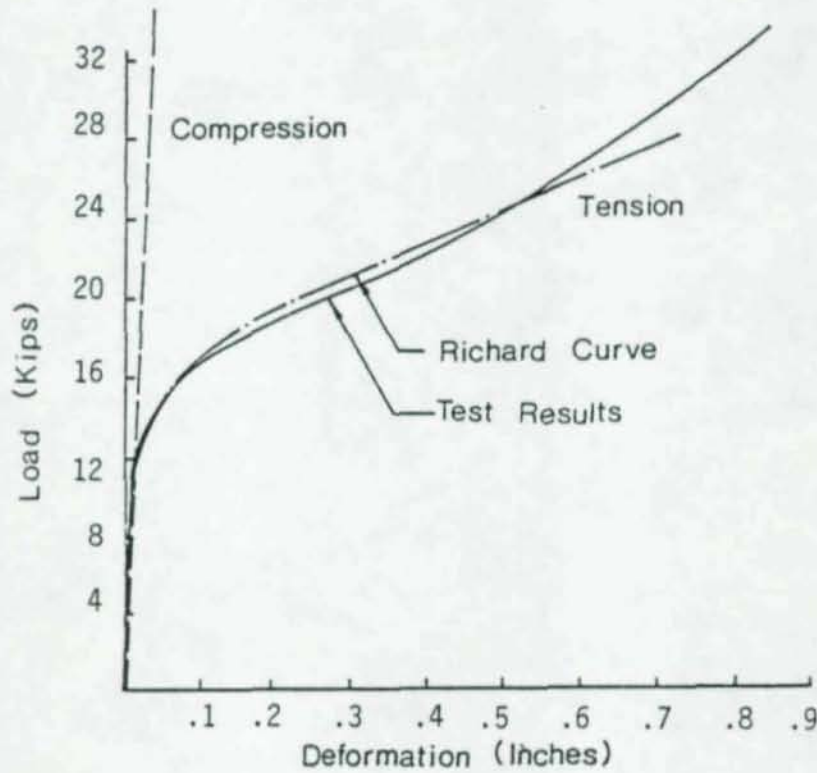


Figure 8. Force Deformation of Framing Angles, Richard Curve versus Test Results.

fastener element simulating the structural action of tension loads. These two elements acting together produce the yield surface illustrated in Figure 9. The elliptical portion of the surface simulates the combination of shear and tension on the angles. The lower part of the surface simulates the action of the double angle in compression and shear. An example of this concept can be illustrated from physical tests of the angles. Figure 10 shows the force deformation curve generated by pulling two 5 x 5 x 3/8" framing angles with 3/4" diameter bolts and 1/2" plate. Figure 11 is the force deformation curve for the same size angle in compression. Plotting the data from the two tests in the form of an ellipse produces the surface in Figure 12.

To obtain input properties for the bar and discrete fastener elements in program INELAS, the following procedure is followed. The bar element in the orthotropic system has an area set equal to 1.0. This is to facilitate the use of a post processing program that plots forces and displacements of the connectors. Input properties for the element are defined below:

EM, K = Young's Modulus or elastic stiffness for
fastener element.

EMP, K_p = Plastic Modulus or plastic stiffness for
fastener element.

SY, R_o = Reference stress or reference load for
fastener element.

PNL = Richard parameter.

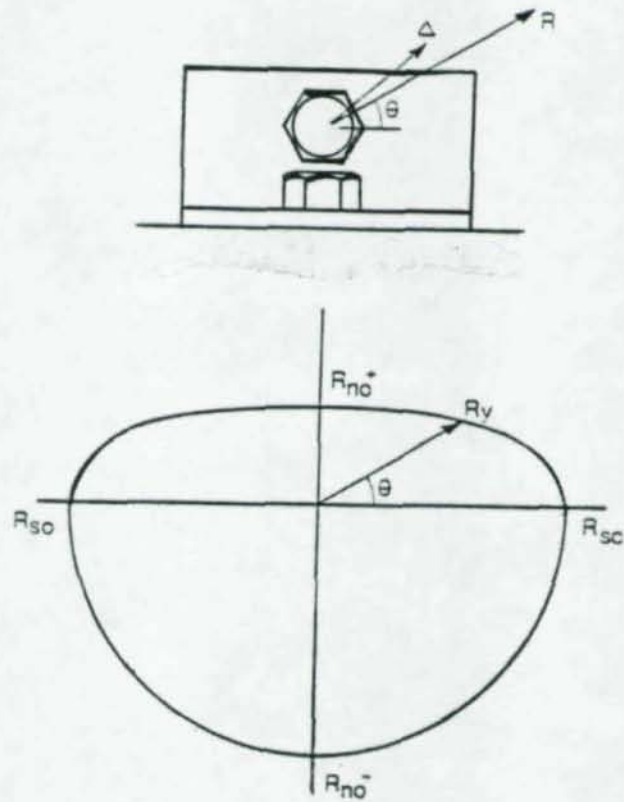


Figure 9. Orthotropic Element Yield Surface.

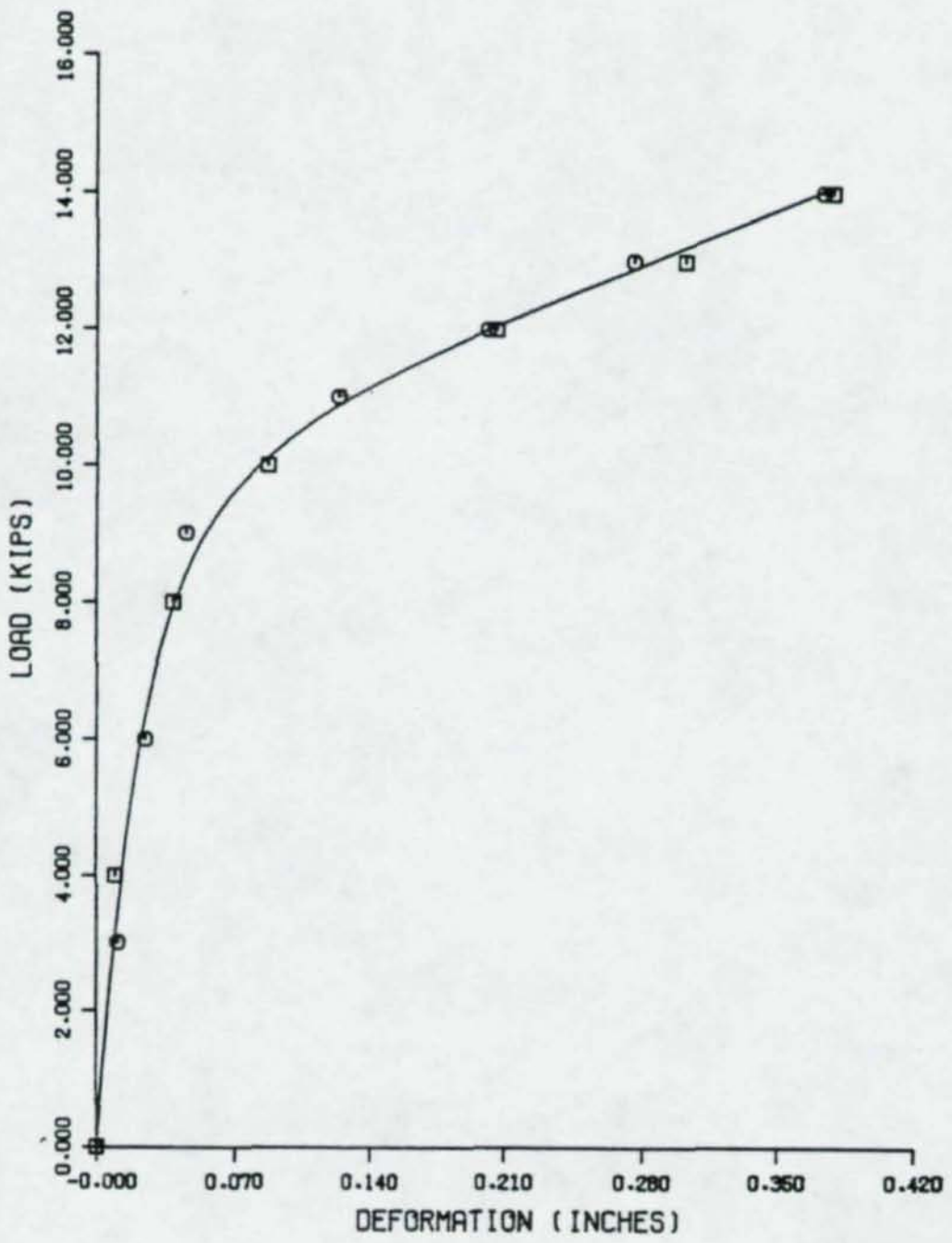


Figure 10. Tensile Force-Deformation Curve for 5 x 5 x 3/8" Framing Angles, 3/4" Diameter Bolt and 1/2" Plate.

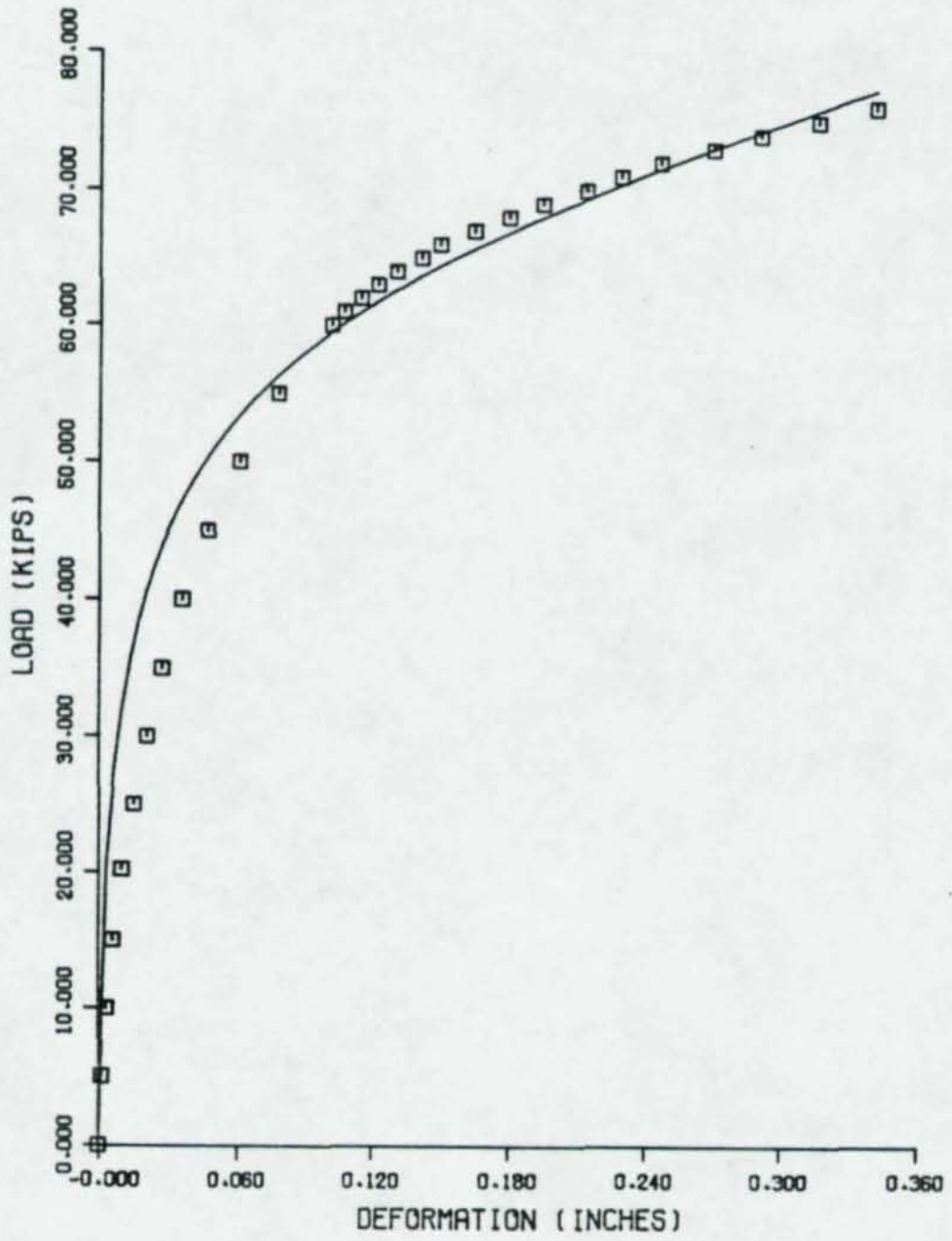


Figure 11. Compressive Force-Deformation Curve for 5 x 5 x 3/8" Framing Angles, 3/4" Diameter Bolt and 1/2" Plate.

$$\left(\frac{R_s}{R_{so}}\right)^2 + \left(\frac{R_n}{R_{no}}\right)^2 = 1$$

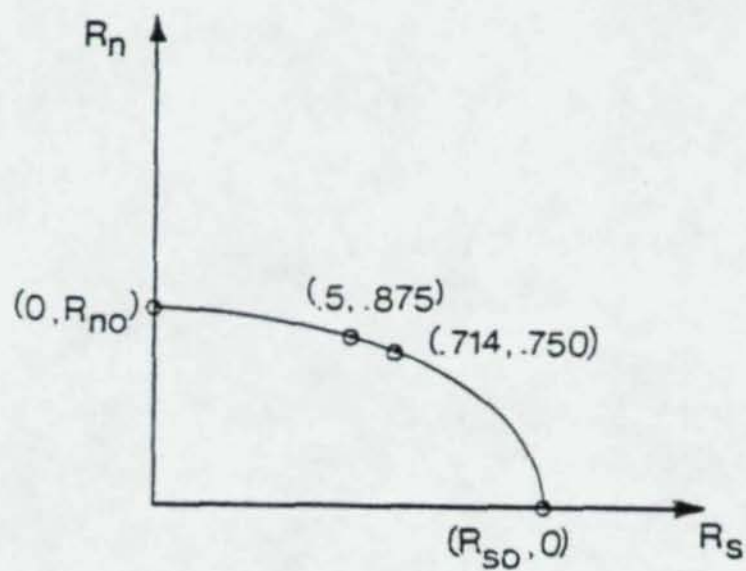


Figure 12. Plotted Yield Surface.

If $A \cong 1.0$ for the bar, then strength for the bar B is

$$\sigma_y * A_a = SY * l. = SY$$

where: σ_y = actual yield (or reference) stress

A_a = area of the two framing angles

Stiffness must also be determined for the formulation of the properties.

$$\text{stiffness} = \frac{AE}{L}$$

and since the area of the bar is unity

$$l * EM + A_a * EM_{\text{actual}} = EM_{\text{input}}$$

$$l * EMP = A_a * EMP_{\text{actual}} = EMP_{\text{input}}$$

The properties must be modified further to develop the proper yield surface and stiffness. Figure 13 illustrates this point from the strength and stiffness considerations. Noting the slopes from the force deformation curves of the same figure, the following may be noted:

$$K_{\text{bar}} = \frac{EM_{\text{input}}}{L}$$

where L is the distance between bolts.

$$\frac{EM_{\text{input}}}{L} = K_{\text{shear}} - K_{\text{tension}}$$

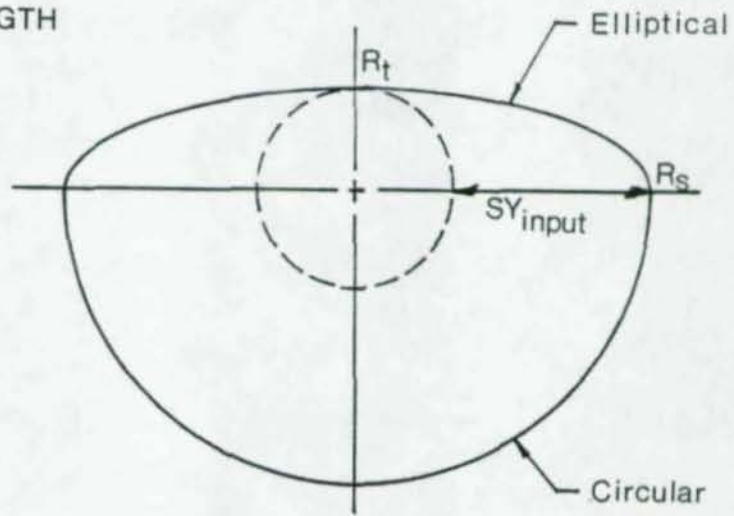
$$\text{so } E_{\text{input}} = L (K_{\text{shear}} - K_{\text{tension}})$$

where:

K_{shear} = is the same for a bolt in double shear

K_{tension} = computed from flexural considerations
(see Figure 14)

STRENGTH



STIFFNESS

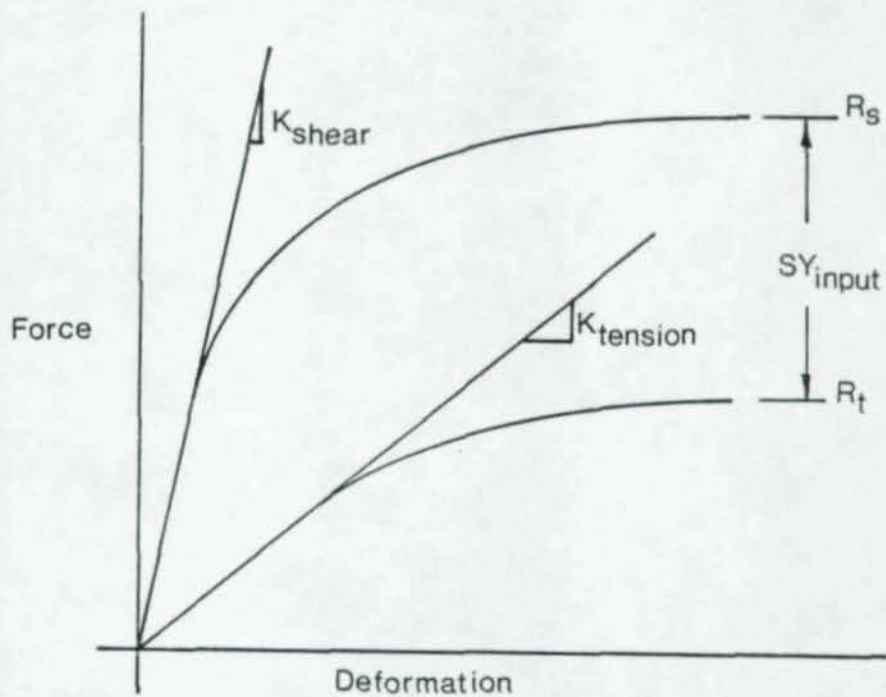
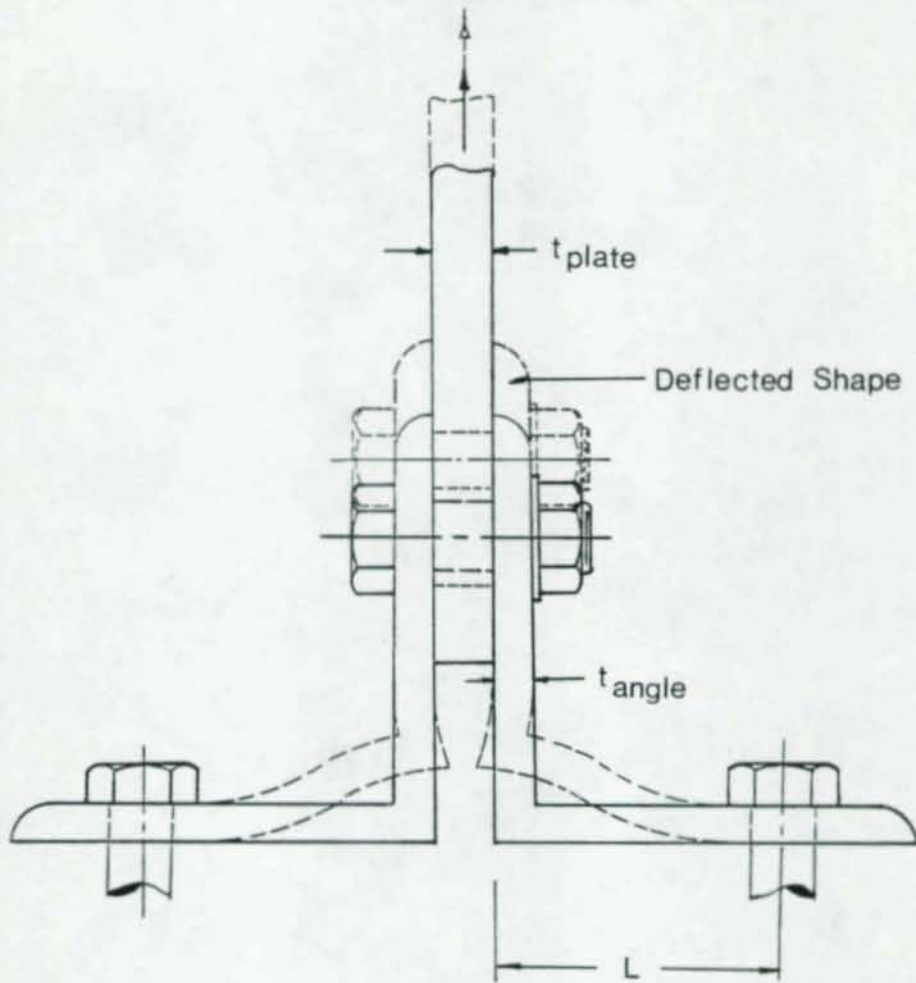


Figure 13. Framing Angle Bar Material Property Formulation.



$$\frac{1}{K_{tension}} = \frac{1}{K_{plate}} + \frac{1}{K_{2 \text{ angles}}}$$

$$K_{plate} = \frac{4E(t_{plate})t_{angle}}{t_{plate} + t_{angle}}$$

$$K_{2 \text{ angles}} = 2 \left[\frac{12 EI}{L^3} \right]$$

Figure 14. Angle Performance for Stiffness.

To illustrate the calculations to obtain K for two three-inch angle segments with leg length equal to 3" and thickness of 3/8", an example is given below:

$$\frac{1}{K_{\text{tension}}} = \frac{1}{K_{2\text{angles}}} + \frac{1}{K_{\text{plate}}}$$

$$\frac{1}{K_{\text{compression}}} = \frac{1}{K_{\text{plate}}}$$

where: $K_{2\text{angles}} = 2 \frac{12EI}{L^3} = 491.4$

which represents the bar element.

and:

$$K_{\text{plate}} = \frac{4Et_{\text{angle}} t_{\text{plate}}}{t_{\text{angle}} + t_{\text{plate}}} = 25,714 \text{ K/inch}$$

which represents the discrete fastener element.

Thus:

$$K_{\text{tension}} = 482 \text{ K/in.}$$

$$K_{\text{compression}} = 25,714 \text{ K/in.}$$

These numbers agree well with physical tests documented in Reference 20 and Figure 10.

The methodology discussed above was used to model a cantilever beam connected by framing angles (10). The model depicts a test done at the University of Illinois. A comparison of the experimental and finite element results is presented in Figure 15. The analytical results agree well with the test results.

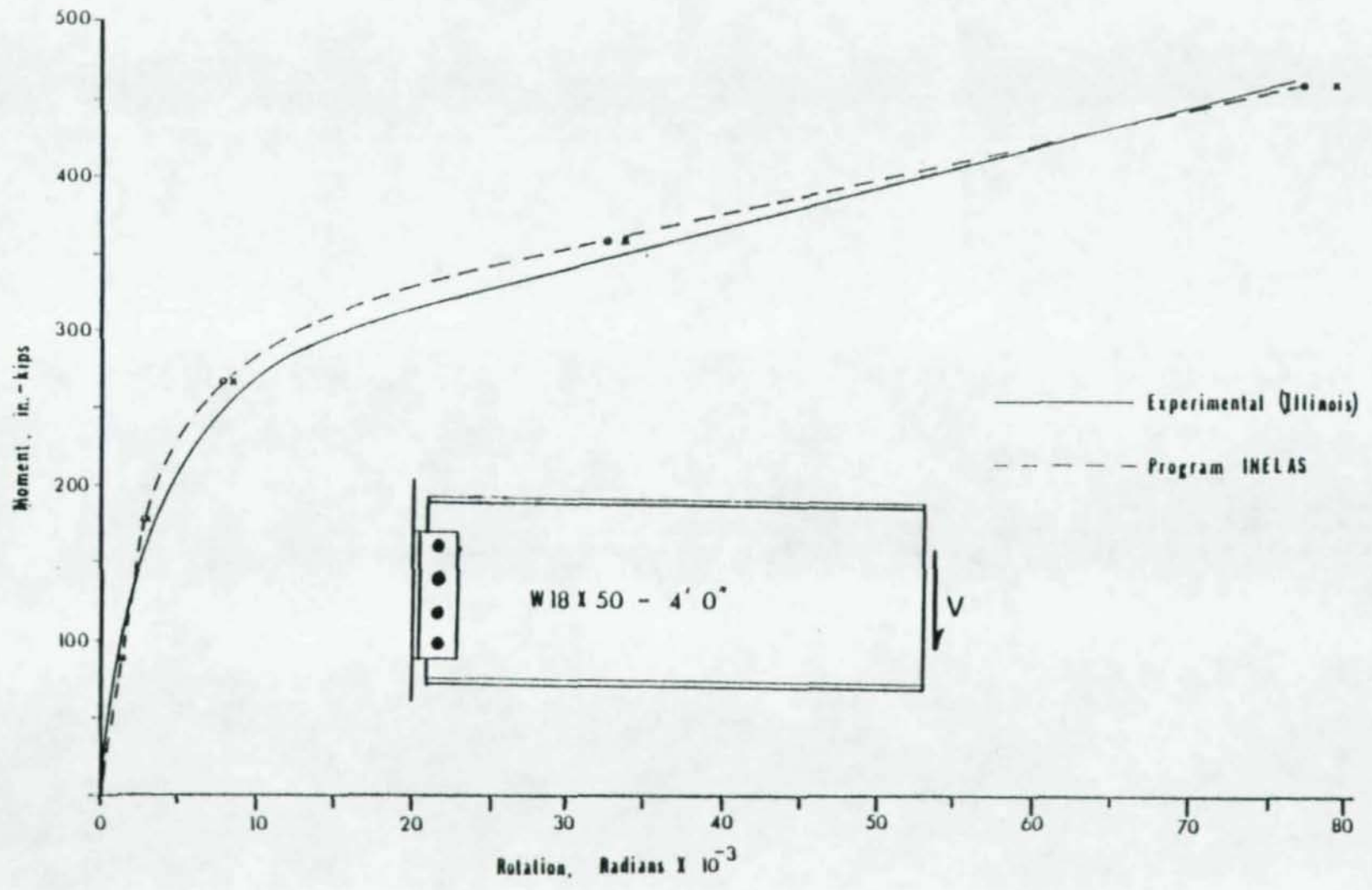


Figure 15. Cantilever Beam Analytical versus Test Results.

CHAPTER 4

ANALYSES OF DIAGONAL BRACING CONNECTIONS

A study by Hormby (10) of the connection shown in Figure 16 was made using the finite element model shown in Figure 17. In this connection the 9/16" gusset plate was welded to the top flange of the W24 x 68 beam. The 4 x 3-1/2 x 1/2" framing angles were welded to the gusset plate and bolted to the web of the W36 x 280 column. In practice this type of connection would be considered flexible since only web angles are used to join the beam to the column. However, this study showed that the gusset plate provided sufficient stiffness; that the beam when loaded with its uniform service load, developed end moments approximately equal to the fixed end moments. Thus the addition of the gusset plate, which is generally designed on the basis of the bracing load only, actually results in a haunched fixed-end beam. These studies are summarized in Table 3 for three different uniform load intensities. In addition to the Hormby study, the six diagonal bracing connections built and tested at the University of Alberta were modeled.

Four separate pieces of software were used in the connection studies. Three of the programs were post processing tools for plotting force and displacement fields and contours and stress surfaces. The major tool was a program called INELAS (1). The program is used for static analysis of structural systems which exhibits linear and/or nonlinear, isotropic and/or anisotropic material behavior.



Figure 17. INELAS Finite Element Model of Diagonal Bracing Connection.

Table 3. Beam End Moments in the Bracing Connection with Uniform Loading.

MOMENTS (Kip-in)

Loads	Actual	Fixed-End		Actual as Percent of Fixed-End	
		Uniform	Haunched	Uniform	Haunched
Working	2757	2520	2814	109%	98%
Yield	4063	3780	4221	107%	96%
2.25 x Yield	5855	5670	6331	103%	92%

There were several components to consider in designing a reliable finite element of the connection. Since the column was supported along its outer flange during the test, it was not included in the model. The gusset plate and beam web were simulated by quadrilateral and triangular plates, whereas the beam flanges were simulated by bar elements. Bolts, welds and framing angles were simulated as discussed in Chapter 3. The combination of these elements produced a two-dimensional model resulting in an efficient and manageable numerical analysis.

In the beginning of these studies it was not clear if the gusset plate alone would be enough to adequately simulate the structural action occurring in the connection. So two models were generated for each test conducted. One model consisted of the gusset and its connectors. The second included the beam and its connectors. An example of the 30° beam-gusset and support conditions is shown in Figure 18.

Neither model depicts the connection as it would occur in the field, but instead establish limits of maximum and minimum rotation the joint will experience. An actual connection would behave somewhere between the two extremes. The gusset model without the beam demonstrates the condition when the beam is very stiff and does not permit the gusset to rotate. The beam-gusset model demonstrates the maximum rotation and connection flexibility by letting the end of the beam rotate freely. The two limiting conditions were modeled to simulate the University of Alberta tests which permitted the free end of the

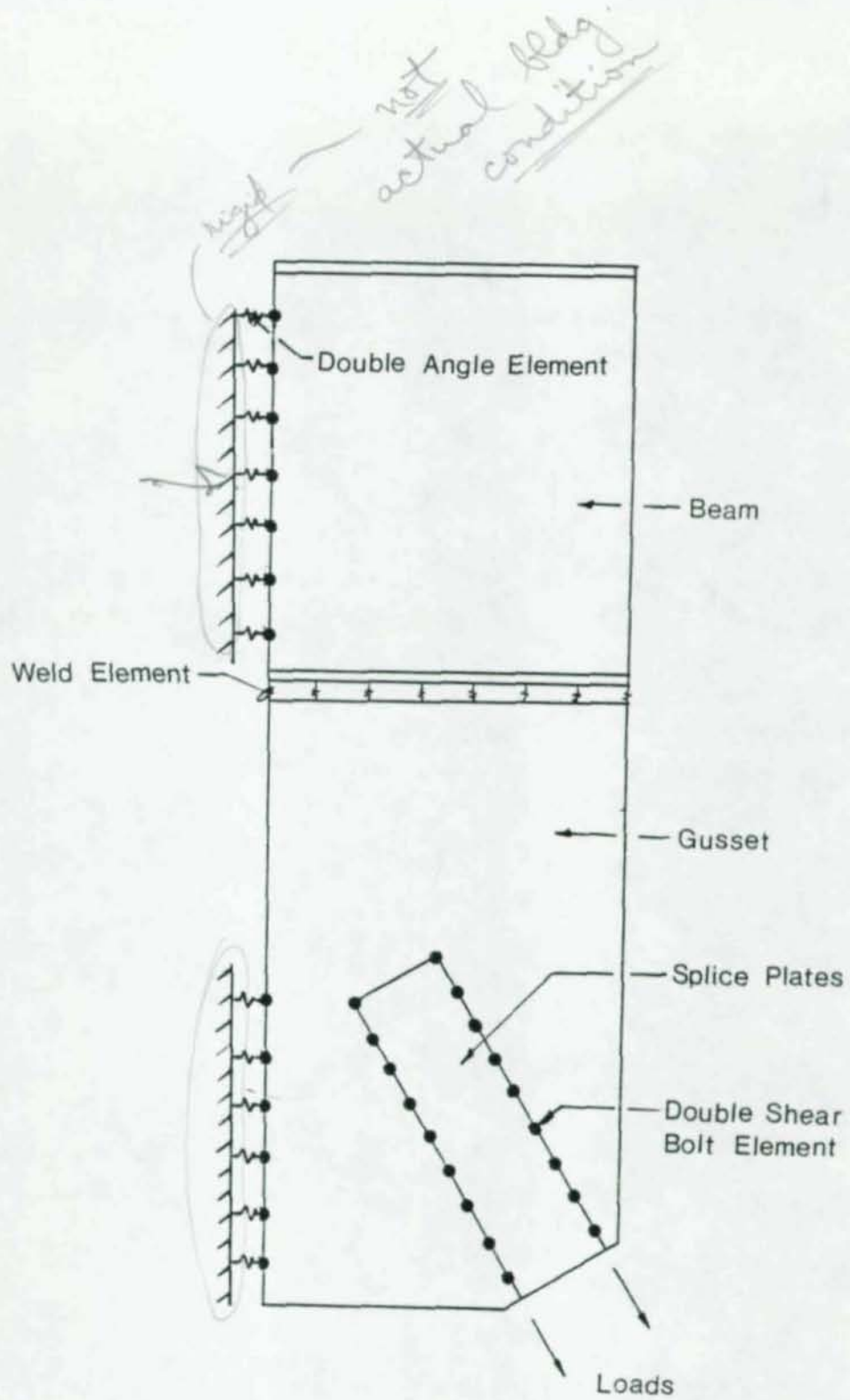


Figure 18. Connection Locations for the 30° Gusset and Beam.

beam to deflect without restraint and to simulate the beam with no rotation.

Table 4 describes the twelve major models generated. Several other models or variations of those models were run to verify the behavior of the connections. Each of the twelve represent corresponding physical tests. Loads were taken from the test conducted at the University of Alberta. Results from all the models were consistent with all twelve test configurations. To reduce the volume and redundancy of information in this report, each model will only be discussed briefly with the exception of the sixty degree, one eighth inch gusset and beam model. This model is probably a more general condition and will be looked at in depth.

The 45° 1/8" gusset model was loaded to 150 kips with increments of load of 0.5, 0.35, and 0.15. The distorted shape is plotted over the original shape in Figure 19. This distorted shape is exaggerated to show the plate behavior more clearly. The rotation of the gusset, the splice plates interaction with the gusset, and the overall deflection pattern is clearly illustrated. A surface and contour plot of effective (von Mises) stress at 75 kips is shown in Figure 20. This corresponds to the first increment of load. For the last increment of load, a similar plot is shown in Figure 21. It is noted that at 150 kips, the peaks of the surface in the stress plots have become much smoother, indicating a significant redistribution of stress as the material yields. At the end of the splice plates the contour pattern matches the tear pattern at failure in the actual physical test.

Table 4. Schedule of Finite Element Models.

Angle	Gusset or Beam Gusset	Gusset Thickness (in)	Load (kips)
45°	Gusset	.125	150
		.375	300
	Beam/ Gusset	.125	150
		.375	300
60°	Gusset	.125	140
		.375	320
	Beam/ Gusset	.125	140
		.375	320
30°	Gusset	.125	158
		.375	320
	Beam/ Gusset	.125	158
		.375	320

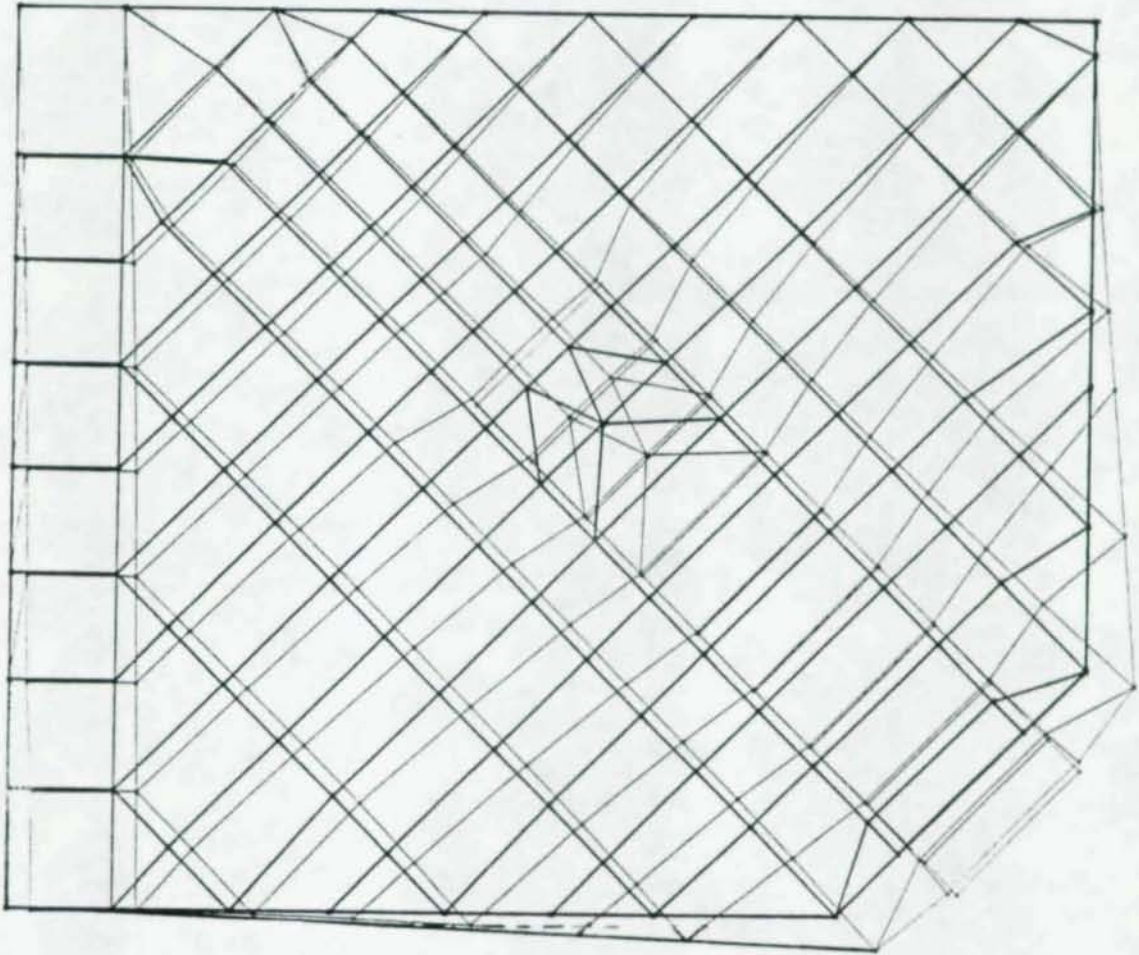


Figure 19. 45°, 1/8" Gusset Undistorted and Distorted Geometry.

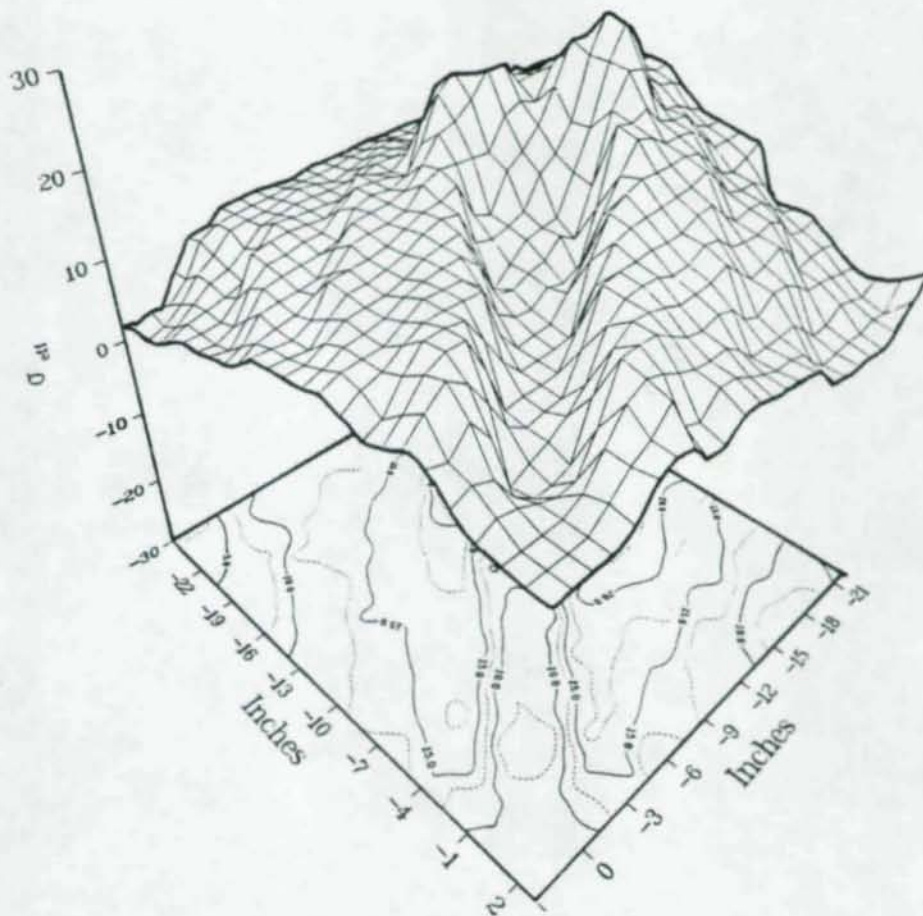


Figure 20. 45°, 1/8" Gusset, Effective (von Mises) Stress Contour and Surface Plots, 75 Kip Load.

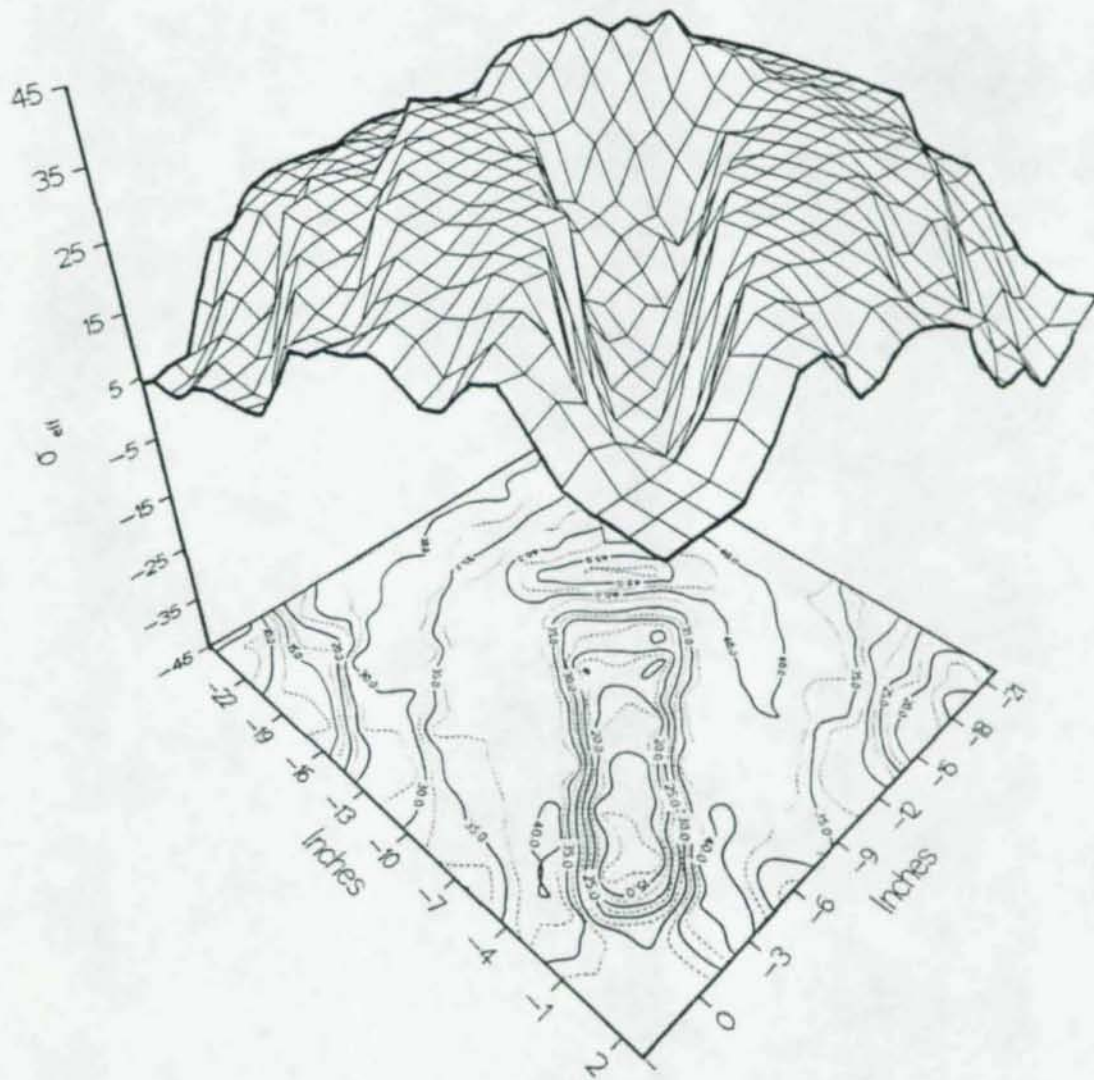


Figure 21. 45°, 1/8" Gusset, Effective (von Mises) Stress Contour and Surface Plots, 150 kip load.

The 3/8" model was loaded to 300 kips and produced the same behavioral pattern as the 1/8" gusset model as did all of the models in the study. In addition to the von Mises stress, maximum shear surface and contour plots were generated. Figure 22 illustrates a similar surface pattern as developed for the von Mises stress. Note the shape typifies the structural action which occurs in the block shear concept.

The gusset plate modeled above was restrained with framing angles on the column side and fixed on the beam side. In actuality, the beam would deflect with the gusset plate as load was applied. To investigate how this effected the model, an expanded model was generated with the beam included to determine its influence. Figure 23 is a plot of this model with the distorted shaped overlayed. As seen in the figure, the beam moves along with the gusset almost as a rigid body pivoting about the lower portion of the gusset. The deflection pattern is similar to the previous model. The reorientation did not significantly alter the force and stress fields in the connections, but deflections were somewhat different due to the reorientation of the gusset and beam. Figure 24 indicates the same effective stress pattern and magnitudes as the gusset model with low stresses in the beam, along with a sharp gradient in the stress field at the gusset to beam connection. As shown previously, the same high stress pattern occurs at the end of the splice plate where the effective stresses are in the 45 ksi range which is well beyond the elastic limit of the material. The 3/8" model of the same configuration performed in a similar manner

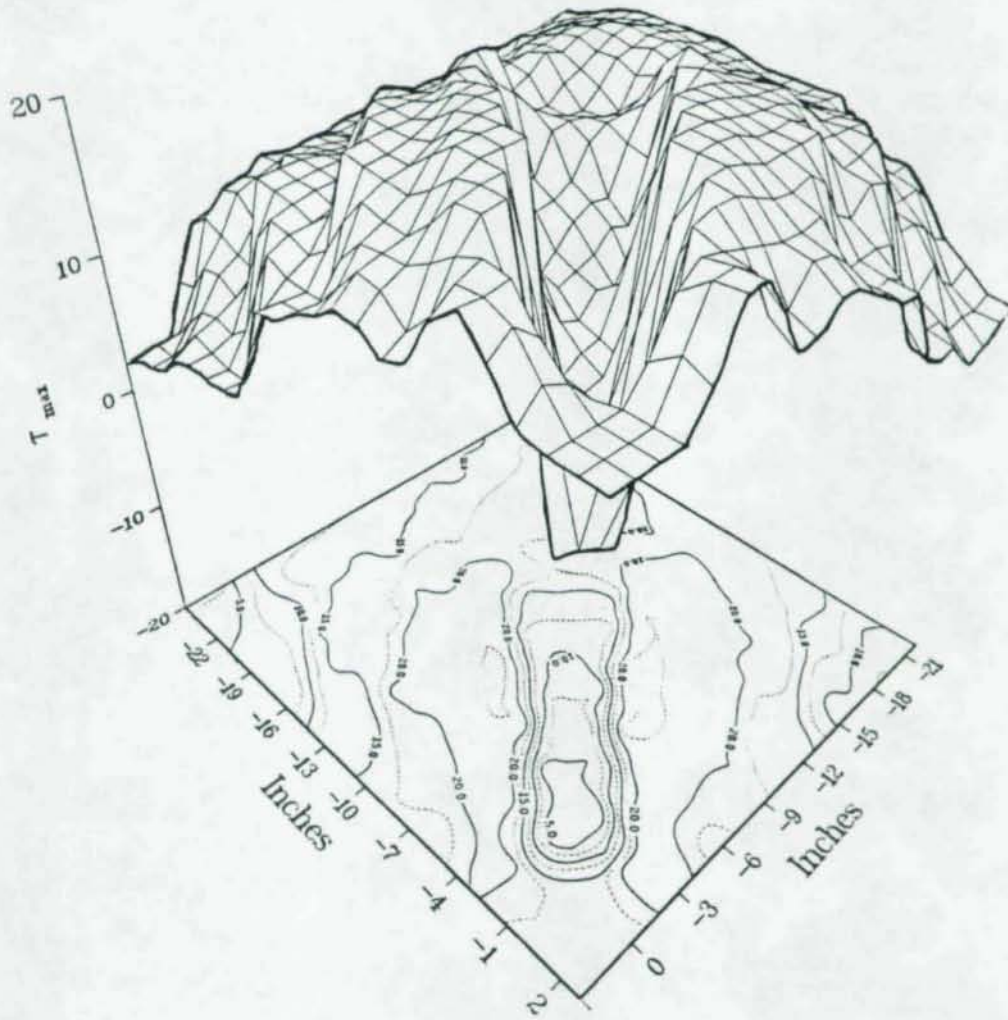


Figure 22. 45°, 1/8" Gusset, Maximum Shear Stress Contour and Surface Plots, 150 kip load.

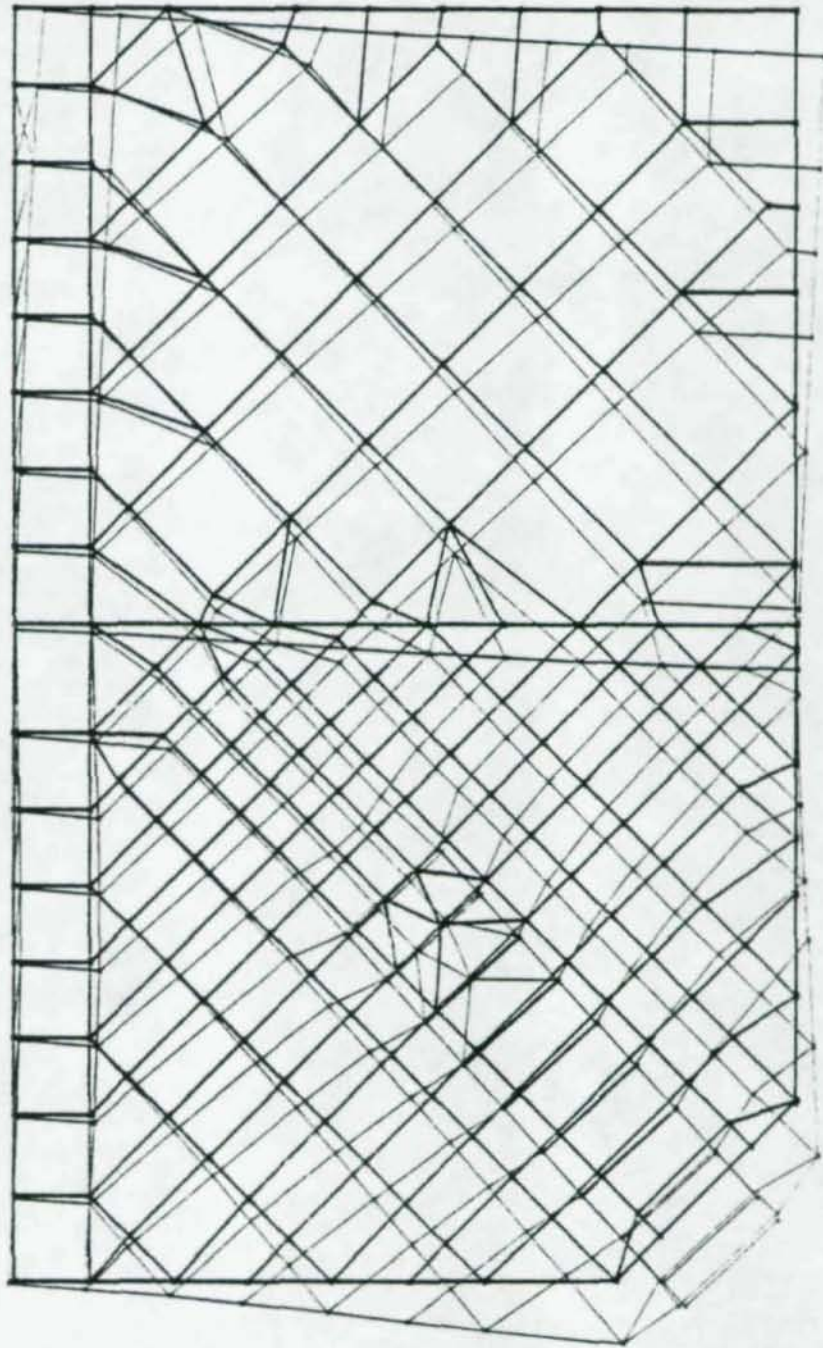


Figure 23. 45° , 1/8" Beam-Gusset Undistorted and Distorted Geometry.

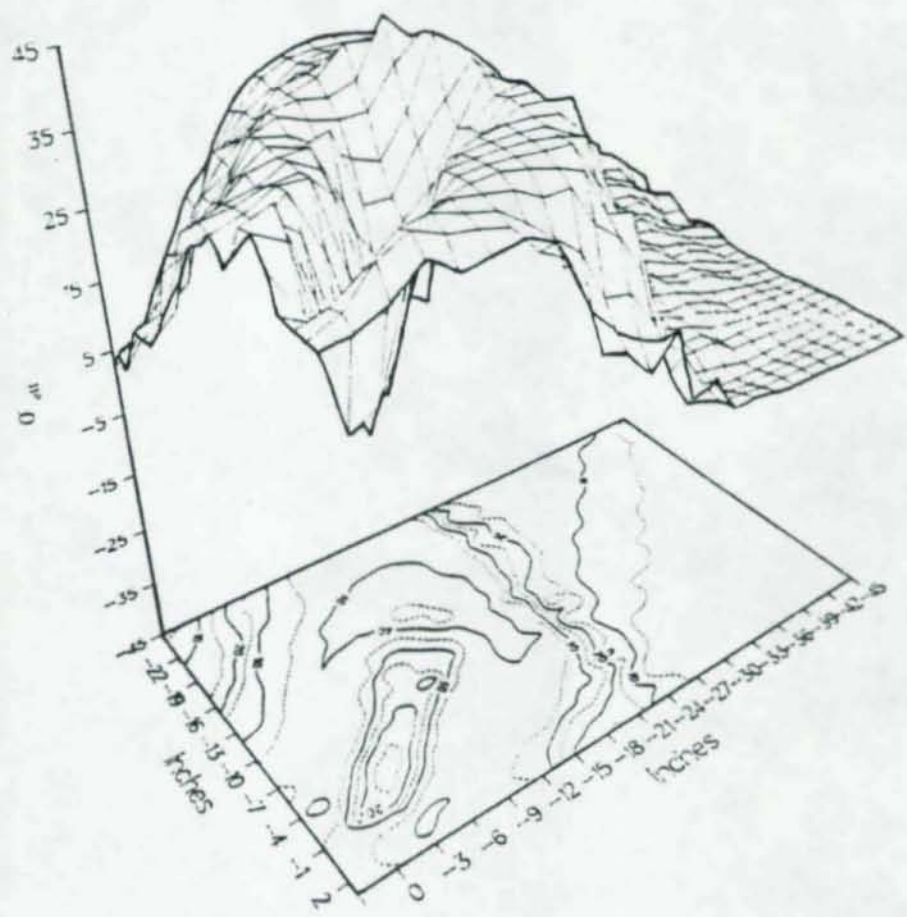


Figure 24. 45°, 1/8" Beam-Gusset Effective (von Mises) Stress Contour and Surface Plots, 150 kip load.

with the exception of greater rotation since the load was increased to 300 kips as illustrated in Figure 25. Again, stress patterns were essentially the same with displacements being changed somewhat by the rigid body rotation of the beam.

The 60° gusset was modeled in a similar fashion. Shown in Figure 26 is the $1/8$ " gusset with the exaggerated distorted shape plotted over it. This model had a total applied load of 140 kips. In Figure 27 the effective stress contour plot shows the same pattern as in the 45° models. The maximum effective stress contour again is 45 ksi at the base, resulting in excessive yielding or failure of the splice plate as before.

Force and displacement distributions in the column and beam connectors were significant findings in the study. Physical tests of the gusset plates were not instrumented to determine loads and displacements at the individual connectors, whereas these analytical methods determine the orientation and magnitude of forces and respective displacements. Traditionally, connectors in gusset plates have been designed by assuming vertical loads were resisted in vertical shear forces by the column connectors, and horizontal loads were resisted in horizontal shear by the beam connectors. If this were the case, framing angles would always take load in the direction of the column in which the angles are very stiff. Figure 28 shows resultant connector loads and displacements from the 140 kip load. From these analysis, it is seen that both the weldments and bolts have significant loads normal to the connection line. The forces and displacements in the splice

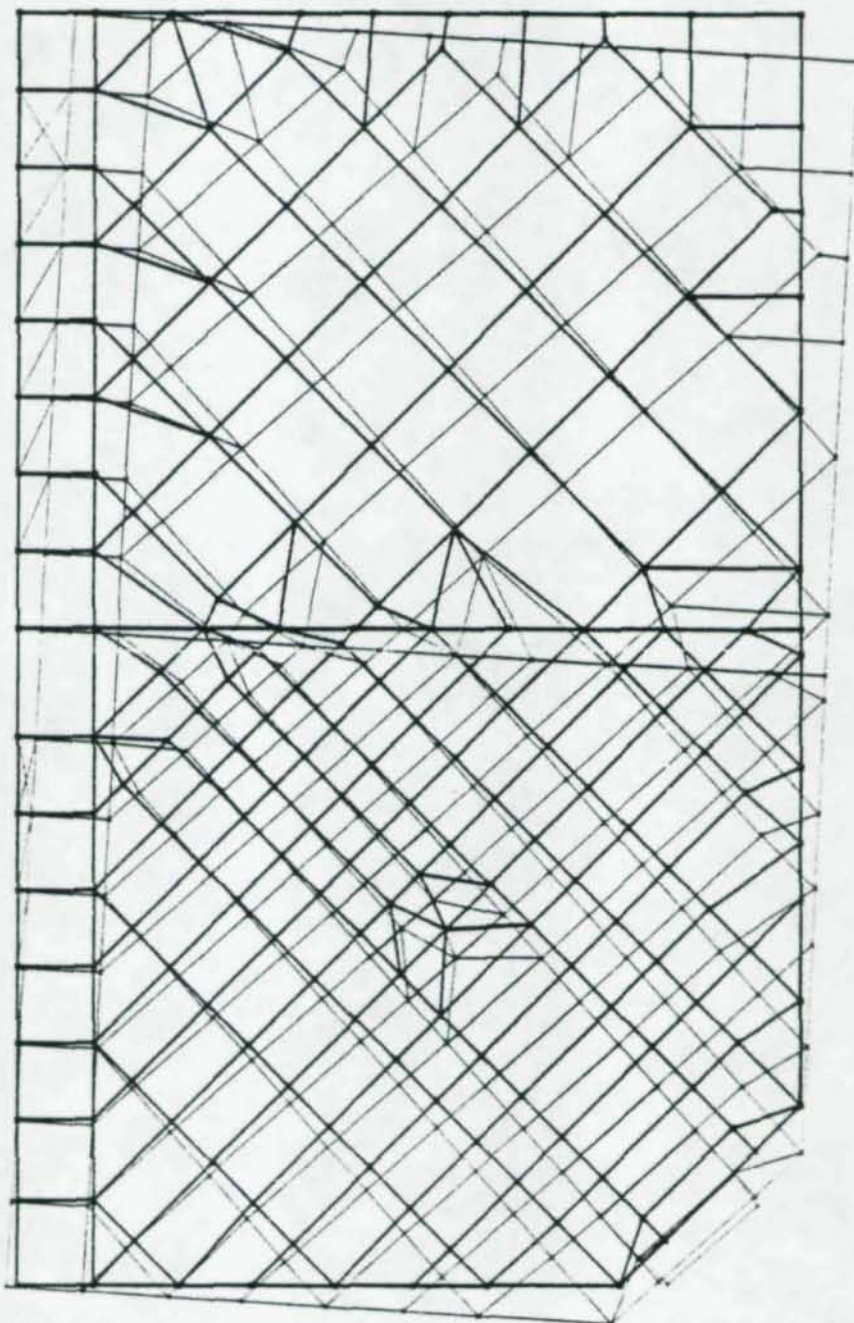


Figure 25. 45° , $3/8$ " Beam-Gusset Undistorted and Distorted Geometry.

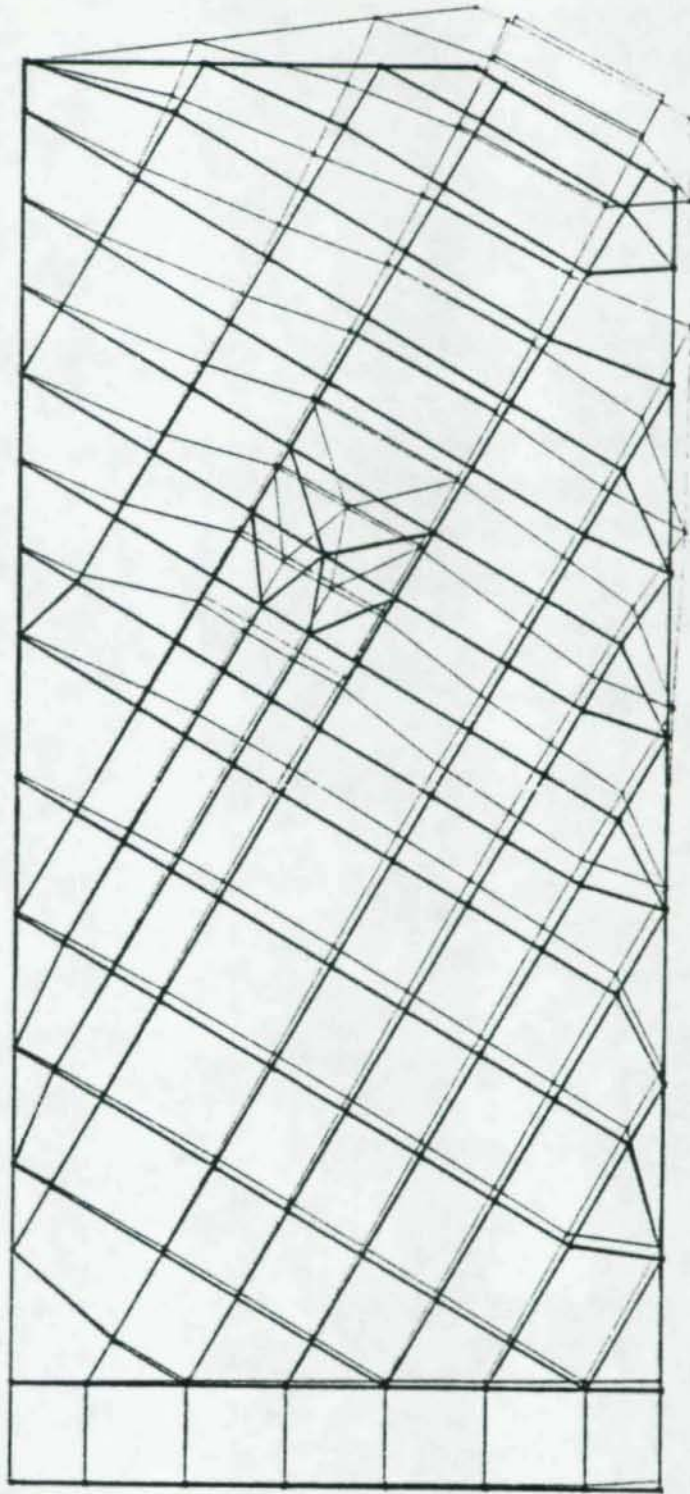


Figure 26. 60° , 1/8" Gusset Undistorted and Distorted Geometry.

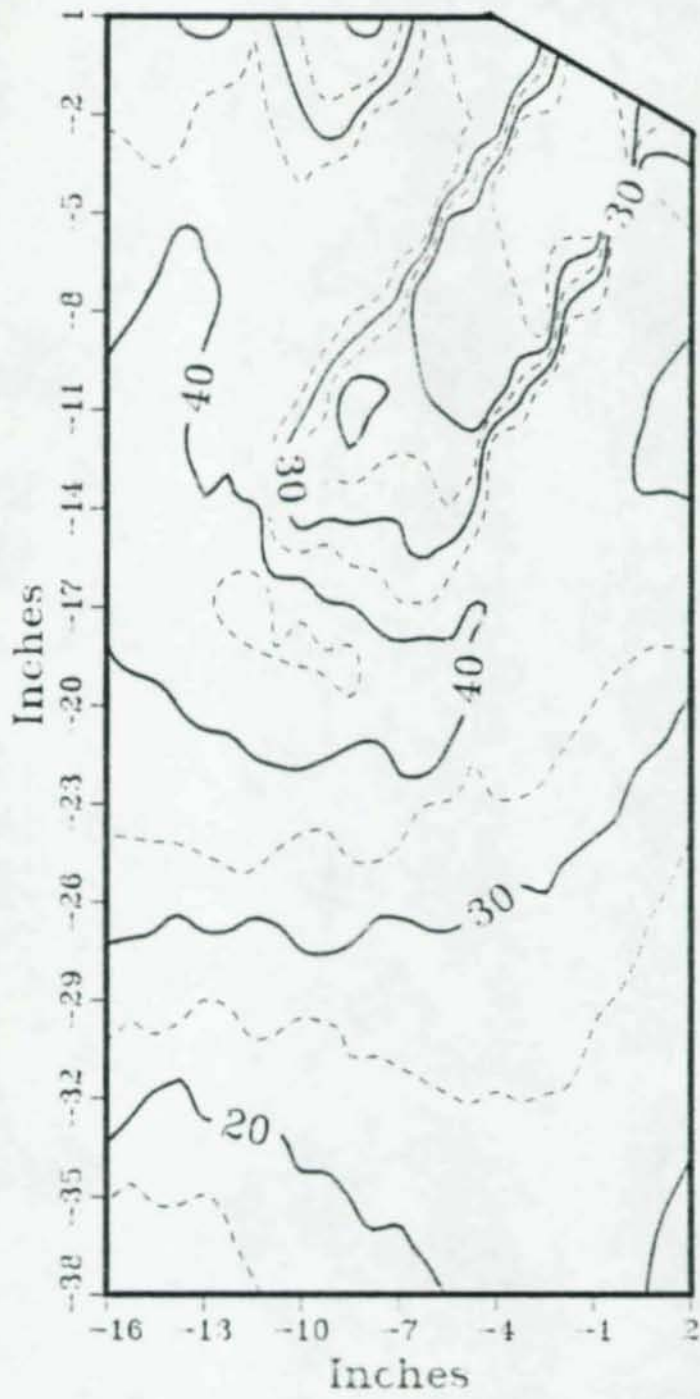


Figure 27. 60°, 1/8" Gusset Effective (von Mises) Stress Contour Plot, 140 kip load.

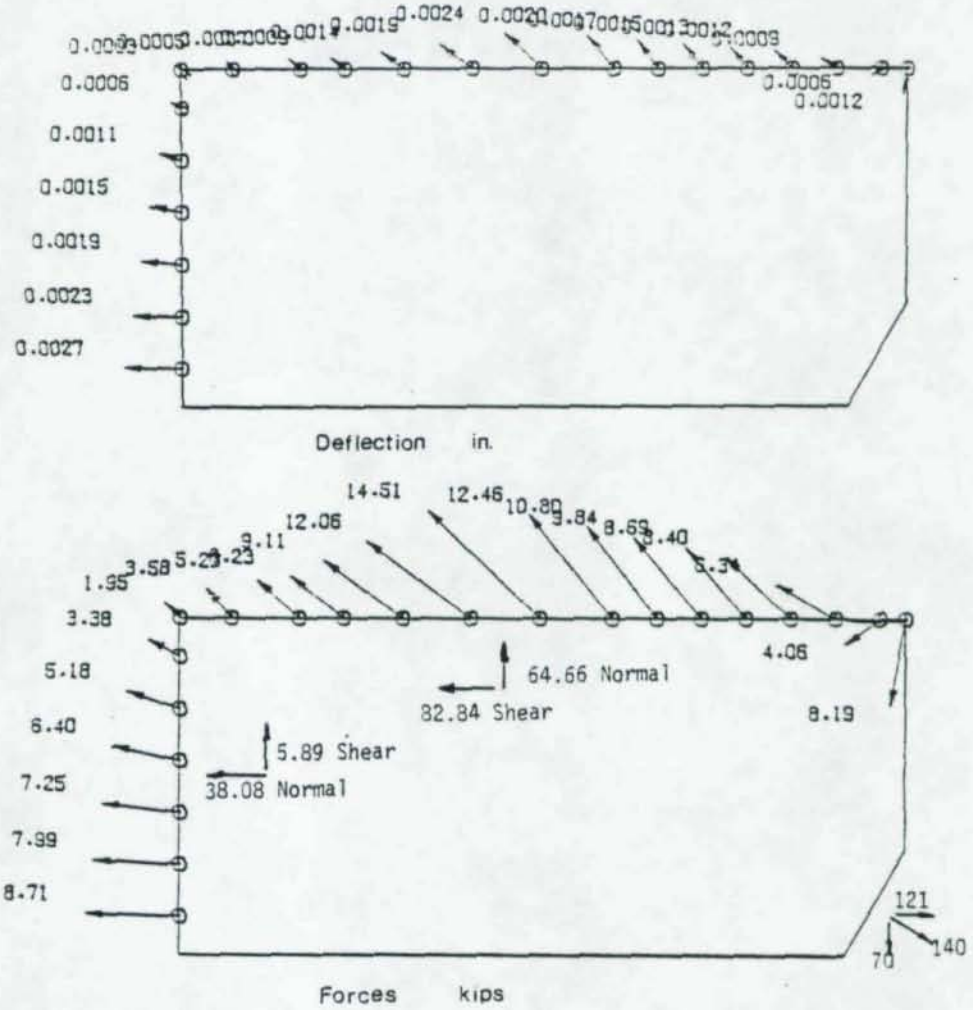


Figure 28. 60°, 1/8" Gusset Force and Deflection Distributions, 140 kip load.

plate to gusset connection are shown in Figure 29, where it is seen that the center bolts have about half the load of the outer bolts. Illustrated in Figure 30 are resultant bolt forces and displacements plotted in the vertical direction to indicate the variation of the magnitude of displacements and forces in the bolt pattern. All of the models studied had yielding in the gusset at maximum load, however the load never redistributed in an even manner to all the bolts. The entire connection distribution of forces in the gusset is given in Figure 31. At the corner of the gusset compression occurs due to the near rigid body rotation of the plate.

The beam-gusset model gave similar results. Figure 32 shows the model with its distorted shape. Force and displacement fields vary somewhat from the gusset model. Figure 33 shows the magnitude and orientation of resultants from the 140 kip load which may be compared to Figure 31. It is noted that the line of action for all the reactions are essentially in line with the direction of applied load for all cases.

The 30° gusset model was generated to complete the span of geometry commonly found in gusset connections. Results from the 1/8" and 3/8" gussets were similar to corresponding results of the 45° and 60° configurations. Shown in Figure 34 is the model and its distorted shape. This gusset was loaded to 158 kips. In the 30° beam-gusset model rotation was not as significant due to the angle of loading and location of the bolts. The distorted shape and model is shown in Figure 35.

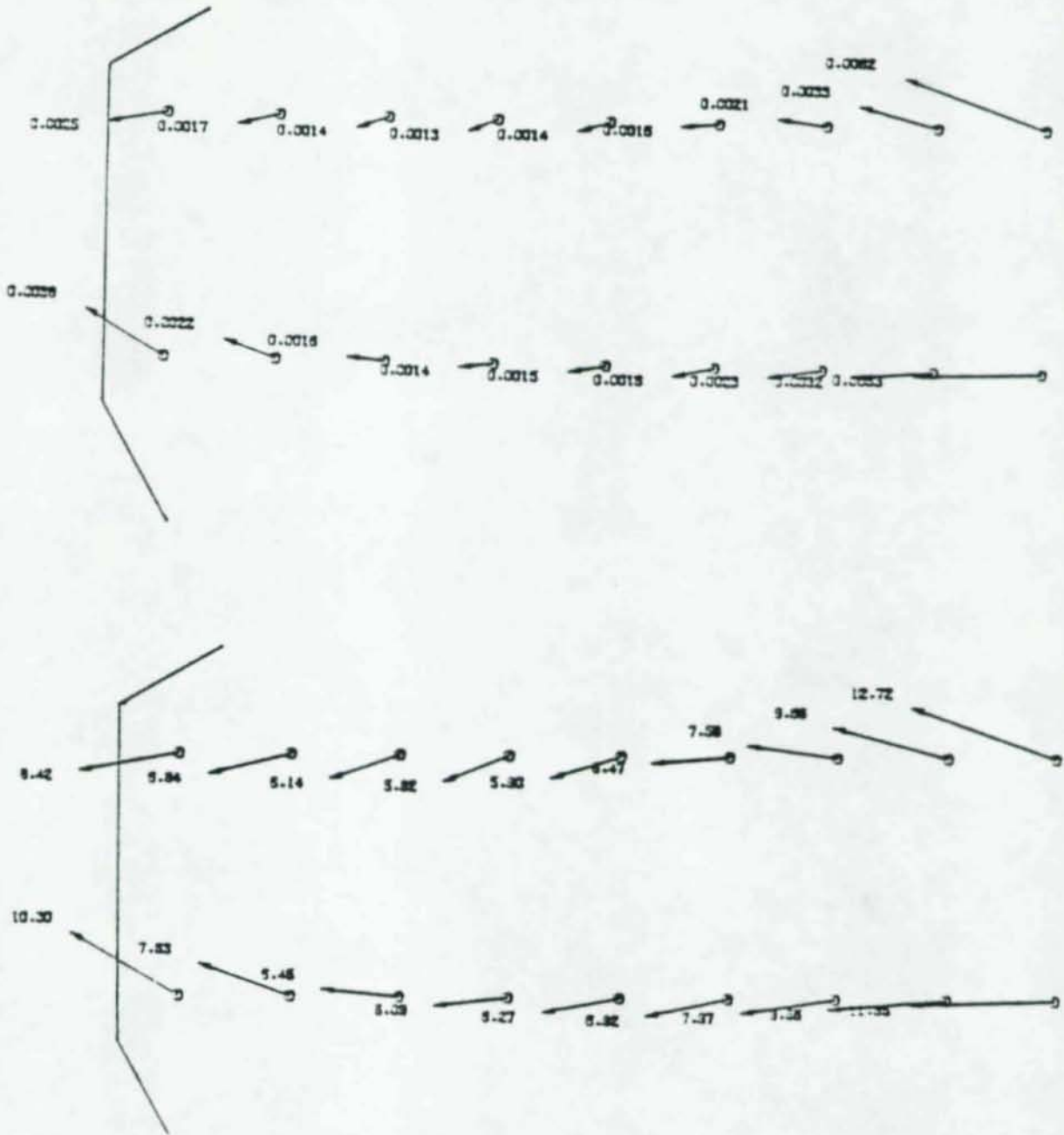


Figure 29. 60°, 1/8" Gusset Splice Plate Connection Force and Deflection Distributions.

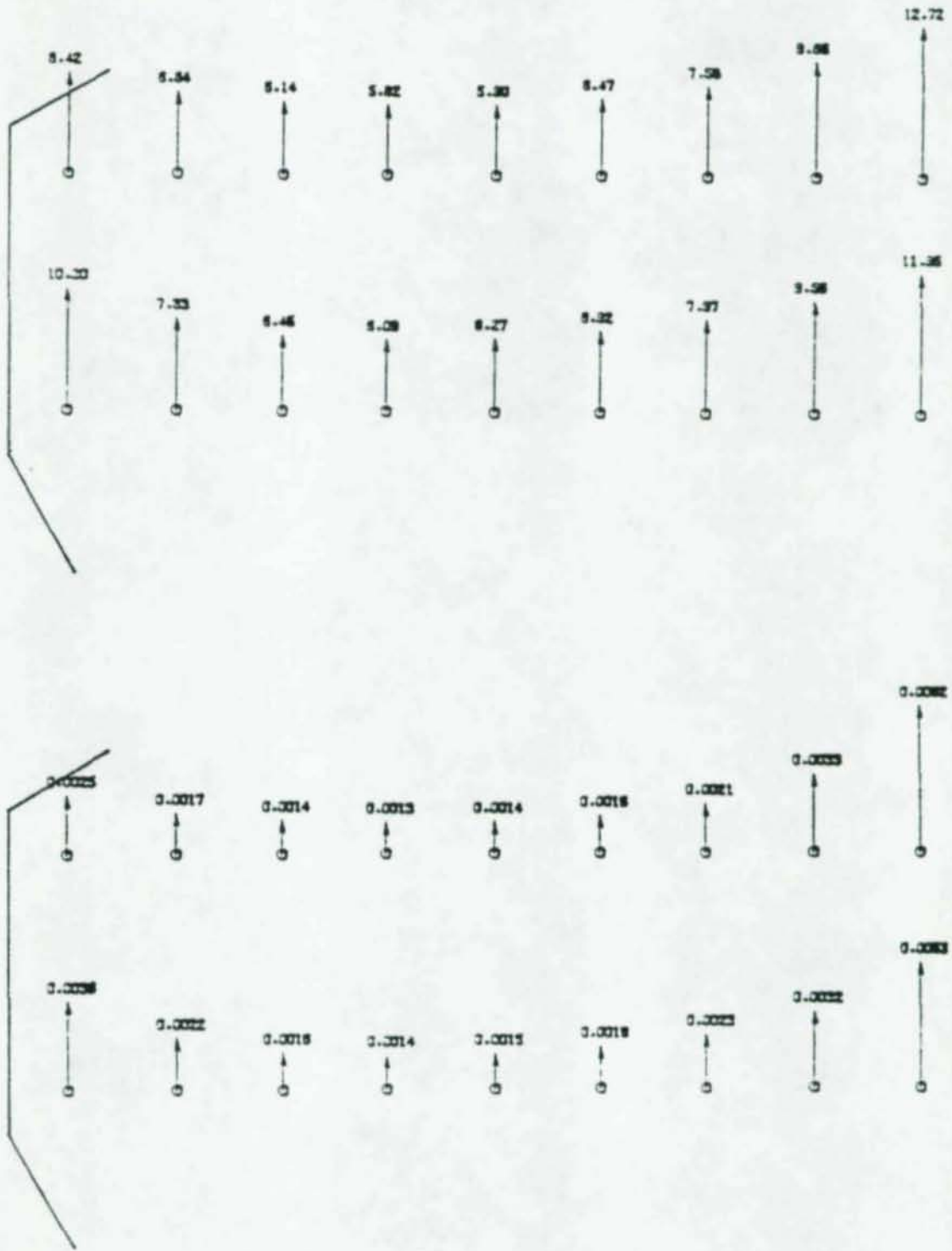


Figure 30. 60°, 1/8" Gusset Splice Plate Connection Force and Deflection Resultants Plotted Vertically.

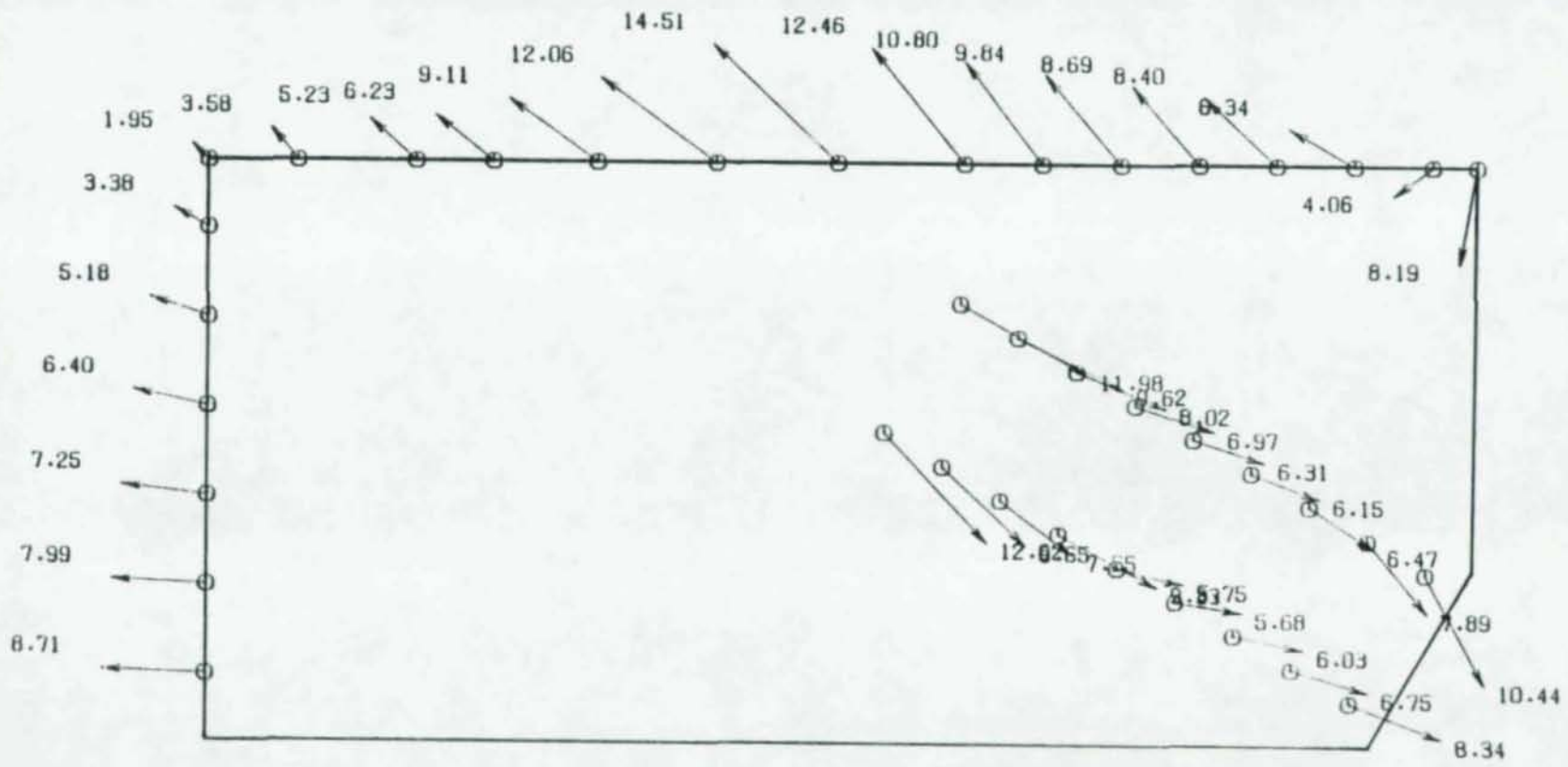


Figure 31. 60°, 1/8" Gusset Total Force Distribution.

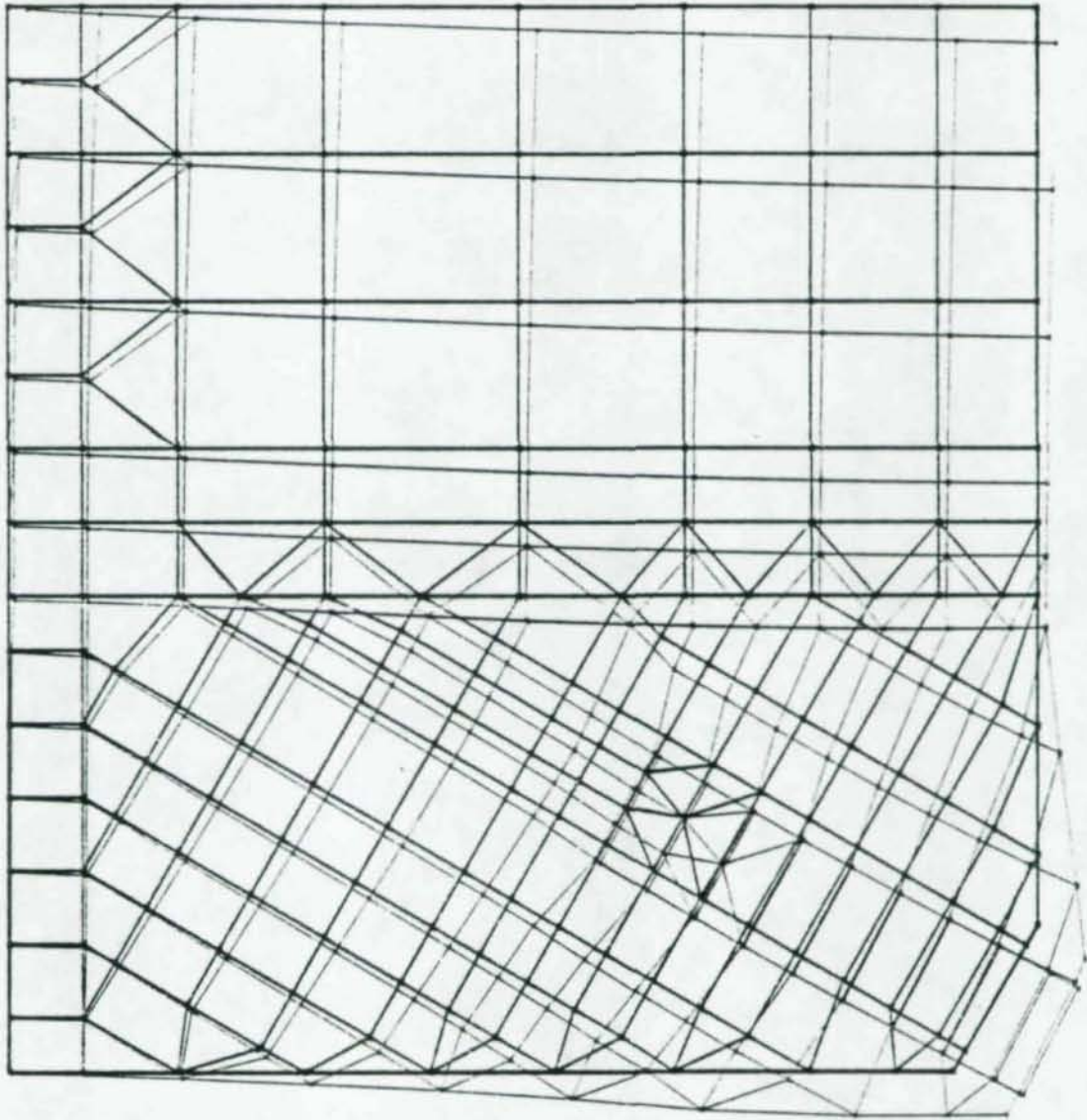


Figure 32. 60° , $1/8''$ Beam-Gusset Undistorted and Distorted Geometry.

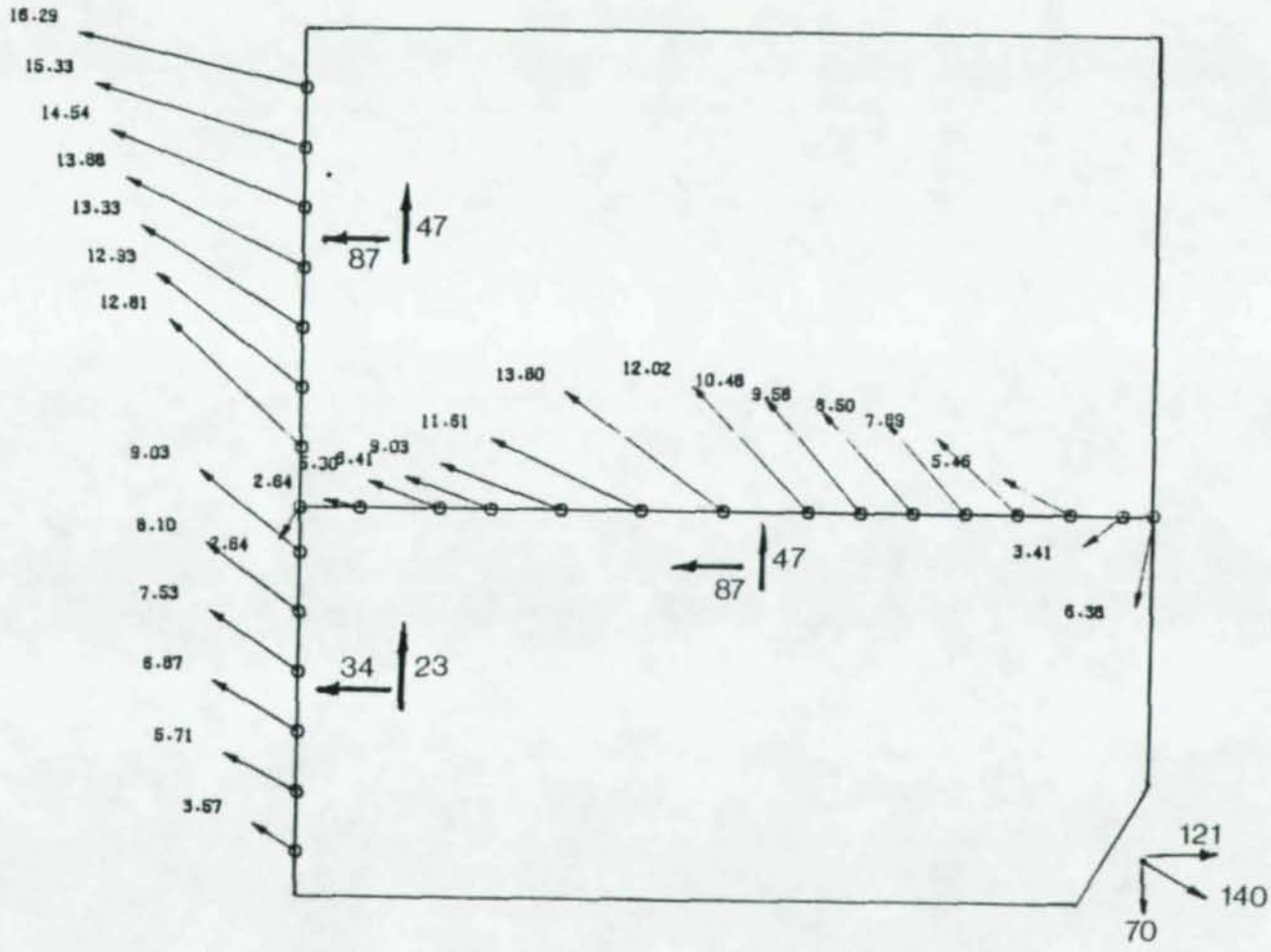


Figure 33. 60°, 1/8" Beam-Gusset Force Distribution, 140 Kip load.

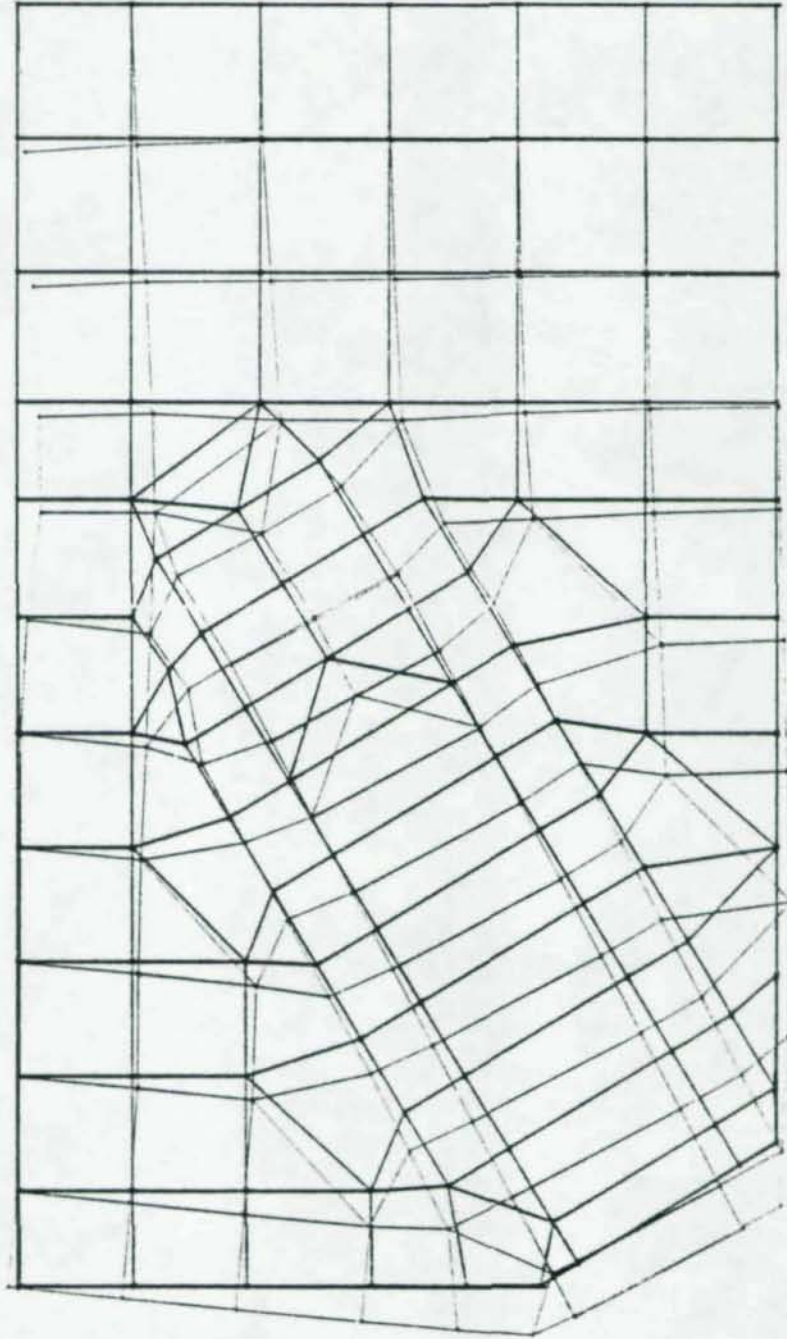


Figure 34. 30°, 1/8" Gusset Undistorted and Distorted Geometries.

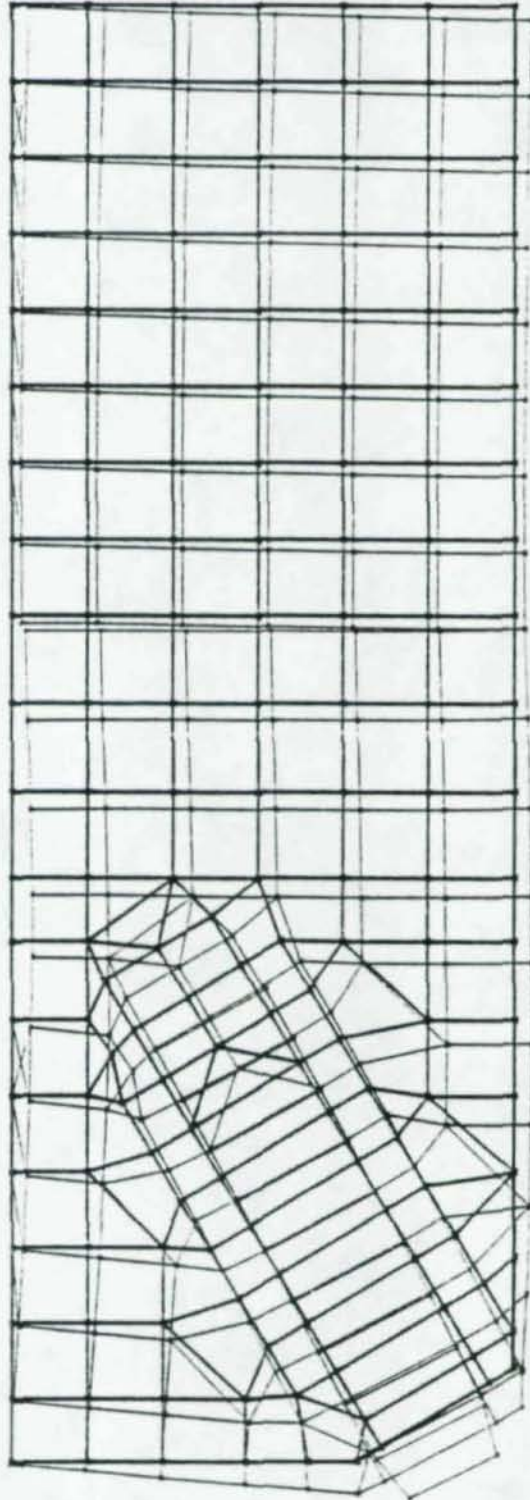


Figure 35. 30° , $1/8$ " Beam-Gusset Undistorted and Distorted Geometries.

CHAPTER 5

ANALYTICAL VERSUS TEST RESULTS

The combined results of the physical tests and analytical studies make it possible to evaluate the validity of the analytical techniques used for connection stress and strain predictions. Three major items were compared to ascertain the validity of the models.

- i) Similarity in deflected shape, yield patterns and failure locations.
- ii) Response of framing angles, welds and bolts.
- iii) Strain magnitudes.

All three items, when compared between analytical and physical tests, compared favorably. The comparisons verify the validity of the techniques used to simulate the gusset plate connections.

The tests done at the University of Alberta had extensive instrumentation, however, only certain strain readings at critical locations were selected as shown in Figures 36 through 41. These values were compared with results from the analytical predictions. Areas of low strain gradients as shown in Figures 22 and 24 agreed quite well with the test results. In areas of high strain gradients, results differed significantly as may be expected. These high gradient areas had strains changing an order of magnitude in less than one half inch. A finer mesh in these areas would possibly provide better results.

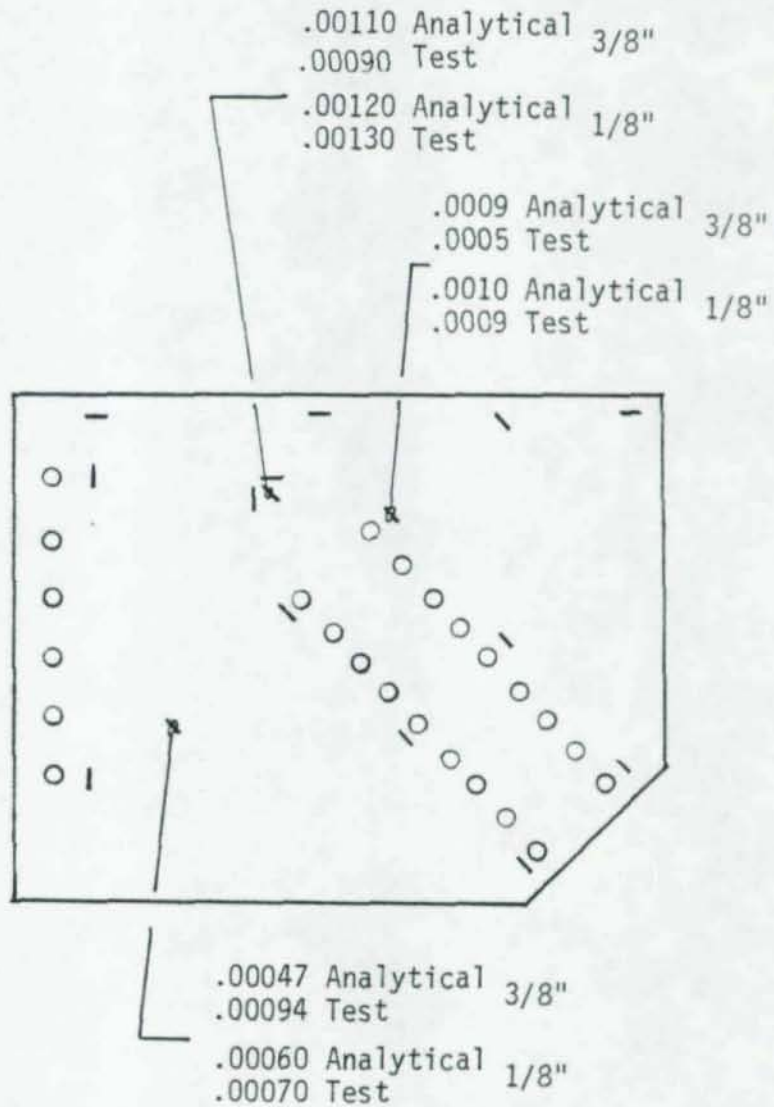


Figure 36. 45° Gusset, Analytical versus Test Results.

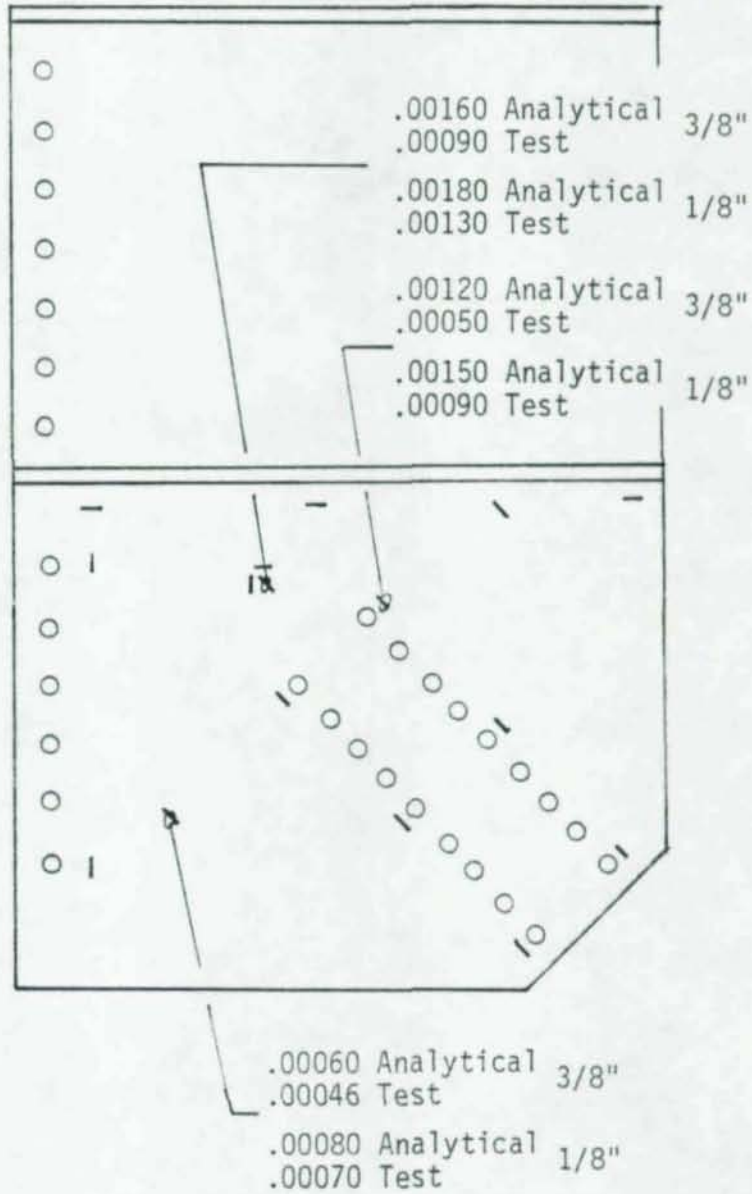


Figure 37. 45° Beam-Gusset, Analytical versus Test Results.

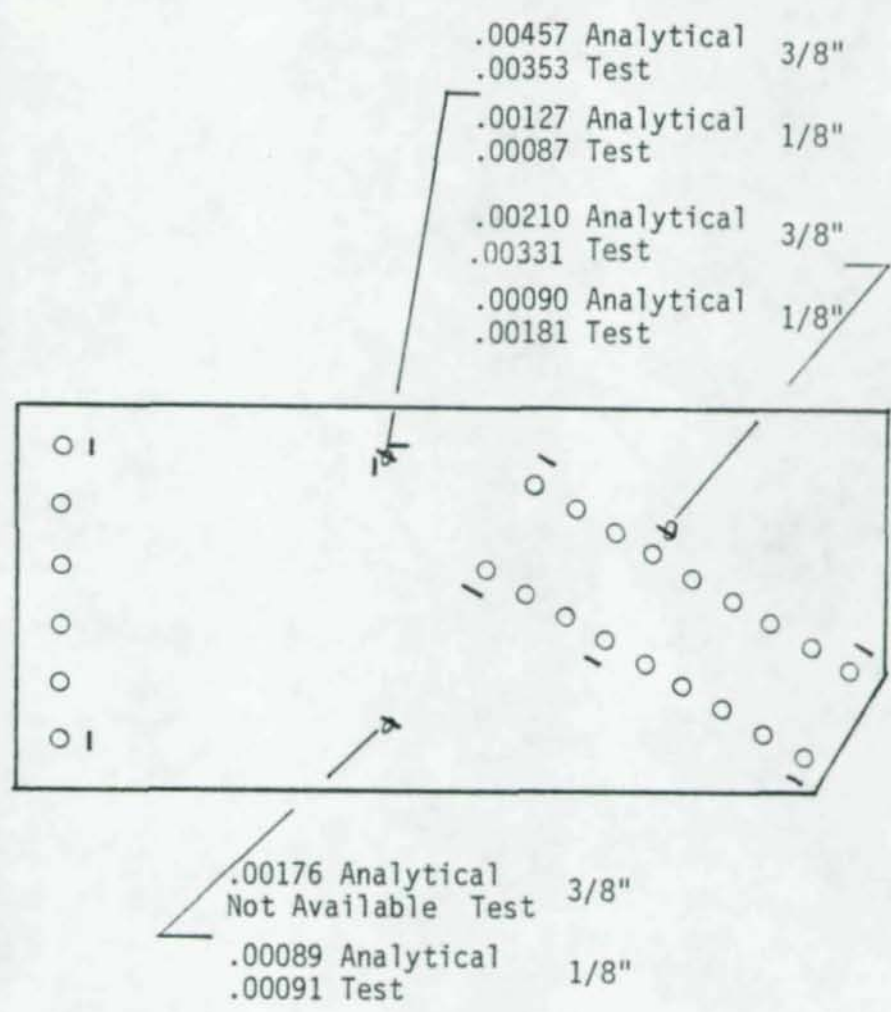


Figure 38. 60° Gusset, Analytical versus Test Results.

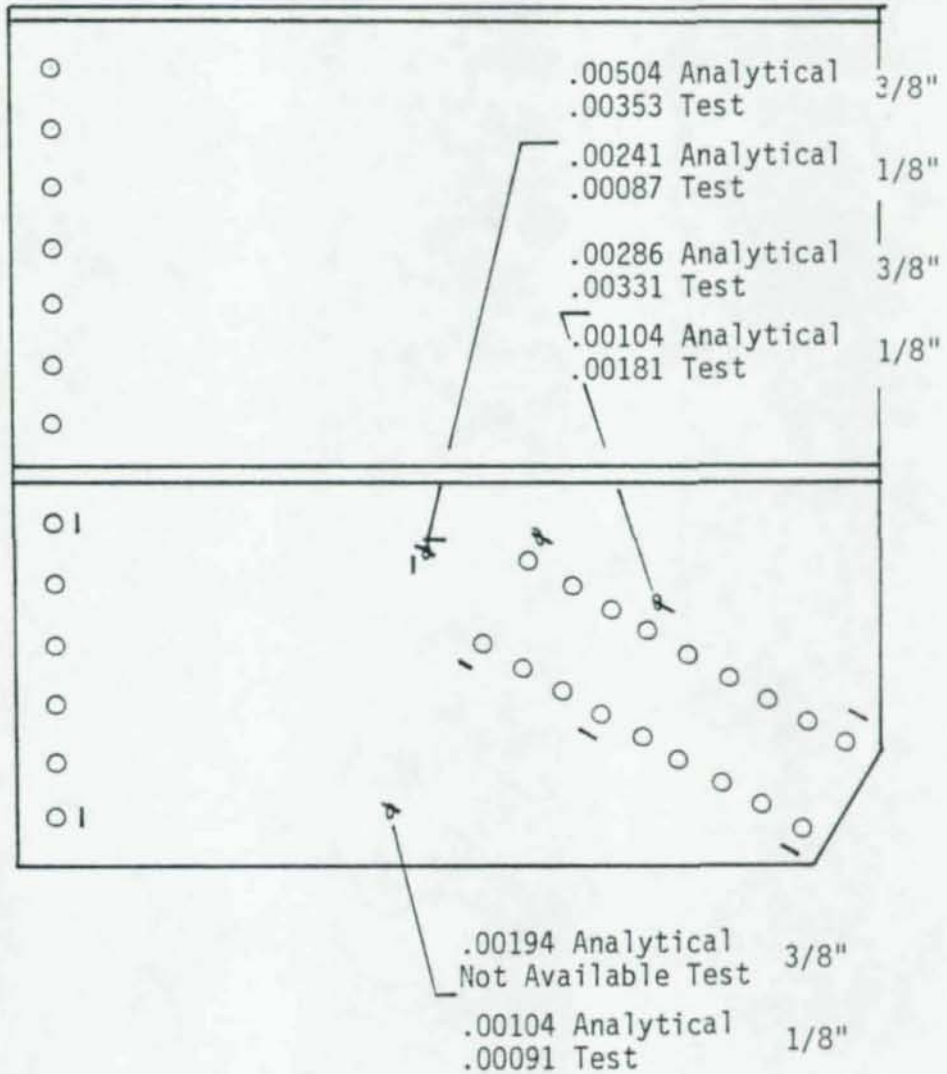
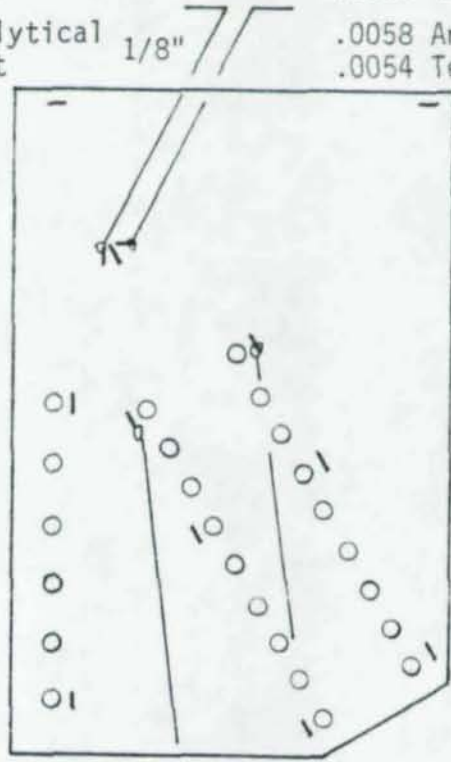


Figure 39. 60° Beam-Gusset, Analytical versus Test Results.

.00042 Analytical	3/8"	.0002 Analytical	3/8"
.00069 Test		.0001 Test	
.00262 Analytical	1/8"	.0058 Analytical	1/8"
.00140 Test		.0054 Test	



.00117 Analytical	3/8"	.00134 Analytical	3/8"
.00140 Test		.00170 Test	
.00304 Analytical	1/8"	.00693 Analytical	1/8"
.00132 Test		.00477 Test	

Figure 40. 30° Gusset, Analytical versus Test Results.

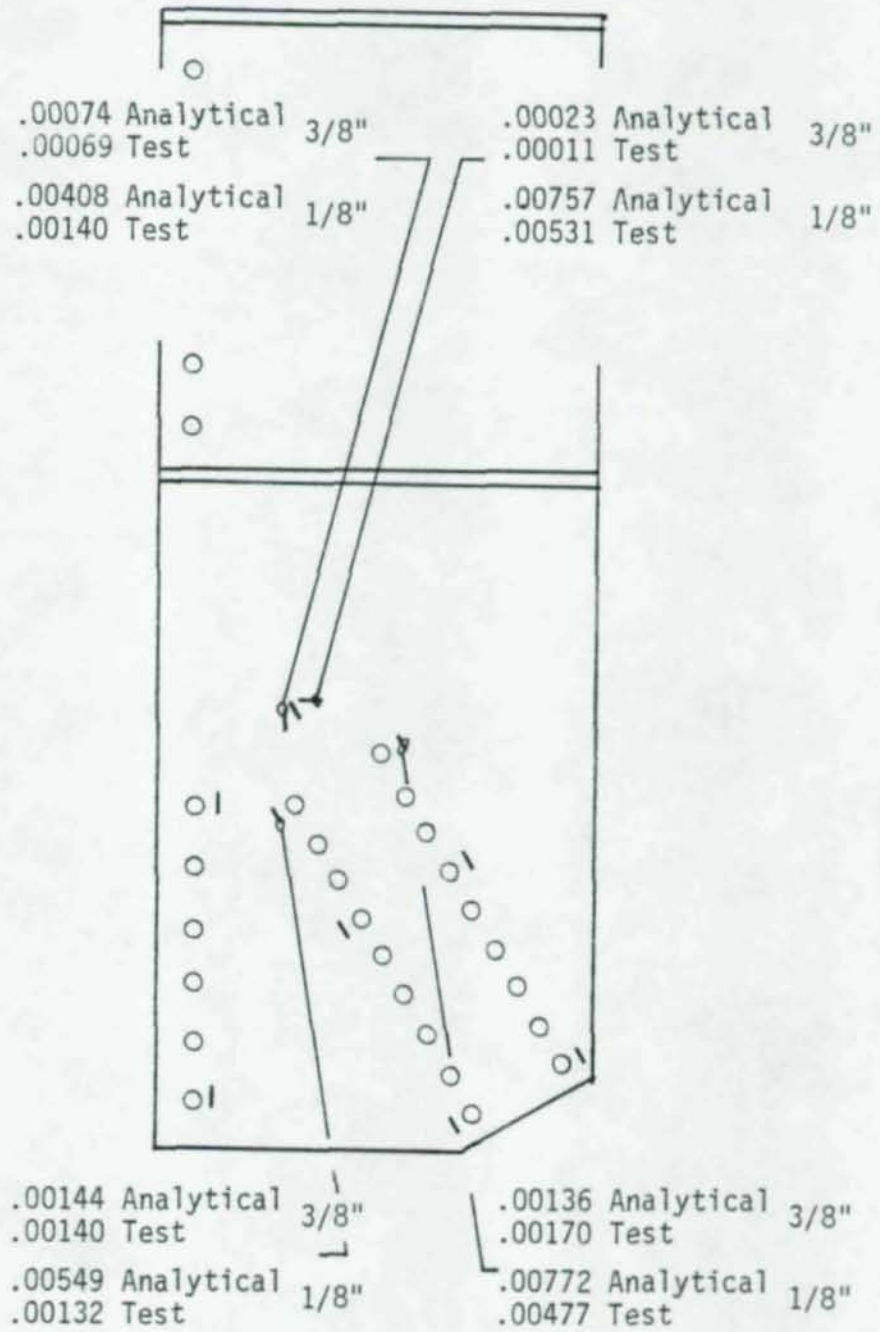
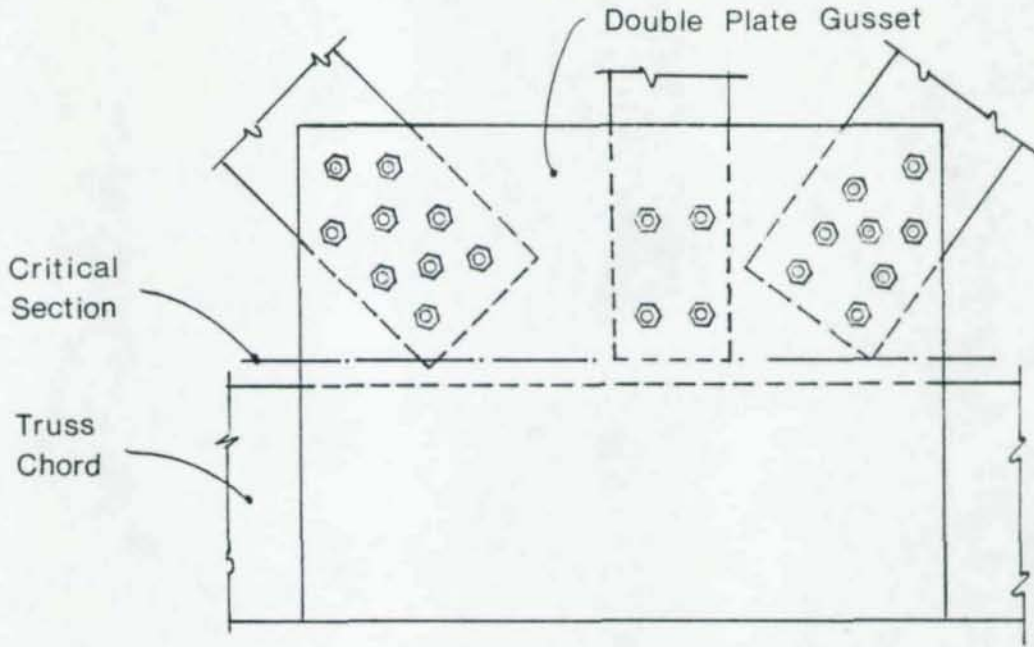


Figure 41. 30° Beam-Gusset, Analytical versus Test Results.

CHAPTER 6

CURRENT DESIGN CONCEPTS

Gusset plate analysis and design procedures have not been fully established. Experimental work done prior to the University of Alberta testing was done by Whitmore (11). Additional analytical work was done by Birkemoe, Eubanks and Munse (12) and Vasarhelyi (13). Whitmore's work in 1952 experimentally measured strains in a scaled version of a typical Warren type bridge gusset plate as illustrated in Figure 42. The model was made of aluminum and had extensive instrumentation. Whitmore observed that the high strains occurred at the ends of tension and compression diagonals. Beam formulas were found to be inaccurate for stress analysis, particularly at the edge of the plate. The "Whitmore criterion" which described a method for determining the maximum normal stress in the gusset was established from this research. This criterion assumes that the member force is distributed evenly over an effective area of the plate which is obtained by multiplying the thickness of the plate by an effective length. The effective length is determined by constructing 30° line segments from the beginning of the bolt pattern to the end of the bolt pattern as shown in Figure 43. The finite element results obtained from this study support the Whitmore criterion. As seen in previous figures, maximum effective stress patterns are similar to the 30° Whitmore pattern. Although a



Warren Truss Connection

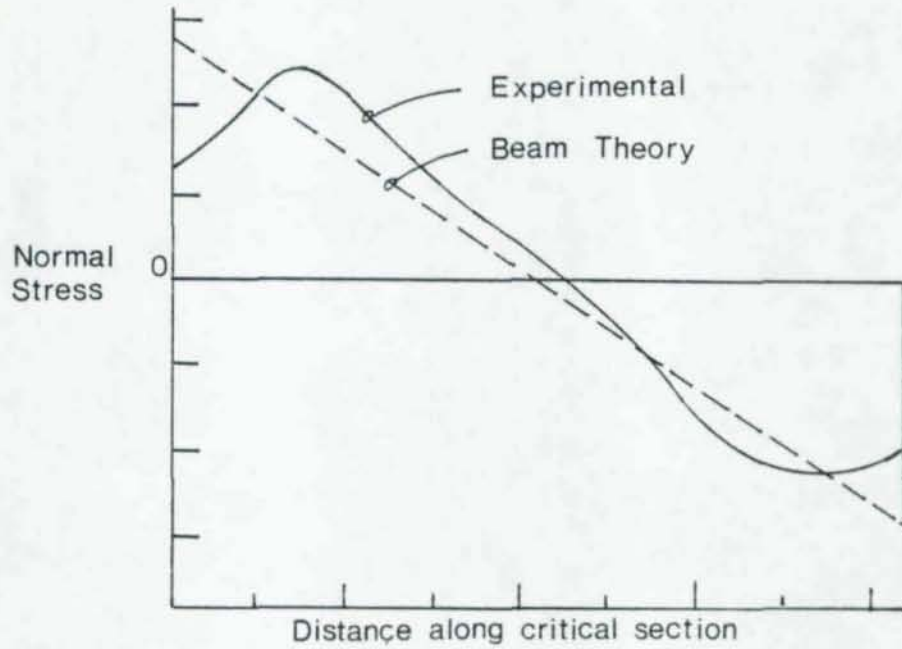


Figure 42. Whitmore Gusset Plate and Stress Distributions.

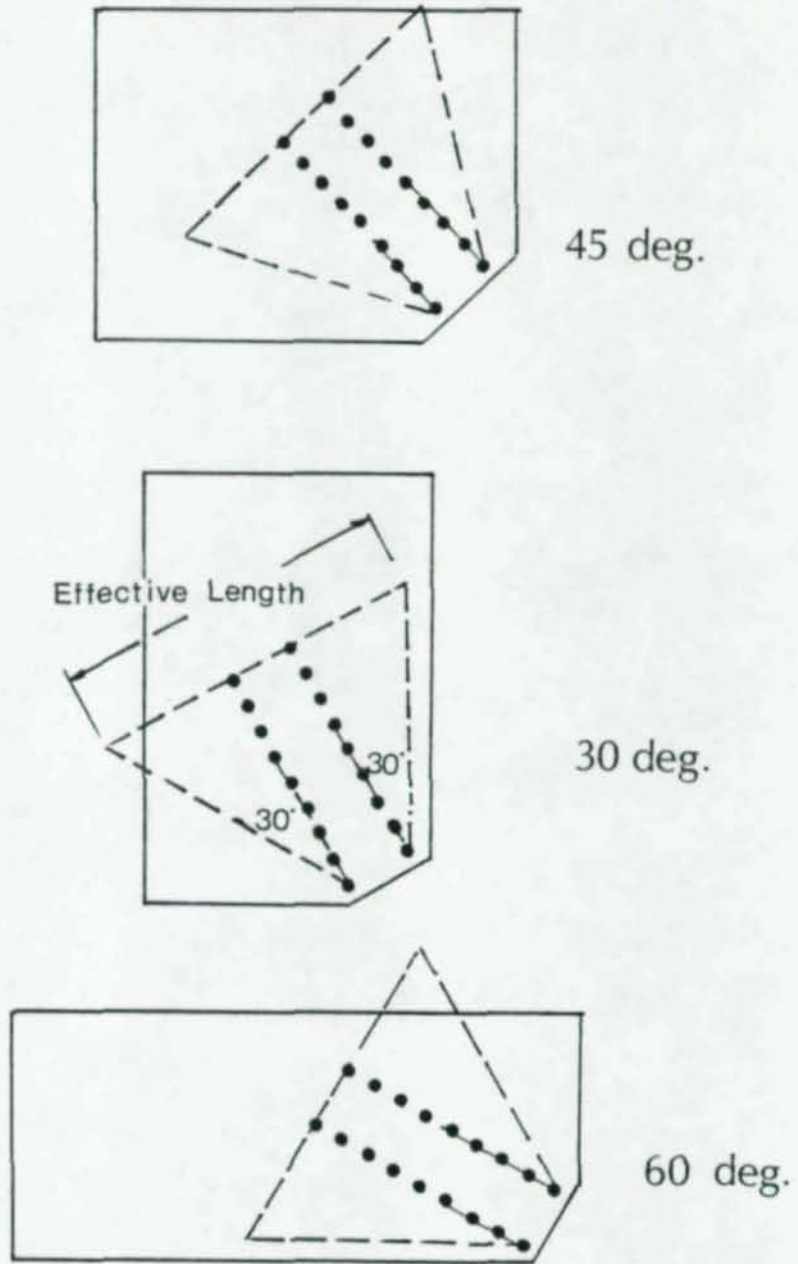


Figure 43. Whitmore Criterion for Effective Area.

good design aid, the Whitmore criterion seems to be supported in concept but analyses may show that the angle could be modified to more accurately depict normal stresses under loadings other than observed in the Whitmore testing.

Extensive analytical studies have not been made for gusset plates. Prior to the development of the finite element method and large computing capability, analysis of gusset plate connections were too complex to adequately describe the influence of material behavior, connectors and boundary conditions. Finite element work was performed by several researchers as this analytical tool became available. Elastic analyses were performed by Vasarhelyi (13), Davis (14), and Desai (15). Non-linear applications were introduced by Struik (16) in 1972. Struik used a nonlinear finite element program to predict effects beyond the elastic range and to estimate the effects of bolt holes in the gusset. Although the analyses were quite thorough, they did not include the nonlinearity of the fasteners. Results presented by Struik were consistent with results gained from studies performed for this paper although displacement field and forces on the connectors were not available. The gusset investigated by Struik was geometrically the same as the specimen Whitmore used in his experimental work in 1952.

CHAPTER 7

BLOCK SHEAR

A possible method for the design of gusset plates may exist in the block shear concept. The concept is discussed in the 8th edition of the AISC commentary section 1.5.1.2 (7). Briefly, the AISC code applies block shear to coped beams as illustrated in Figure 44. The acceptance of these results by the AISC committee came from tests at the University of Alberta and the University of Texas. These tests demonstrated that the failure load may be predicted by combining ultimate shear strength over the net section subject to shear stress with the ultimate tensile strength of the net section subject to tensile stress. Thus, the formula:

$$R_{BS} = 0.30 A_v F_u + 0.50 A_t F_u$$

where:

R_{BS} = Resistance to block shear, kips

A_v = Net shear area, in.²

A_t = Net tension area, in.²

F_u = Specified minimum tensile strength, ksi

Initial work leading up to this formula was done by Birkemoe and Gilmore (17). Their work included physical testing of connections subject to block shear failure.

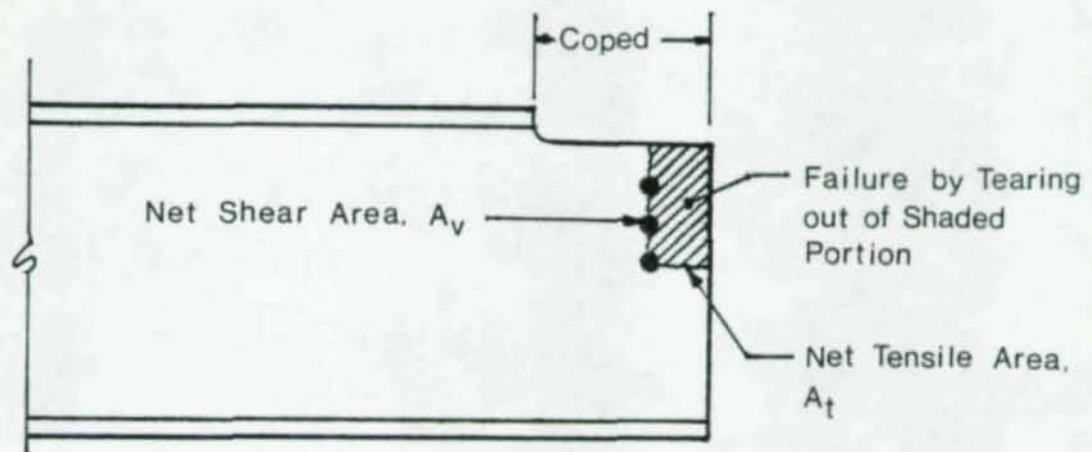


Figure 44. Block Shear Failure Mode for Coped Beams.

Yura, Birkemoe and Ricles (18) did additional work extending tests to include two rows of bolts, as well as additional single bolt testing. Their results indicated that the block shear formula with two rows of bolts overestimated the capacity of the connection. Ricles and Yura (19) made additional studies with a linear finite element analysis to predict failure patterns in the two row bolted connections. These prompted a modified block shear formula which assumes a linear distribution along the tensile failure area of the specimen. Previously tensile stress was assumed constant. Figure 45 illustrates both the linear and constant distributions for a typical specimen. To support this concept they purposed the following formulas:

Block shear capacity = tensile strength + shear yielding;

$$R_f = F_u \left[(g + e_n) 0.5 t_w - \frac{g + \frac{d_h}{2}}{g + e_n} t_w d_h \right] + 0.6 F_y (e_g + \Sigma s) t_w$$

or for design purposes:

$$\text{Block shear capacity} = 0.5 F_u A_{u \text{ net}} + 0.6 F_y A_{v \text{ gross}};$$

$$R_f = 0.5 F_u [(g + e_n) t_w - 1.5 d_h t_w] + 0.6 F_y (e_g + \Sigma s) t_w$$

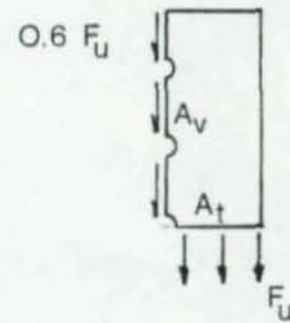
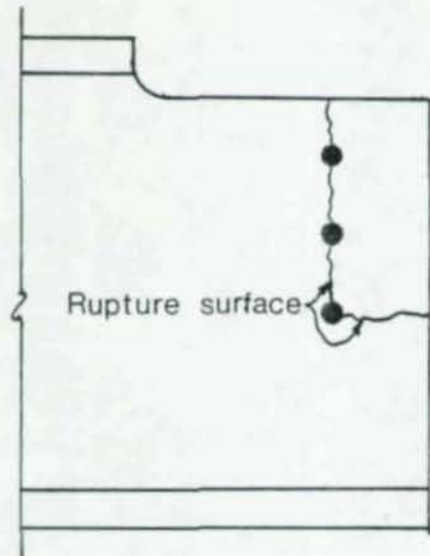
where:

A_t = net area of web in tensile stress plane of connection;

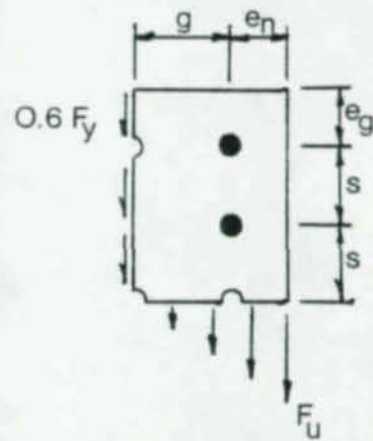
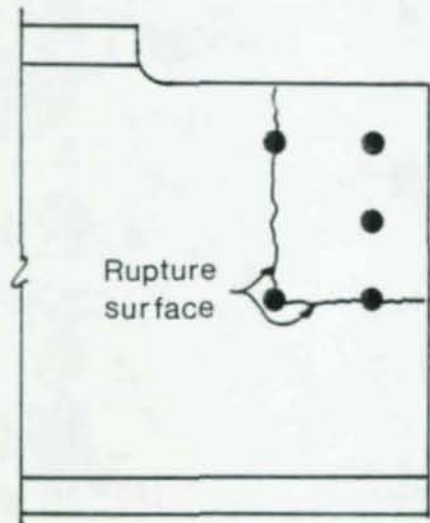
A_v = net area of web in shear stress plane of connection;

d_b = diameter of bolt;

d_h = the effective diameter of the bolt hole ($d_b + 1/8$);



Constant Stress Distribution



Linearly Varying Stress Distribution

Figure 45. Constant and Linear Stress Distributions in Block Shear.

e_g = edge distance from center line of the bolt hole to free edge;

e_n = end distance from center line of the bolt hole to free end;

F_u = static ultimate tensile stress of material;

F_y = static yield stress of material;

g = gage length of bolt line;

s = center-to-center spacing of bolts.

These formulas gave results which compared favorably with physical tests.

As seen in contour plots of the gusseted connections studied in this paper, the diagonal brace connection to gusset plate fails in a similar manner to the coped beams tested. Figure 46 illustrates this point. The similarity in the two problems has prompted the idea of modifying the block shear formula from the AISC specification to a design tool for designing the bracing connection. Thus, a modified block shear criterion may be applicable to determining the gusset plate size and thickness. This modified procedure would use the gross section along the bolt lines in large connections. An argument for using the gross section may be based on the fact that the interior bolts may never slip into bearing as illustrated in Figure 30. For the gusset test, specimens there are two rows with nine bolts each at 2-1/4" on center, spaced five inches apart as illustrated in Figure 2. Thus, using the block shear concept with shear forces along the bolt lines and tension along the end of the splice plate,

$$P_{ultimate} = A_{vg} F_{vu} + A_{tg} F_{tu}$$

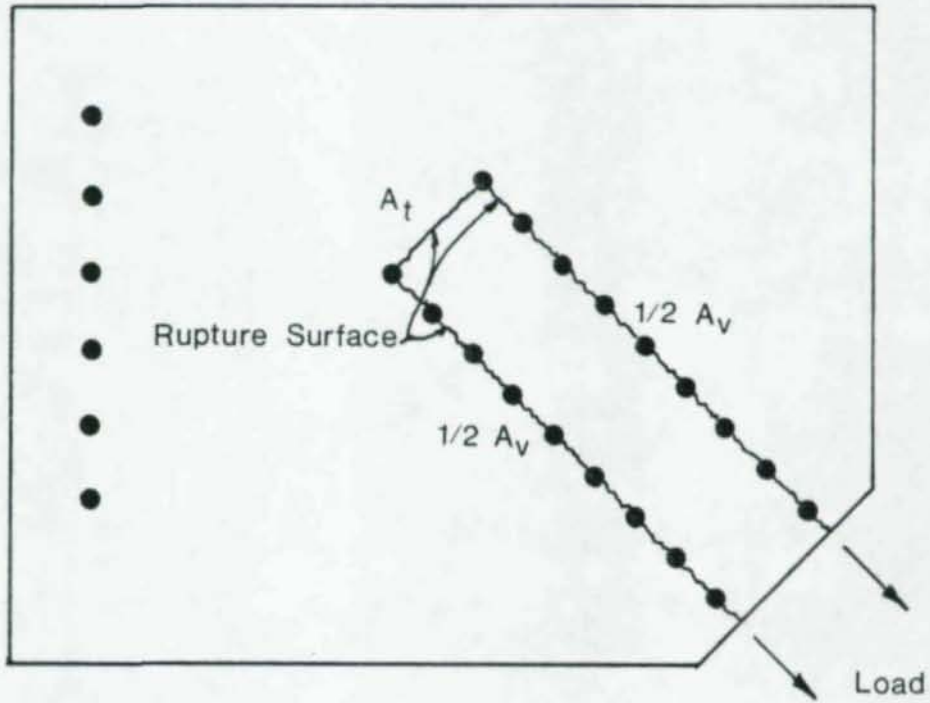


Figure 46. Gusset Plate Block Shear Failure.

where:

A_{vg} = gross shear area;

A_{tg} = gross tensile area;

F_{vu} = ultimate shear strength;

F_{tu} = ultimate tensile strength.

Applying this to the 1/8" gusset configuration yields the following:

$$A_{vg} = t (\ell v) = (.125) (8 \times 2\frac{1}{2}) 2 = 4.5 \text{ in.}^2$$

$$A_{tg} = t (\ell t) = (.125) (5) = .625 \text{ in.}^2$$

$$F_{vu} = .6 F_y = 25.6 \text{ ksi}$$

$$F_{tu} = 55.5 \text{ ksi}$$

$$(4.5) 25.6 + (.625) (55.5) = 150 \text{ kips.}$$

The loads at which tearing occurred at the ends of the splice plates in the 60°, 45° and 30° gussets were 140, 150 and 158 kips respectively. In the case of small connections where there are five or less bolts in a row, it may be appropriate that the net section along the bolt line be used to compute the strength of this connection. Additional tests are needed to establish this design concept for small connections.

CHAPTER 8

SUMMARY

The analytical models of gusset connections which include the plate and the connectors have been shown to predict the strain distributions in gusset plates in an adequate manner. Comparing the results of these models with physical tests have verified the analytical techniques used in the study. Findings from the finite element models showed that significant normal load is transmitted to welds and double angle connections. In general, the reaction of the connections were oriented closely to the applied load. These studies also support the Whitmore criterion for gusset plate design.

A recommended alternate procedure was introduced utilizing block shear theory. Previous work in beam connections provide a foundation to support the use of the block shear failure theory and should be investigated in further studies for the design of gusset plates. Preliminary findings show positive results predicting failure loads in the gusset plates with good accuracy.

Work done in this study has provided insight into the structural action of this connection which may lead to efficient design guides and procedures. Further research may provide the structural design profession with needed design tools that ultimately minimize assumptions and produce a more reliable and economical gusset connection.

APPENDIX

	Page
45° 1/8" Gusset Model	76
45° 3/8" Gusset Model	87
45° 1/8" Beam-Gusset Model	95
45° 3/8" Beam-Gusset Model	100
60° 1/8" Gusset Model	104
60° 3/8" Gusset Model	108
60° 1/8" Beam-Gusset Model	113
60° 3/8" Beam-Gusset Model	119
30° 1/8" Gusset Model	123
30° 3/8" Gusset Model	129
30° 1/8" Beam-Gusset Model	134
30° 3/8" Beam-Gusset Model	139

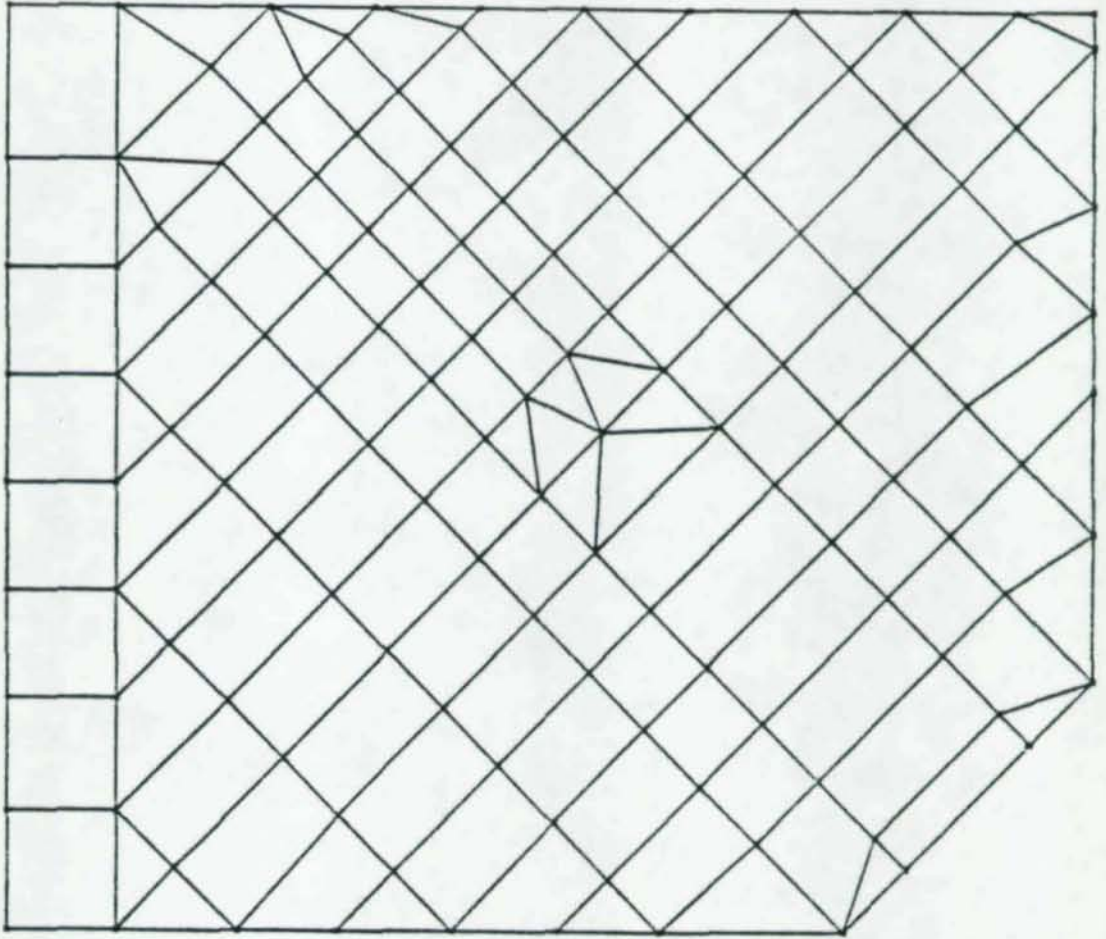


Figure A.1. Undistorted 45° Gusset Grid.

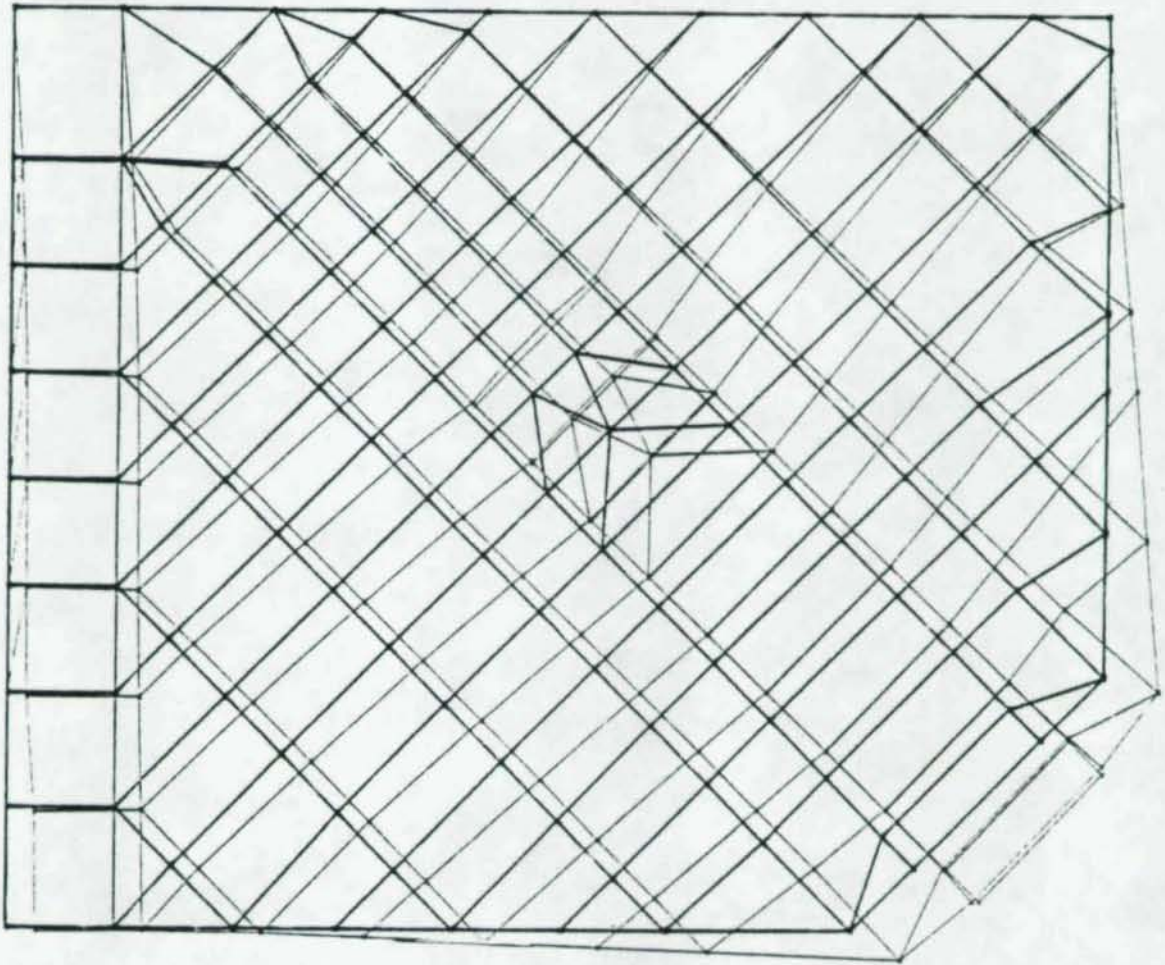


Figure A.2. 1/8" 45° Gusset Grid and Distorted Geometry.

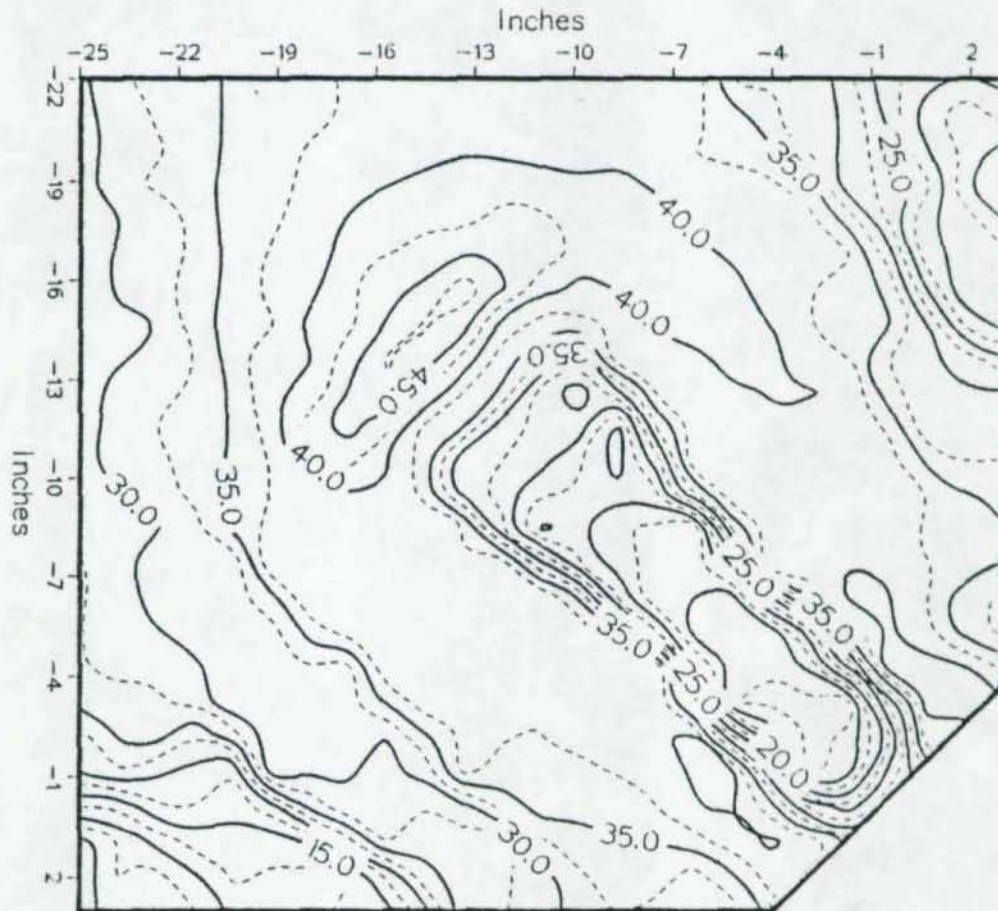


Figure A.3. Effective Stress Contour Plot 1/8" 45° Gusset, P = 150K.

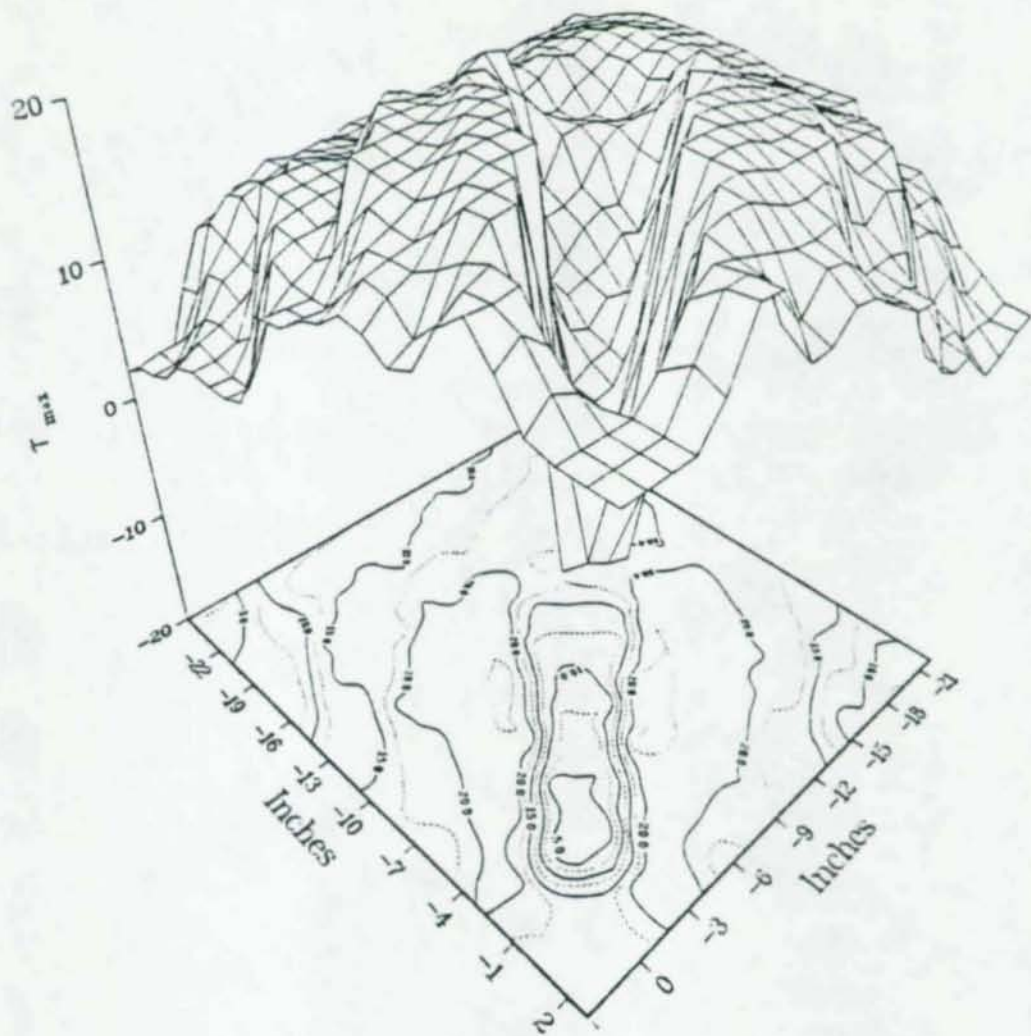


Figure A.4. Maximum Shear Surface and Contour Plot, $1/8''$ 45° Gusset, $P = 150K$.

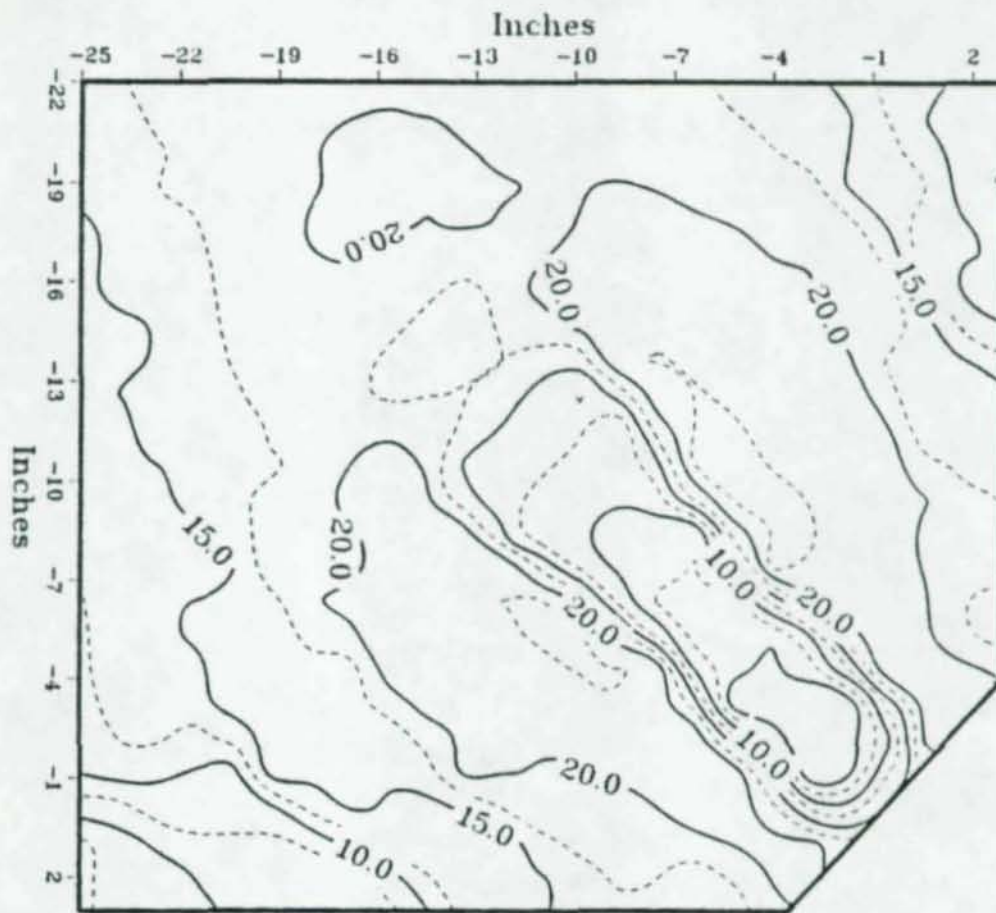


Figure A.5. Maximum Shear Contour Plot, 1/8" 45° Gusset, P = 150K.

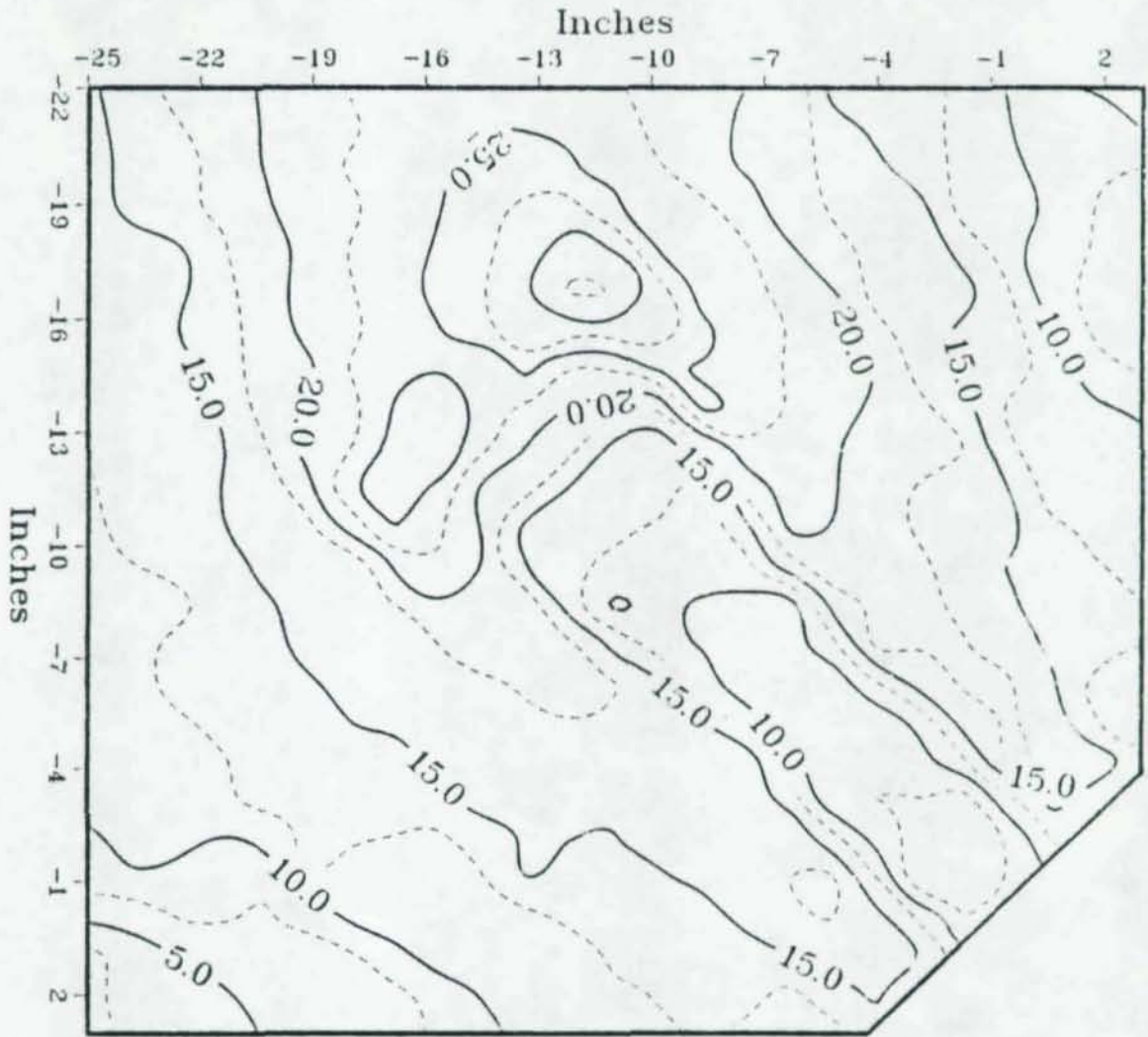


Figure A.6. Effective Stress Contour Plot, 1/8" 45° Gusset, P = 75K.

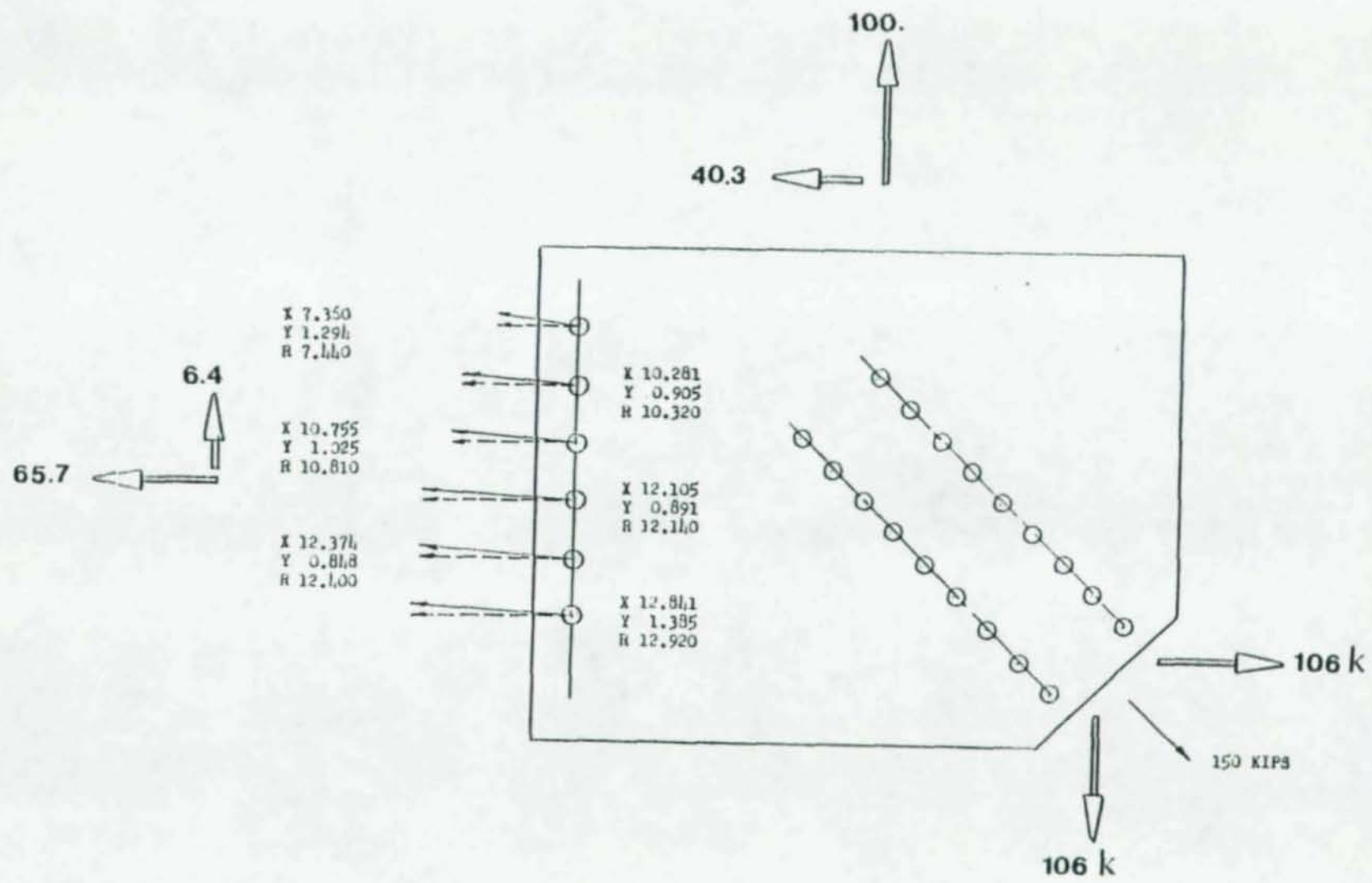
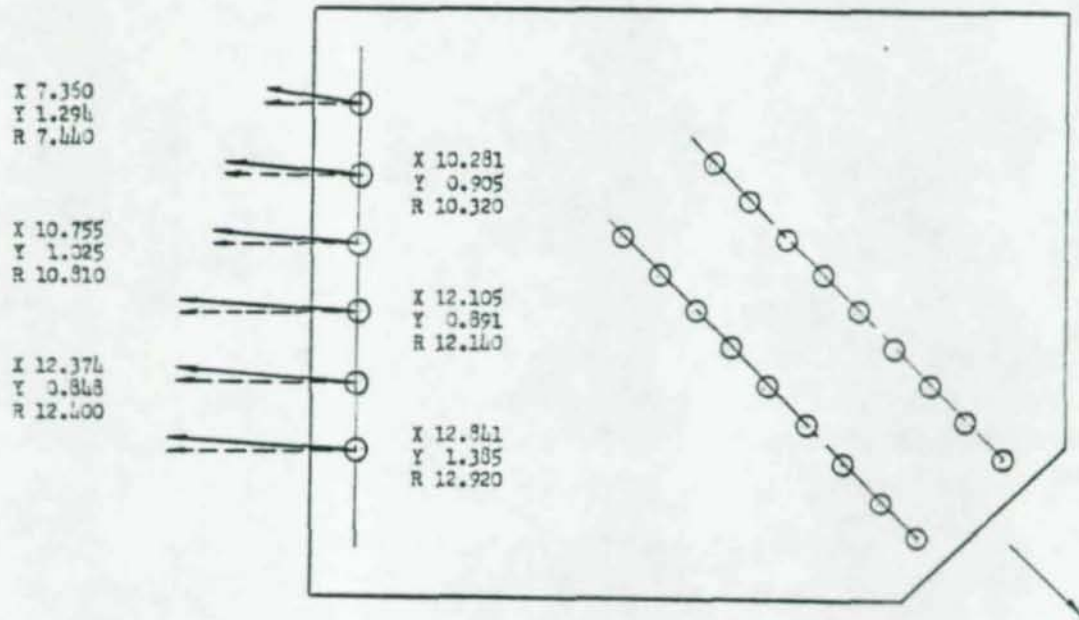
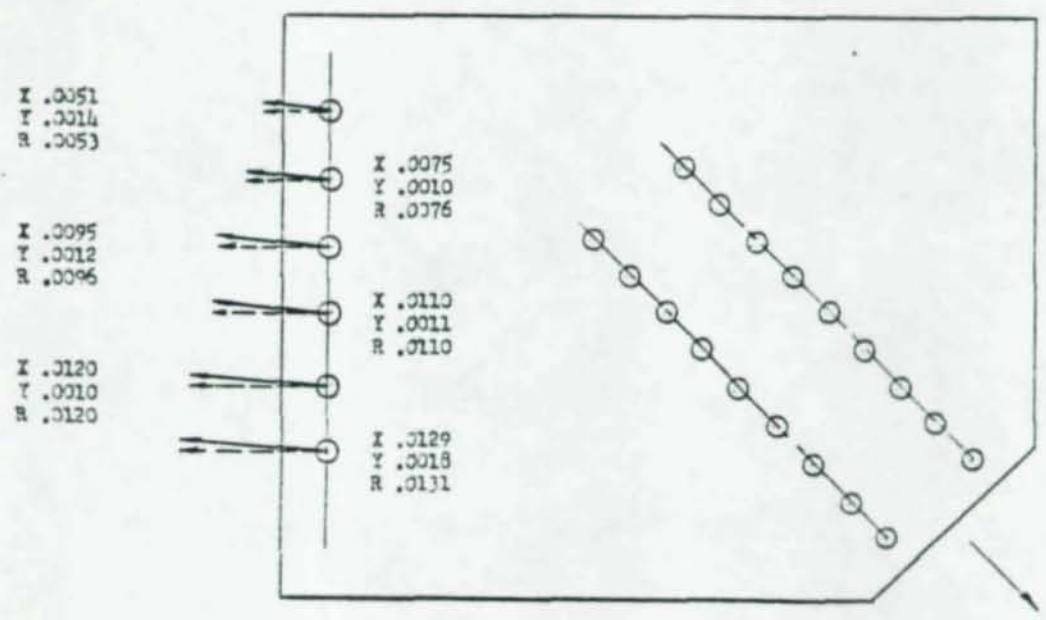


Figure A.7. Resultant Bolt Forces, 1/8" 45° Gusset, P = 150K.



1/8" Plate 45° Connection: Resultant Bolt Forces



1/8" Plate 45° Connection: Resultant Bolt Displacements

Figure A.8. Resultant Forces and Displacements, 1/8" 45° Gusset, P = 150K.

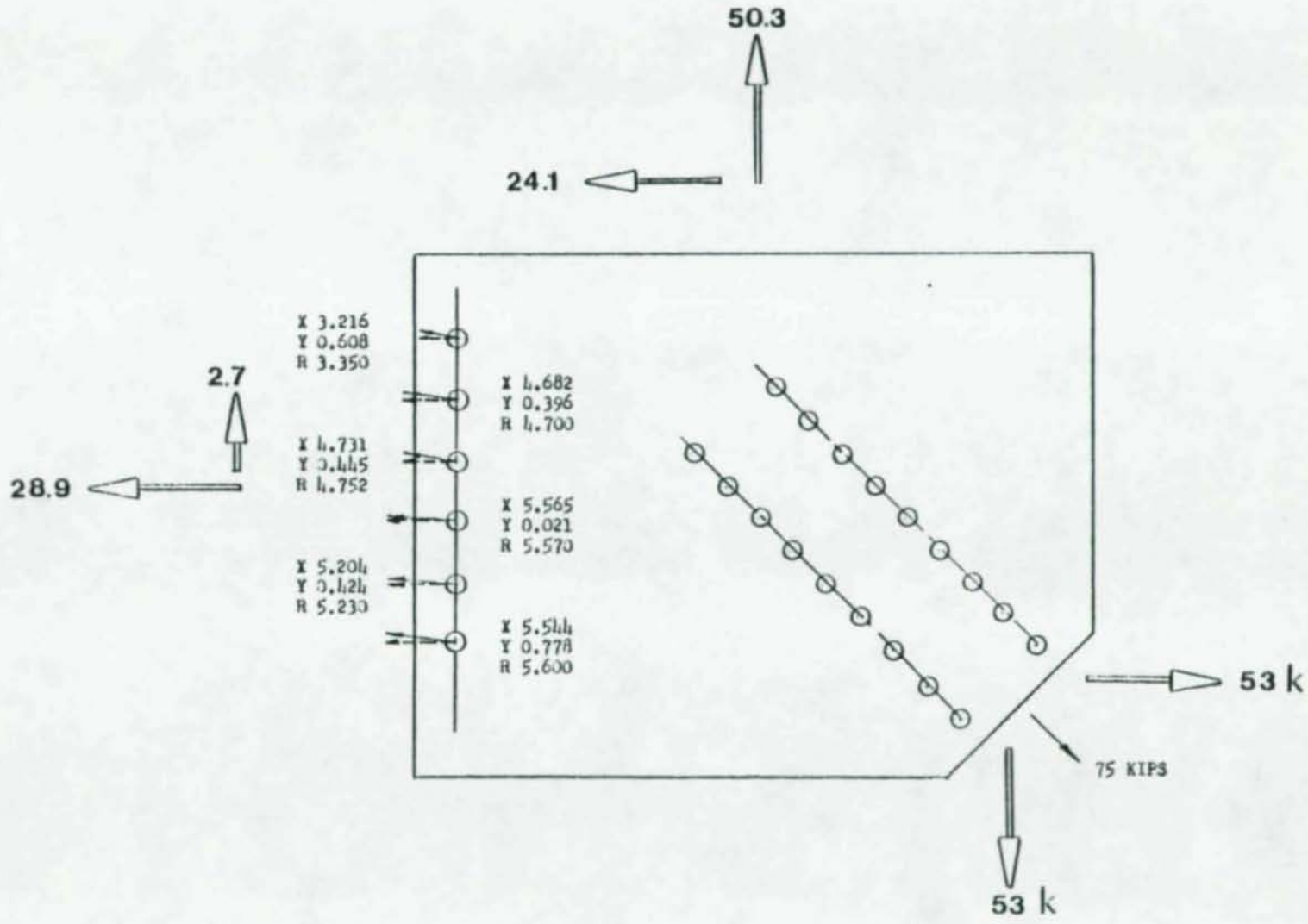
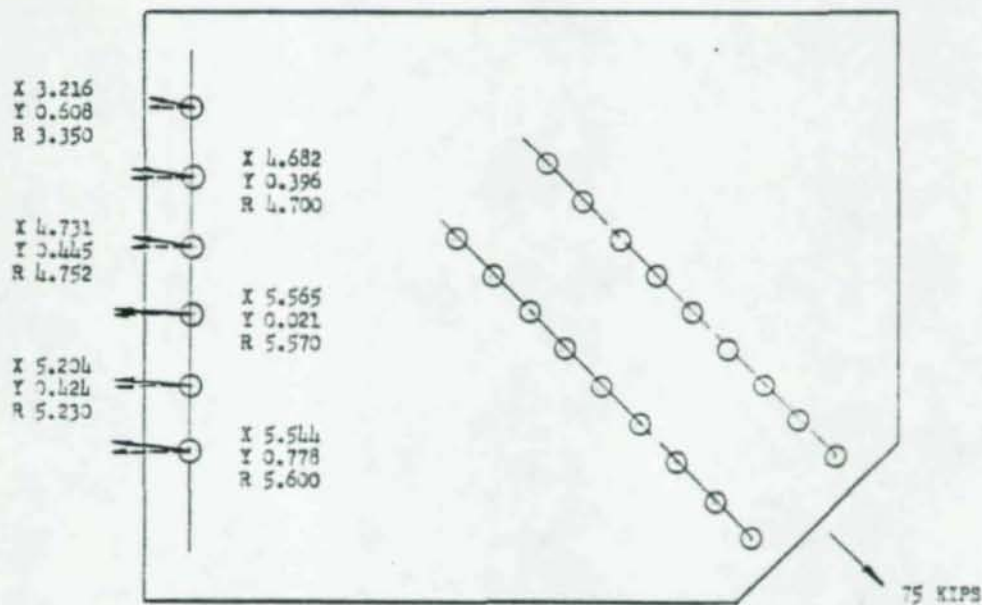
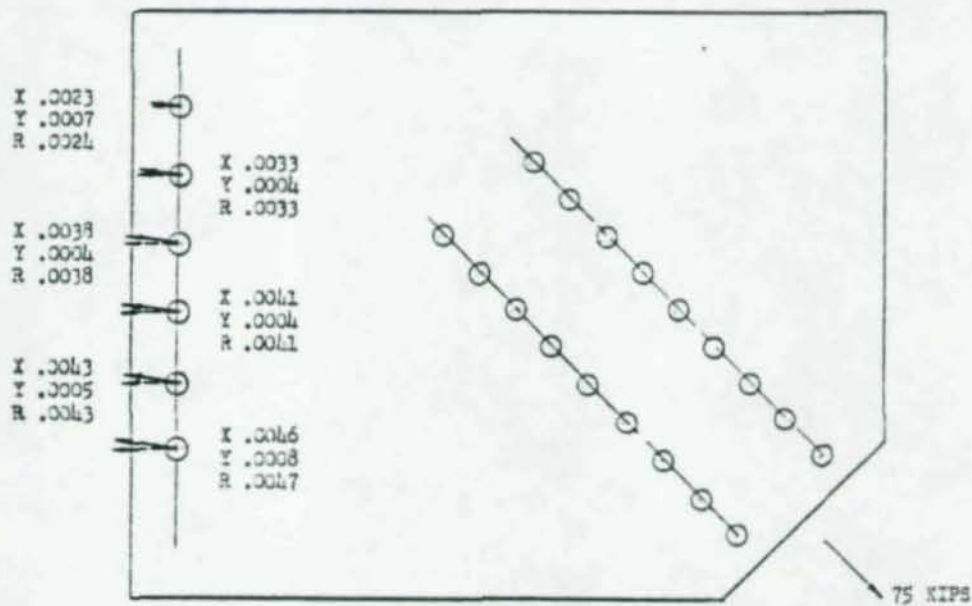


Figure A.9. Resultant Bolt Forces, 1/8" 45° Gusset, P = 75K.



1/8" Plate 45° Connections: Resultant Bolt Forces



1/8" Plate 45° Connections: Resultant Bolt Displacements

Figure A.10. Resultant Bolt Forces and Displacements, 1/8" 45° Gusset, P = 75K.

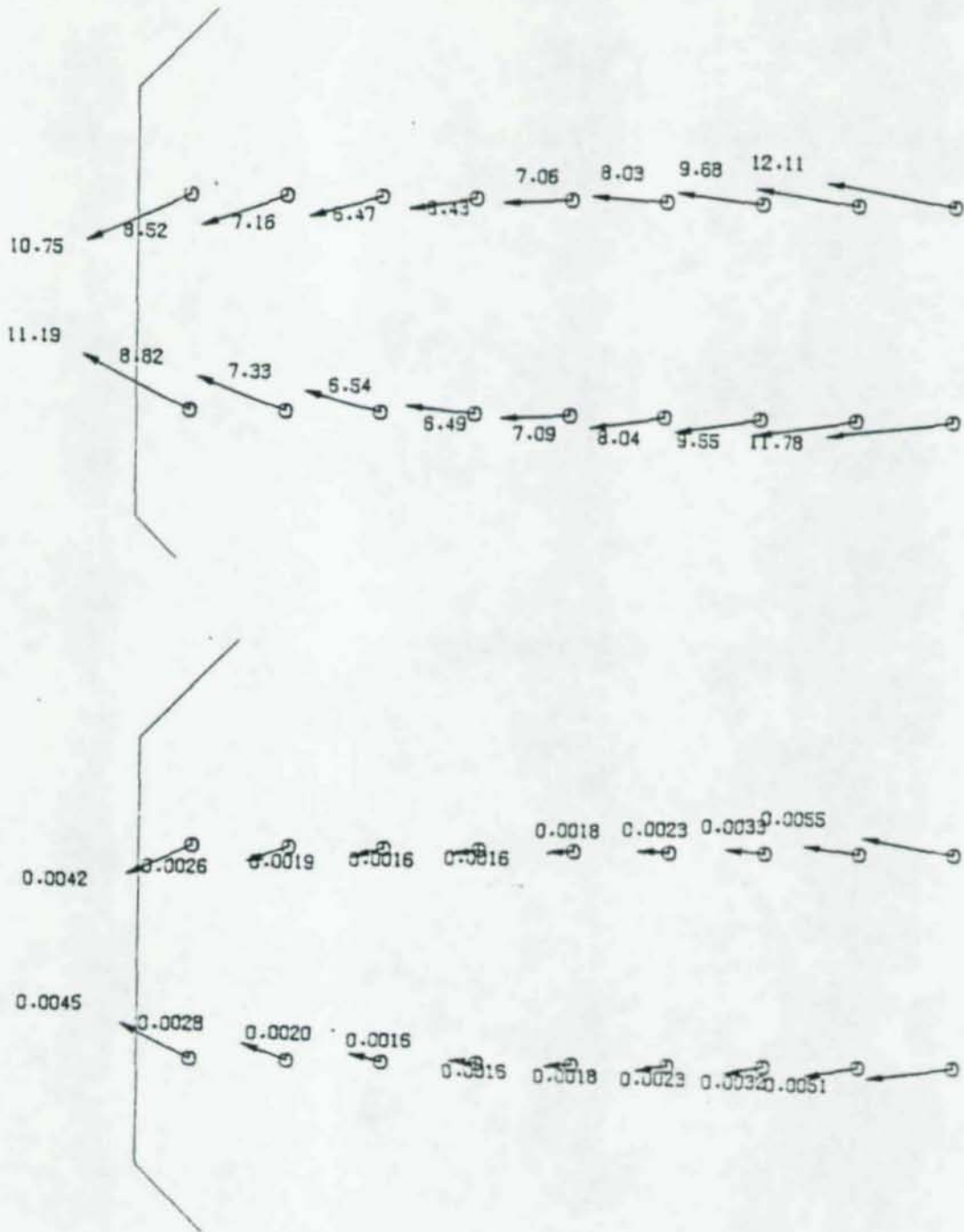


Figure A.11. Resultant Forces and Displacements, 1/8" 45° Gusset Splice Plate, P = 150K.

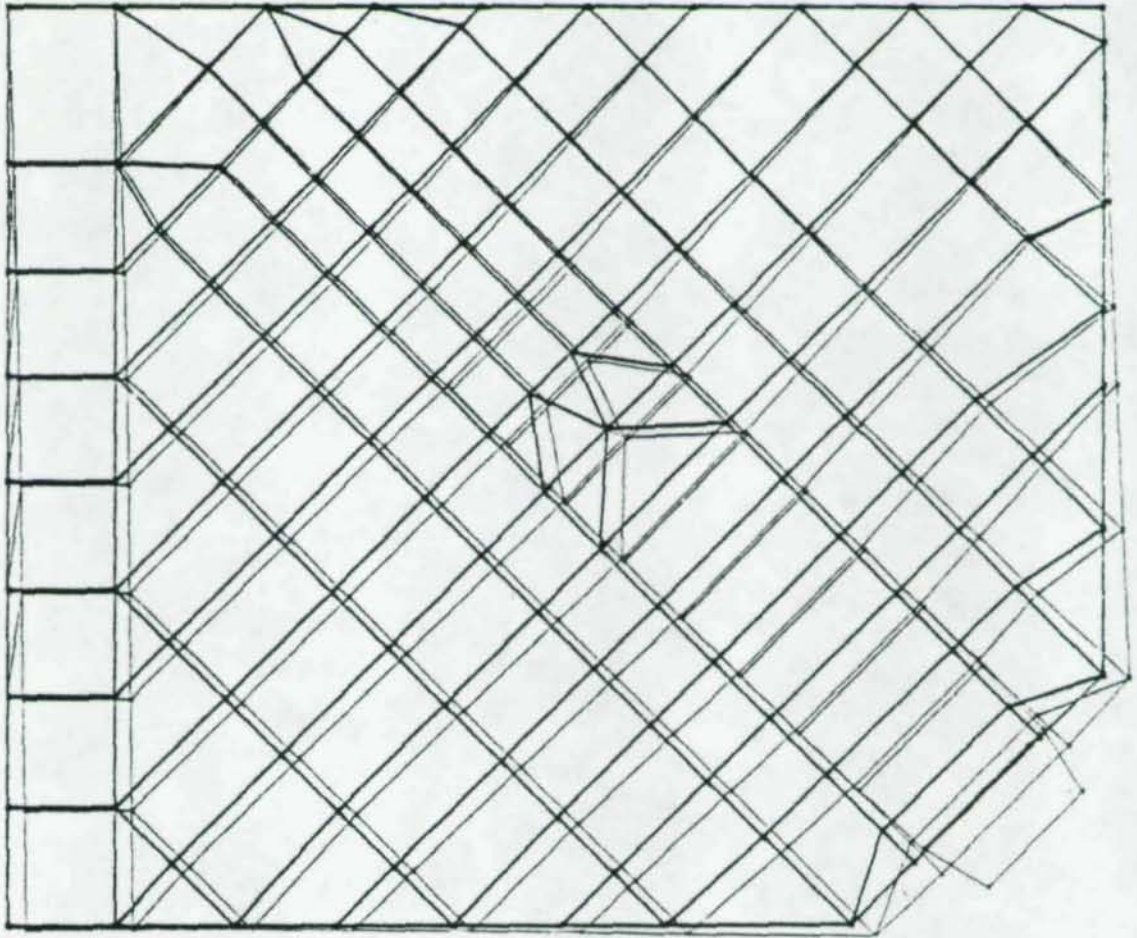


Figure A.12. 3/8" 45° Gusset Grid and Distorted Geometry.

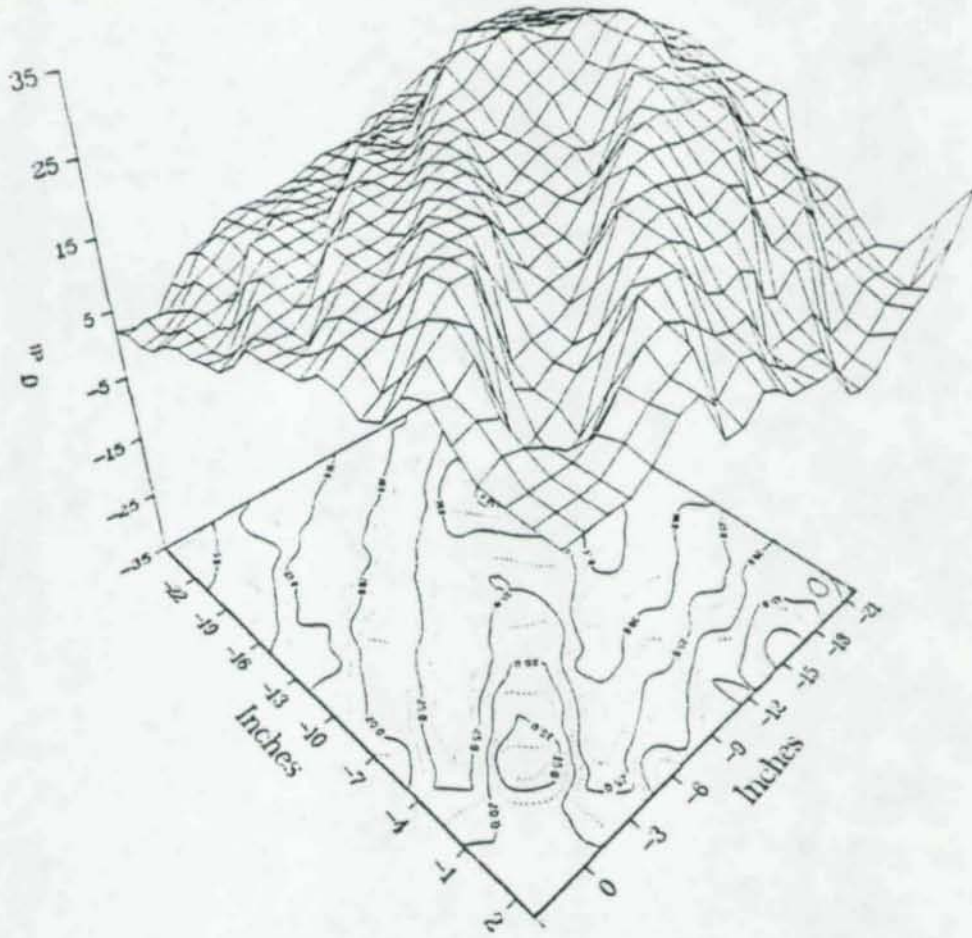


Figure A.13. 3/8" 45° Gusset Effective Stress Surface Contour Plot,
P = 300K.

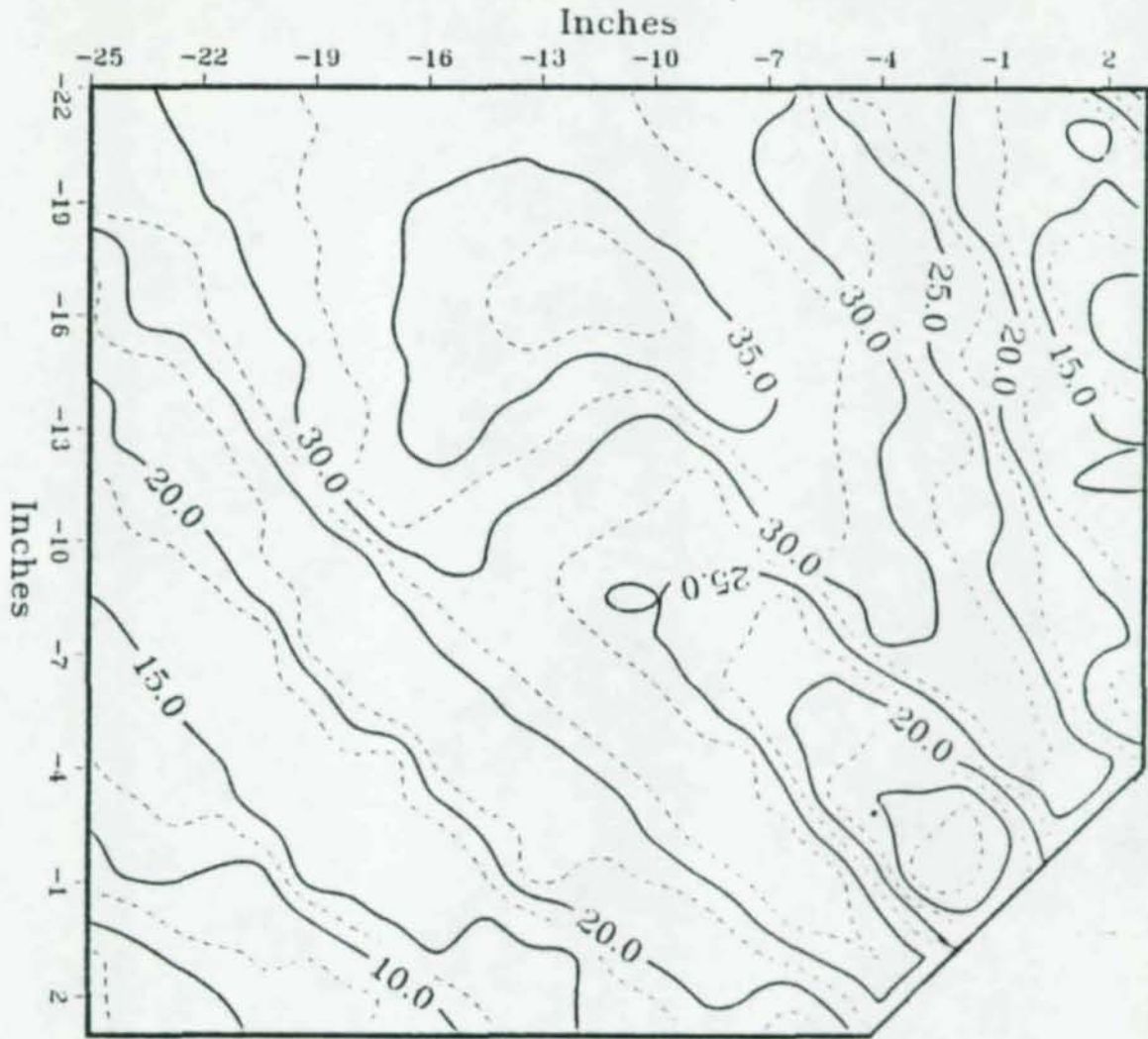


Figure A.14. 3/8" 45° Gusset Effective Stress Contour Plot, P = 300K.

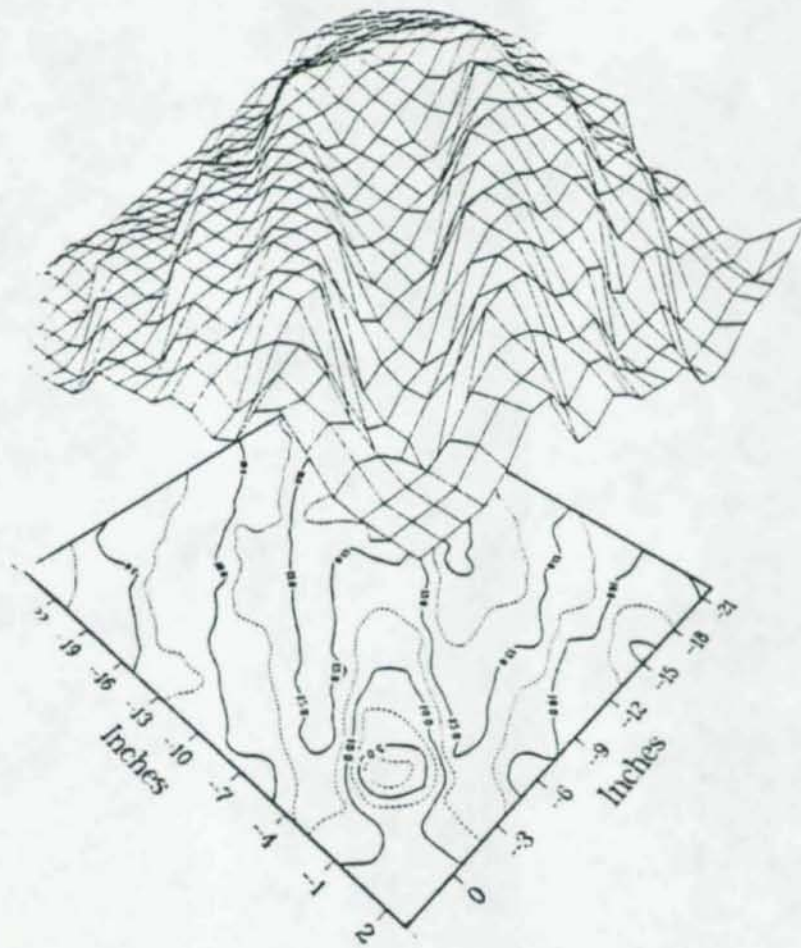


Figure A.15. 3/8" 45° Gusset Maximum Shear Stress Surface Contour Plot, P = 300K.

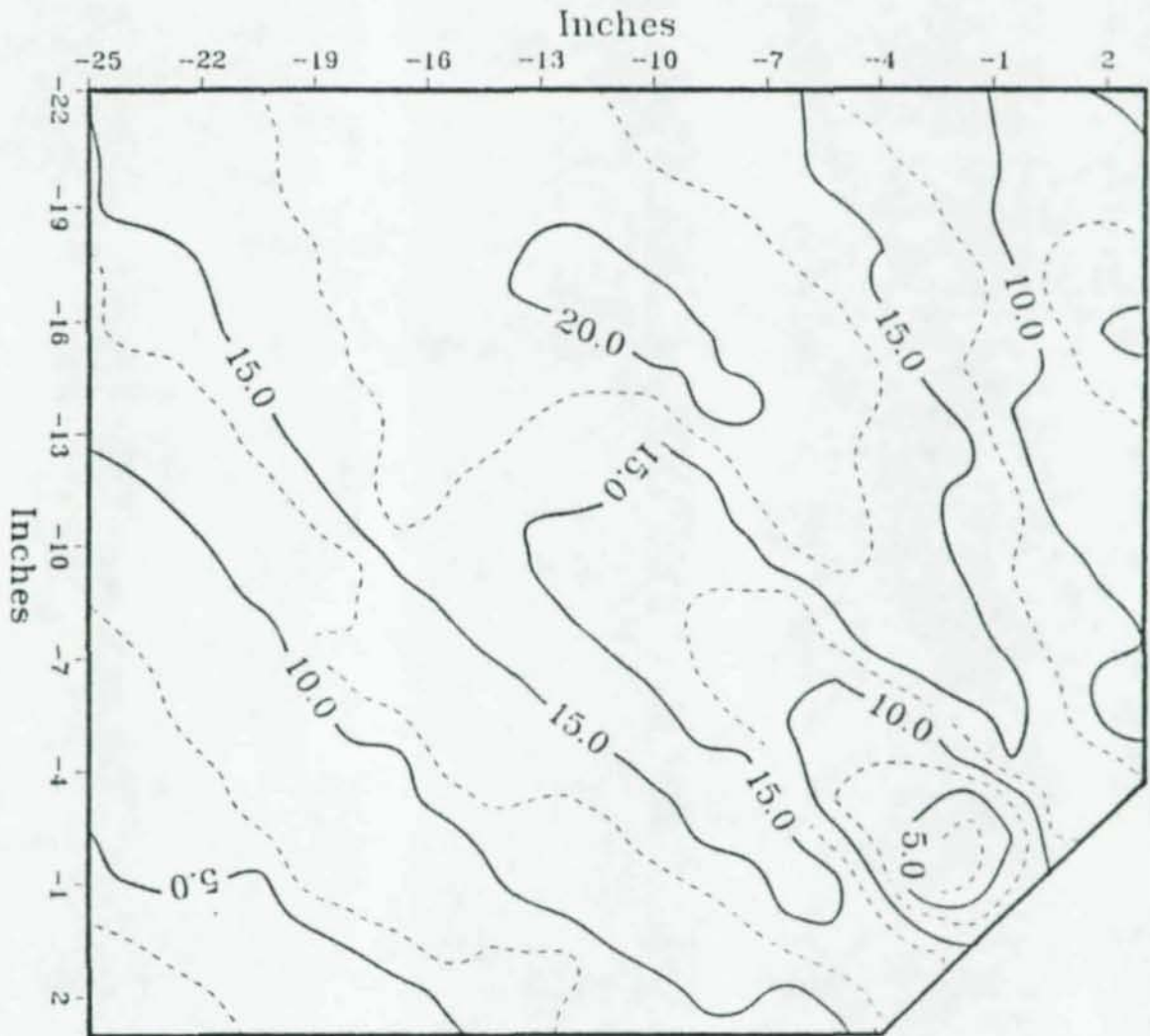


Figure A.16. 3/8" 45° Gusset Maximum Shear Stress Contour Plot,
P = 300K.

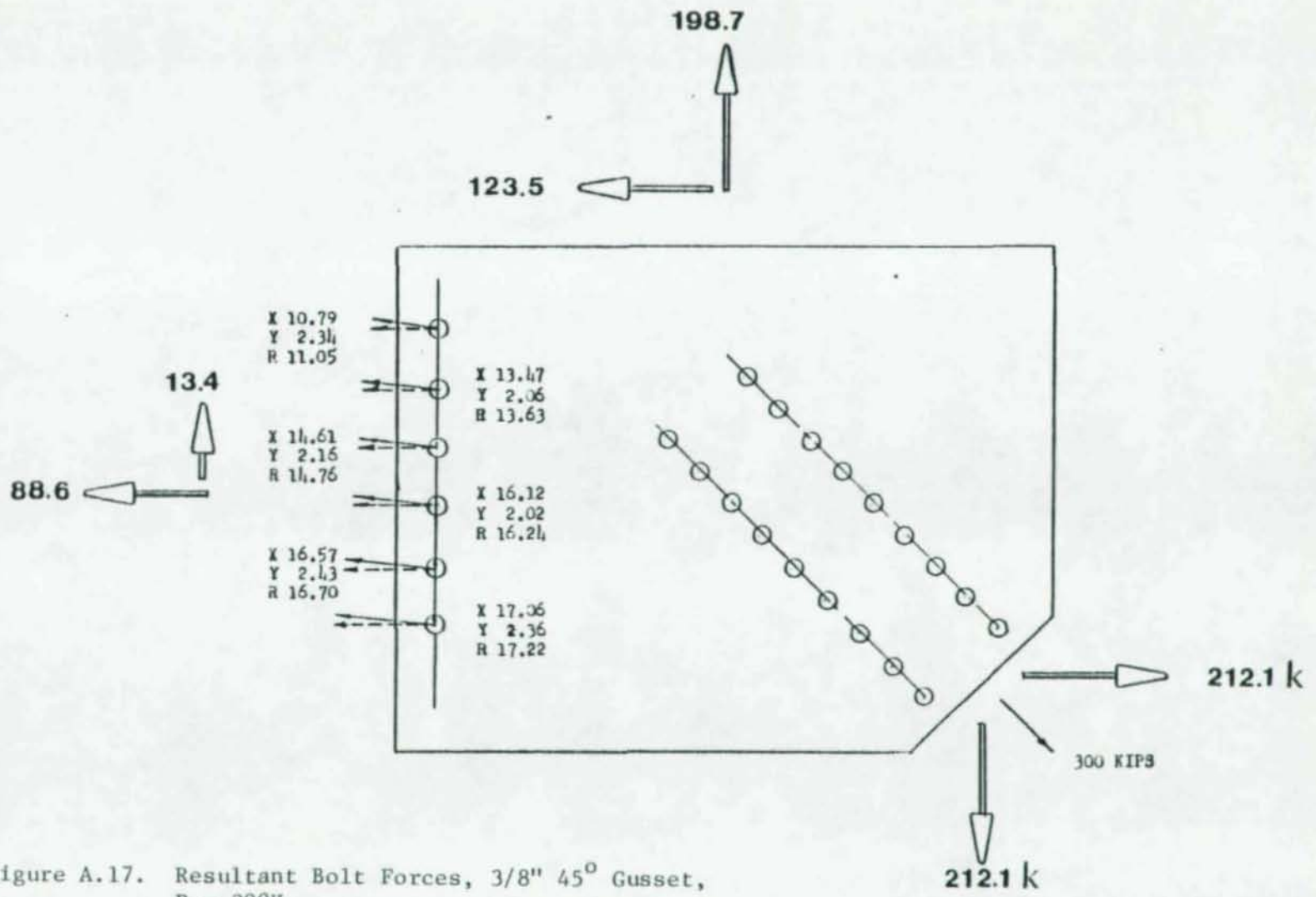
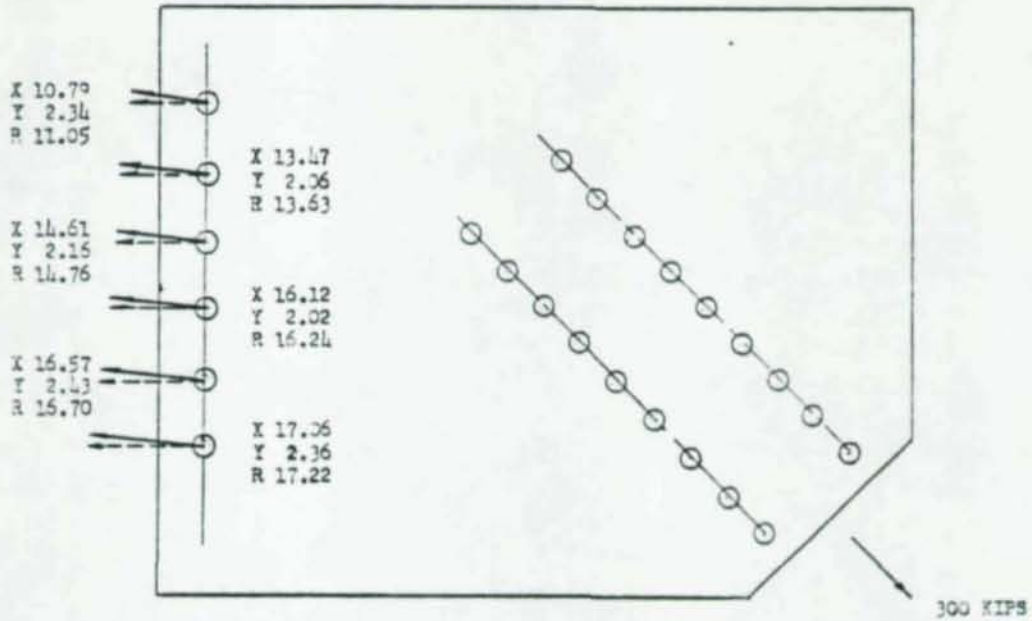
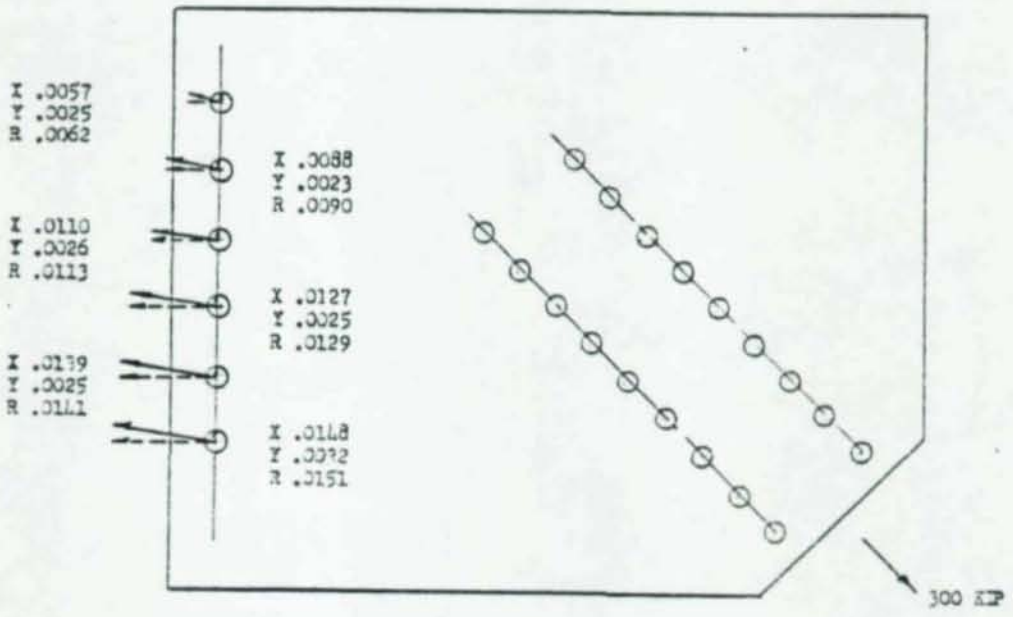


Figure A.17. Resultant Bolt Forces, 3/8" 45° Gusset, P = 300K.



3/8" Plate L5° Connection: Resultant Bolt Forces



3/8" Plate L5° Connection: Resultant Bolt Displacements

Figure A.18. Resultant Force and Displacements, 3/8" 45° Gusset, P = 300K.

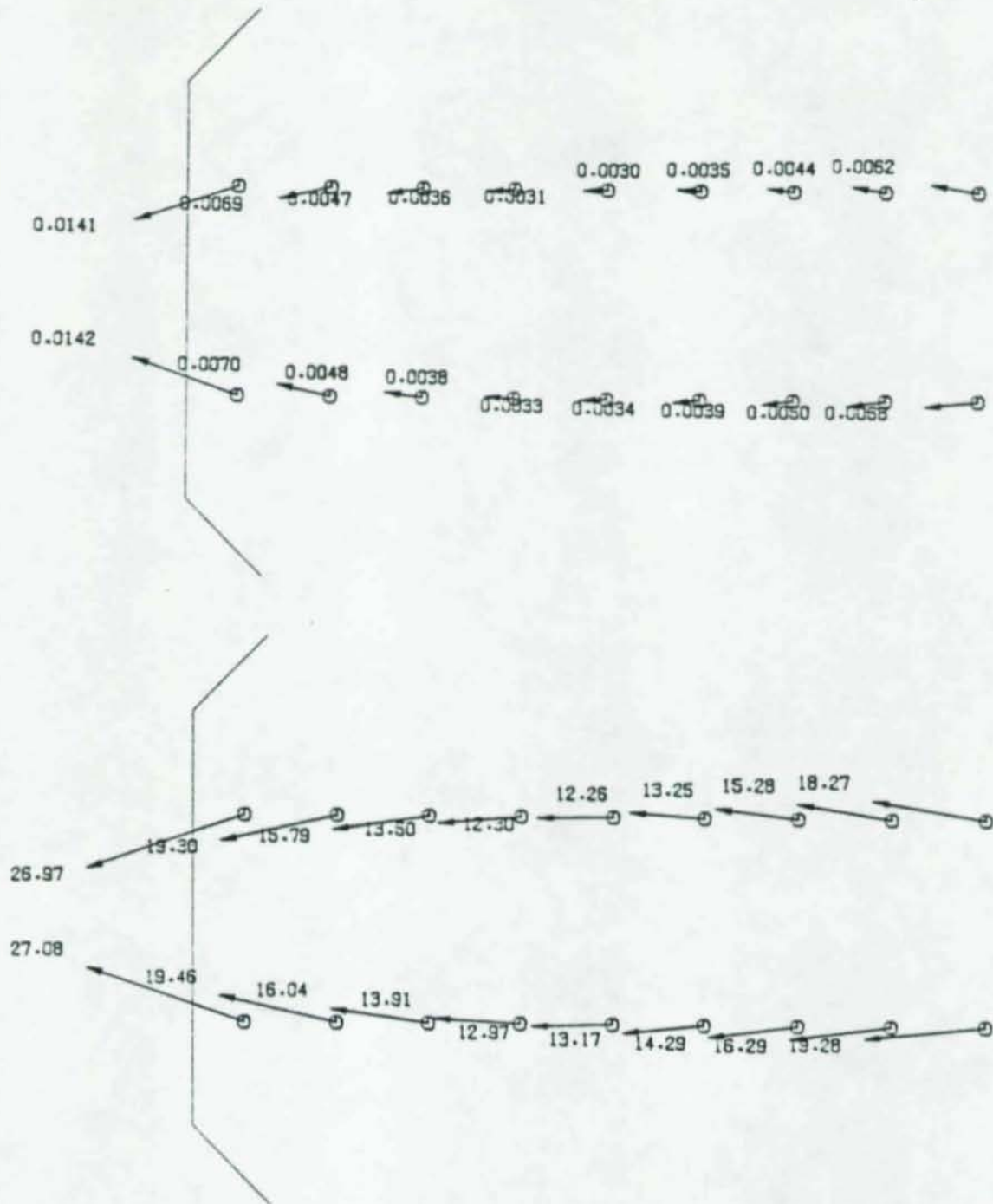


Figure A.19. Resultant Forces and Displacements 3/8" 45° Gusset Splice Plate, P = 300K.

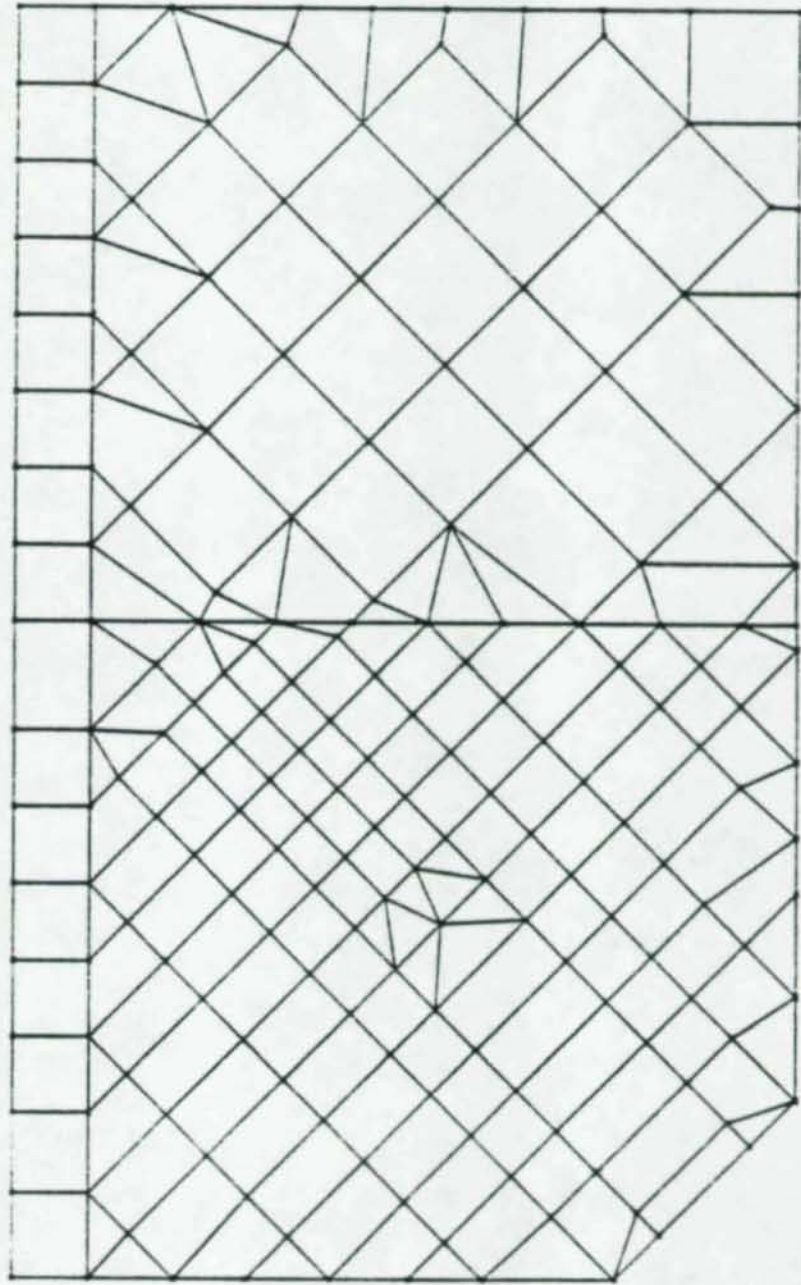


Figure A.20. 45° Beam-Gusset Undistorted Grid.

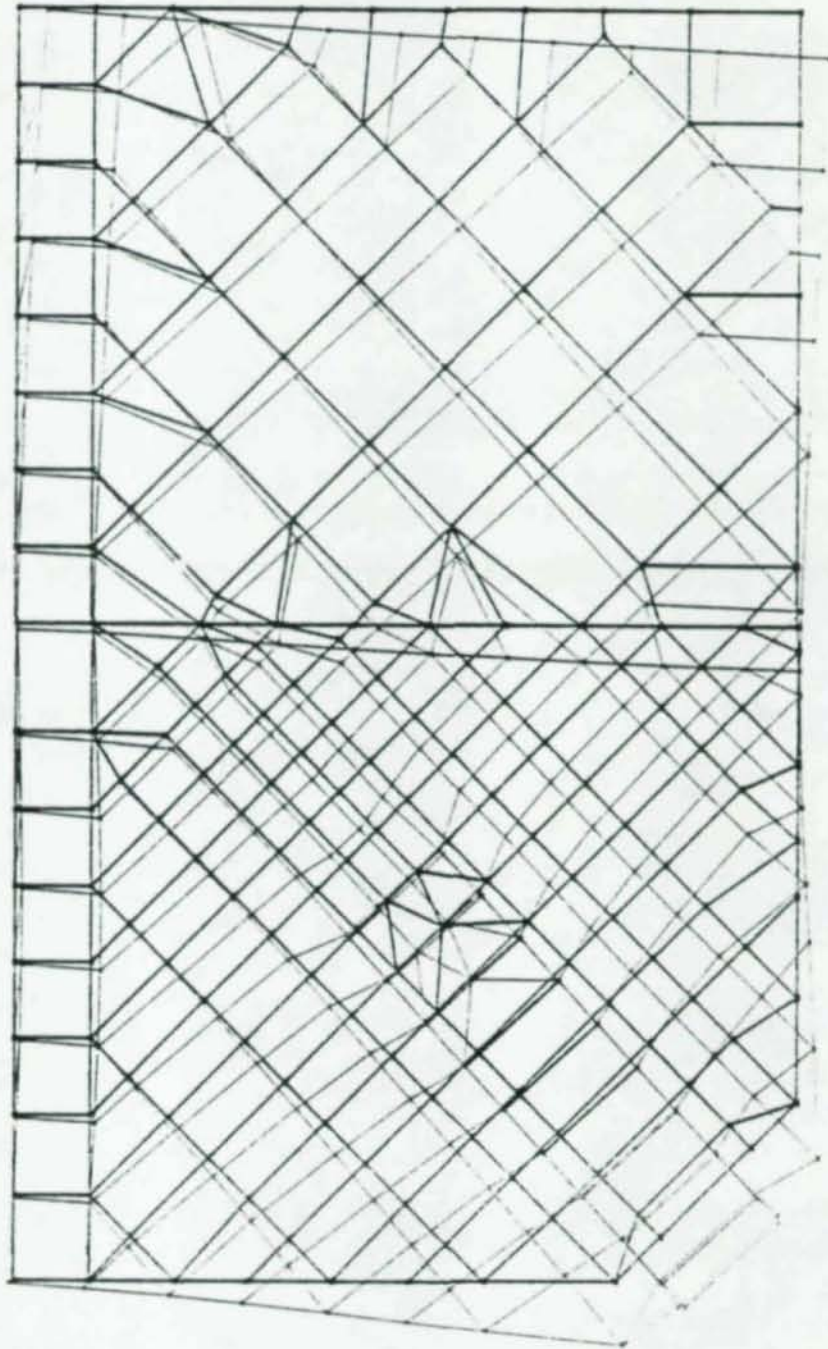


Figure A.21. 1/8" 45° Beam-Gusset Grid and Distorted Geometry.

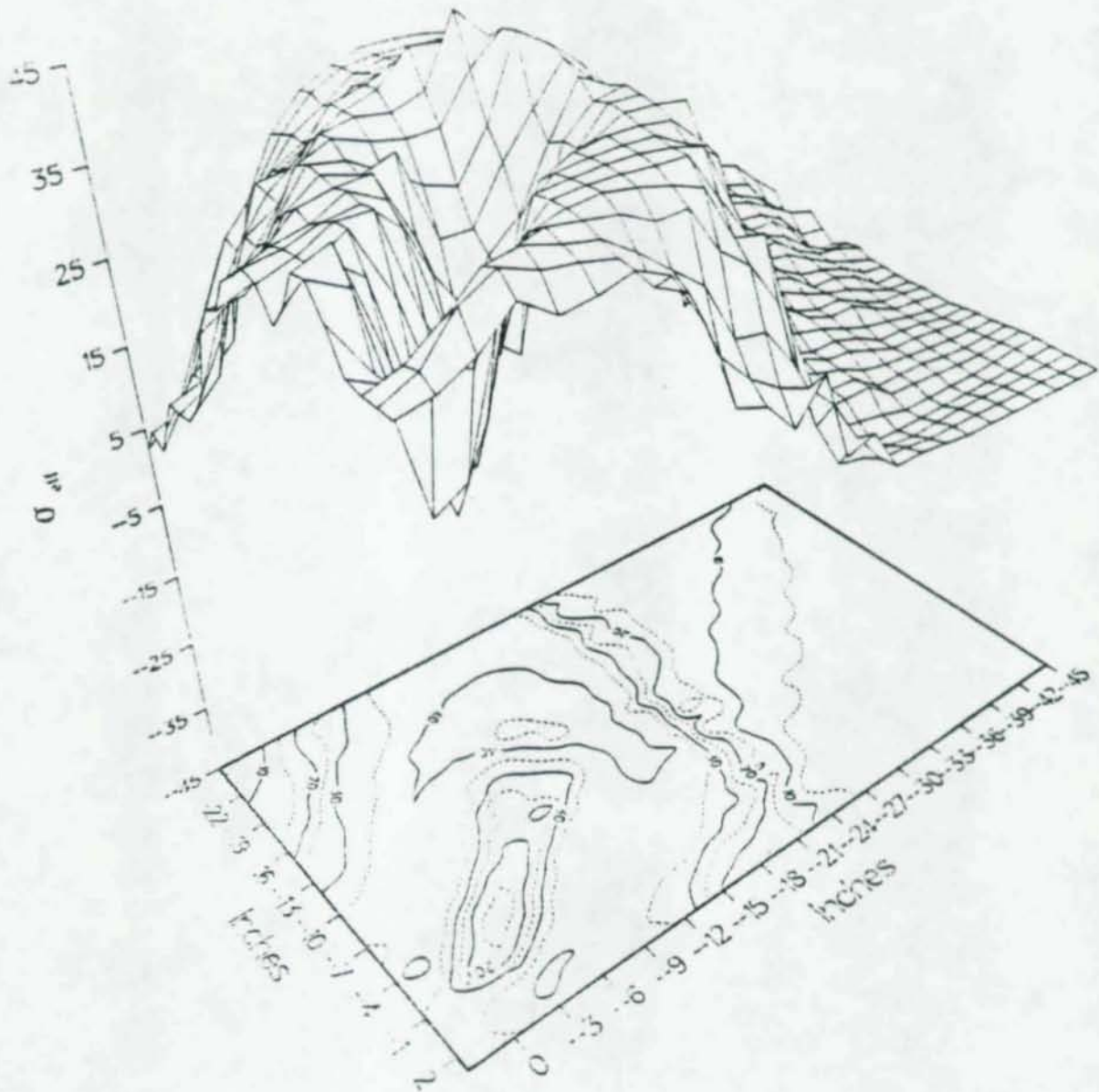


Figure A.22. 1/8" 45° Beam-Gusset Effective Stress Surface Contour Plot, P = 150K.

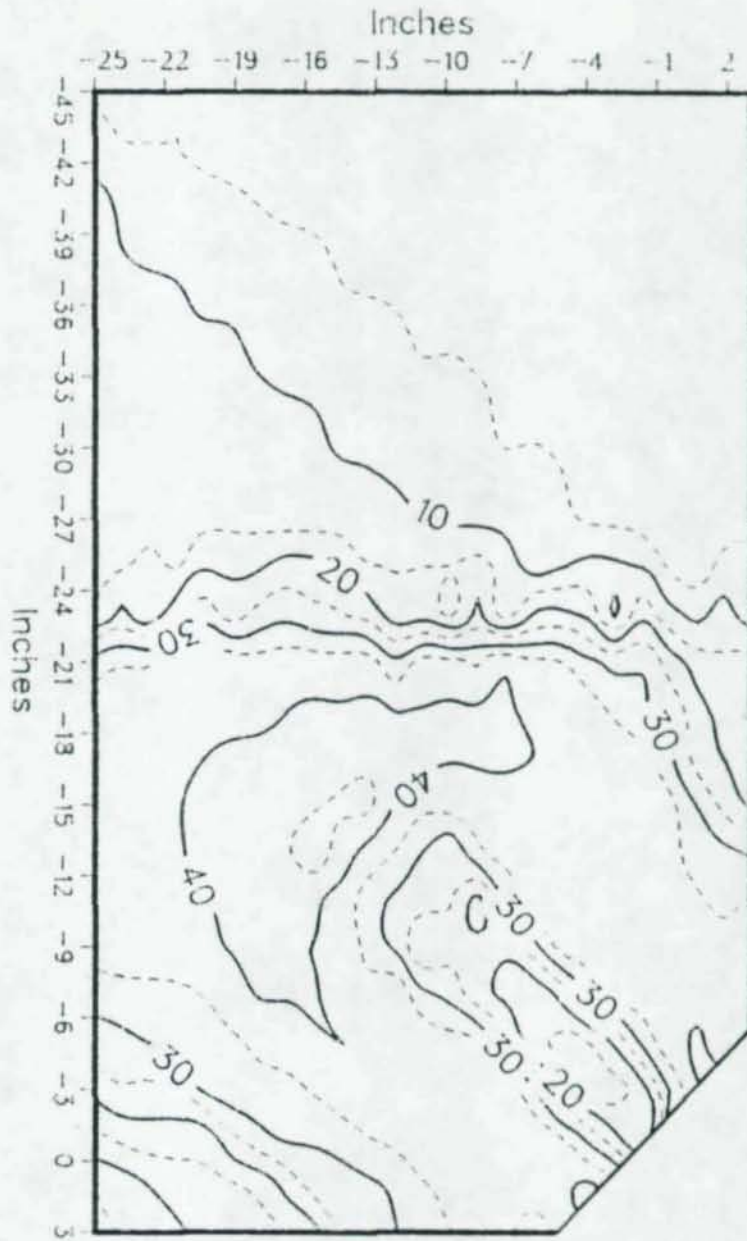


Figure A.23. Effective Stress Contour Plot, 1/8" 45° Beam-Gusset, P = 150K.

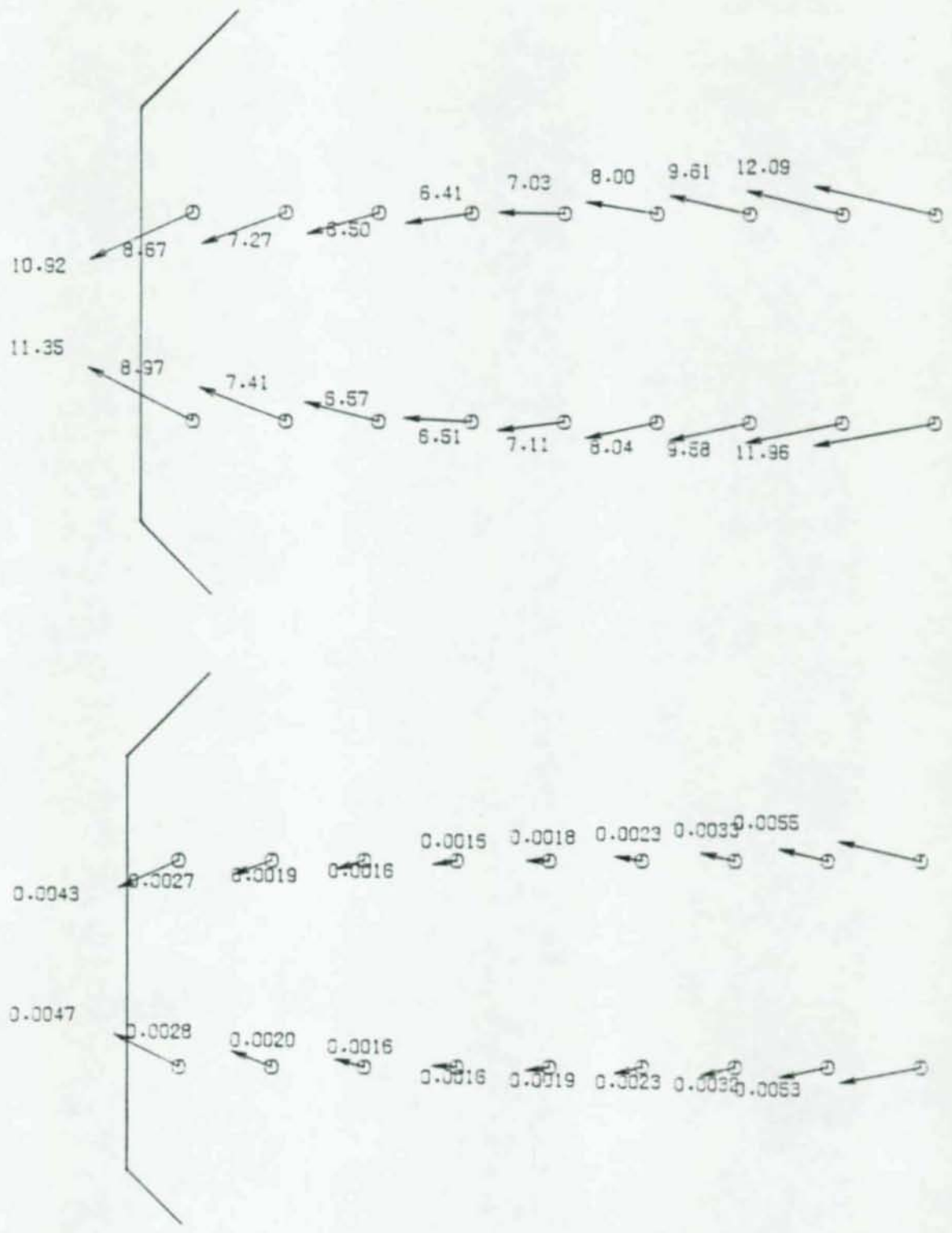


Figure A.24. Resultant Forces and Displacements 1/8" 45° Beam-Gusset, P = 150K.

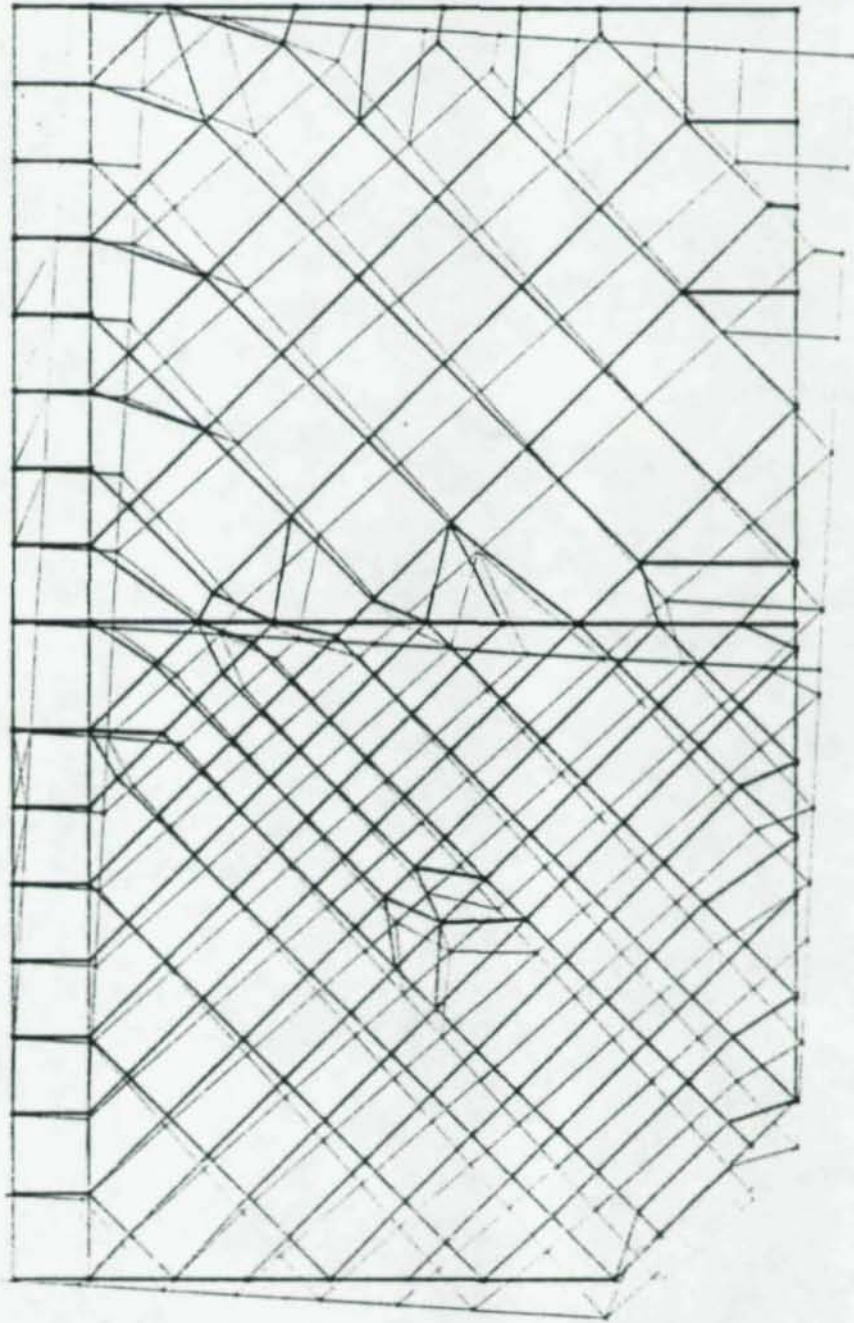


Figure A.25. $3/8''$ 45° Beam-Gusset Grid and Distorted Shape.

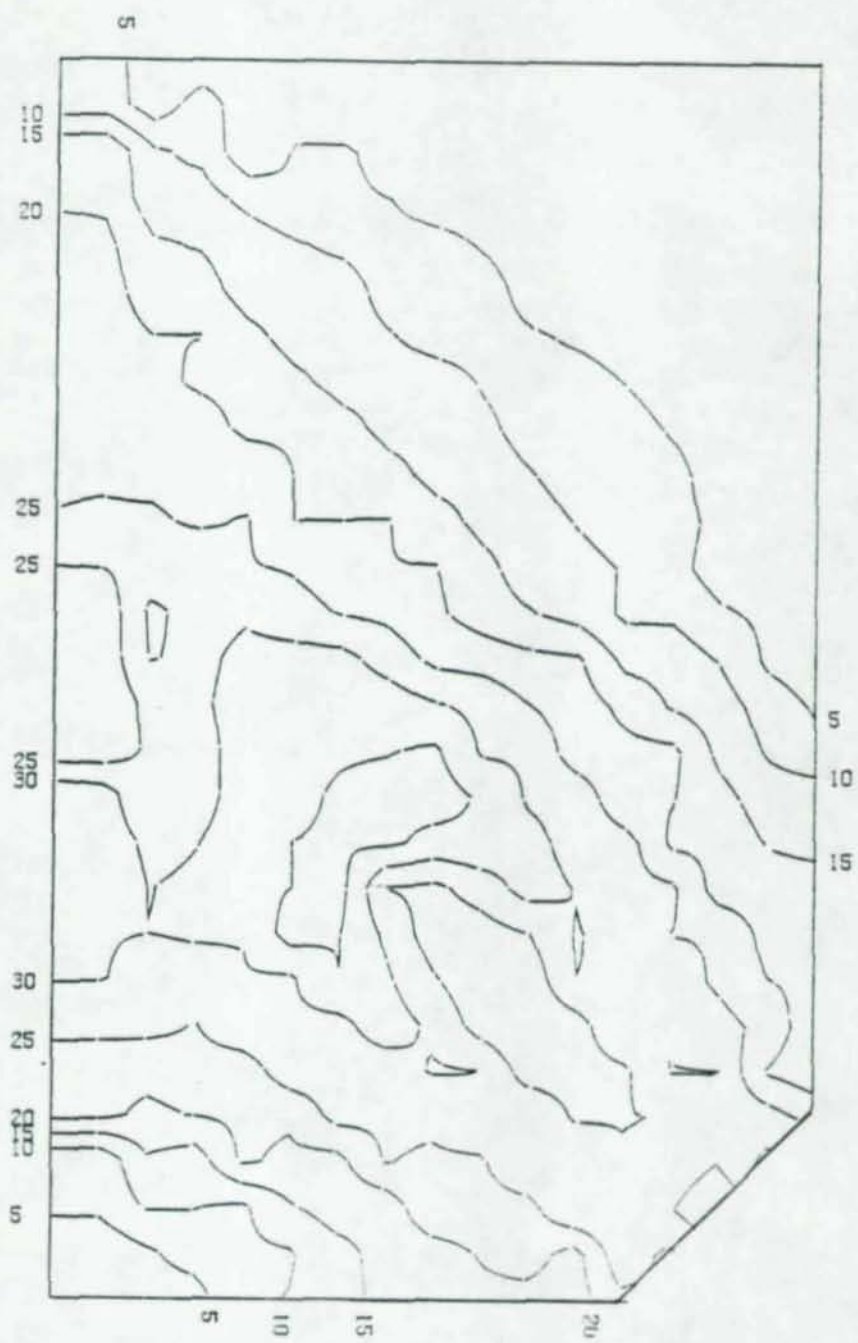


Figure A.26. Effective Stress Contour Plot, 3/8" 45° Beam-Gusset, P = 300K.

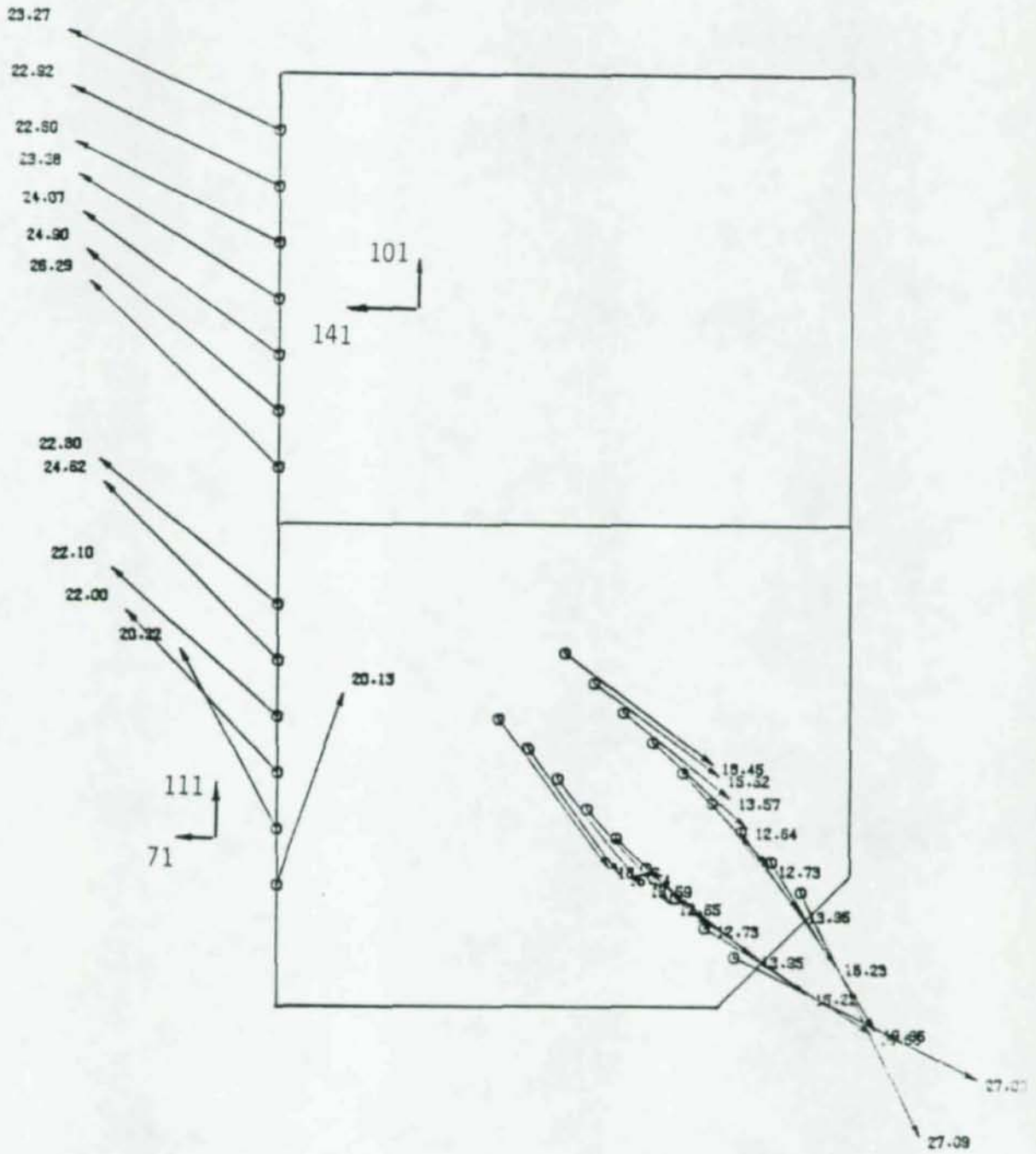


Figure A.27. Resultant Forces 3/8" 45° Beam-Gusset, P = 300K.

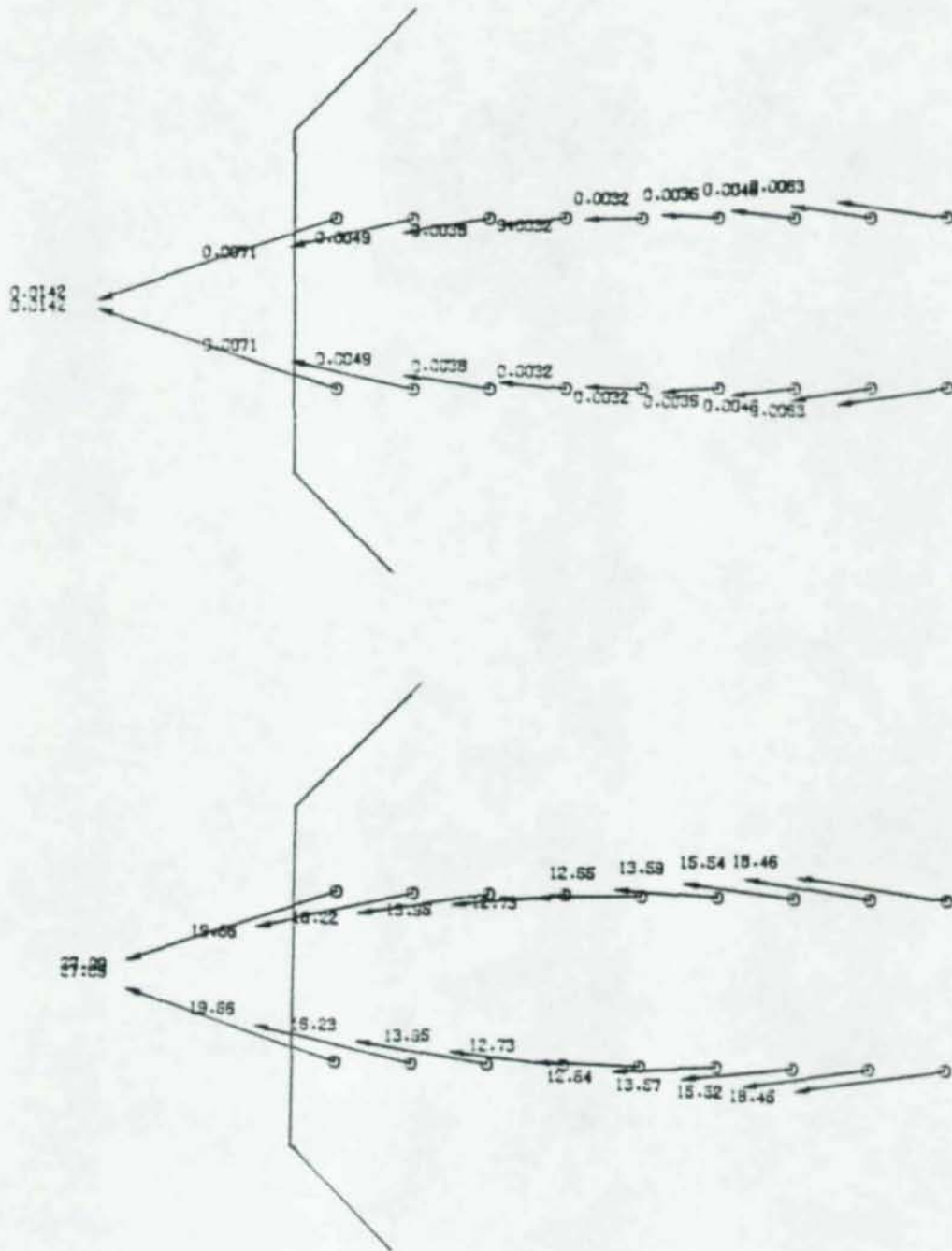


Figure A.28. Resultant Forces and Displacements 3/8" 45° Beam-Gusset Splice Plate, P = 300K.

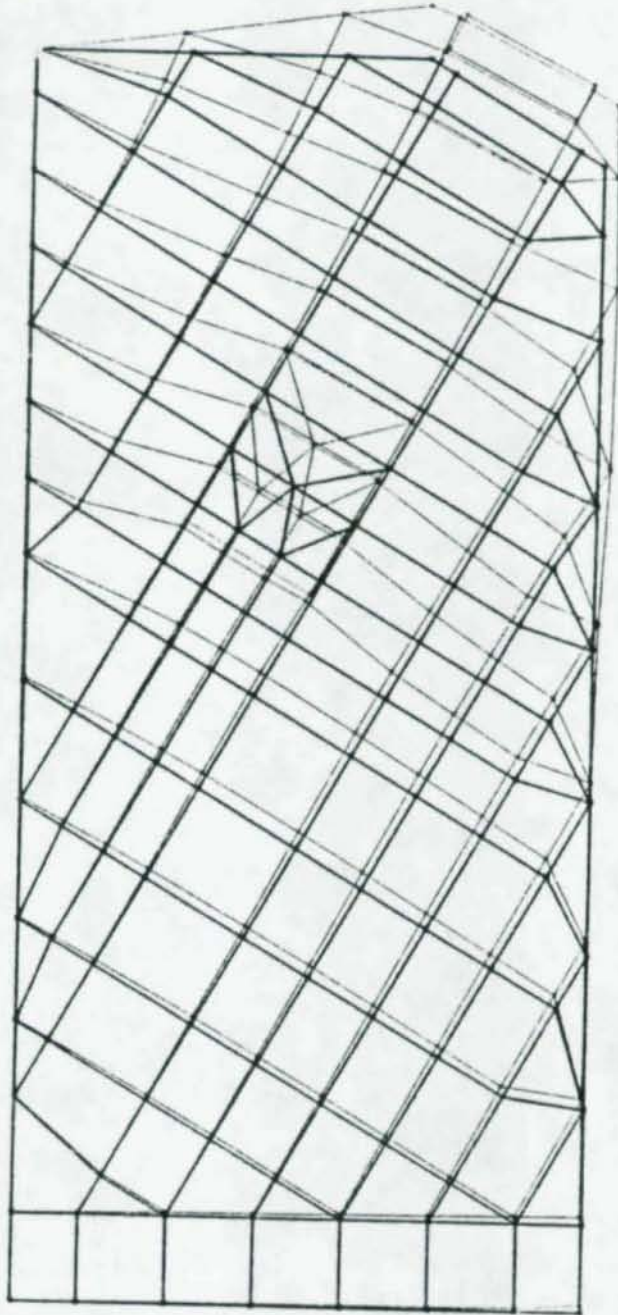


Figure A.29. 1/8" 60° Gusset Grid and Distorted Geometry.

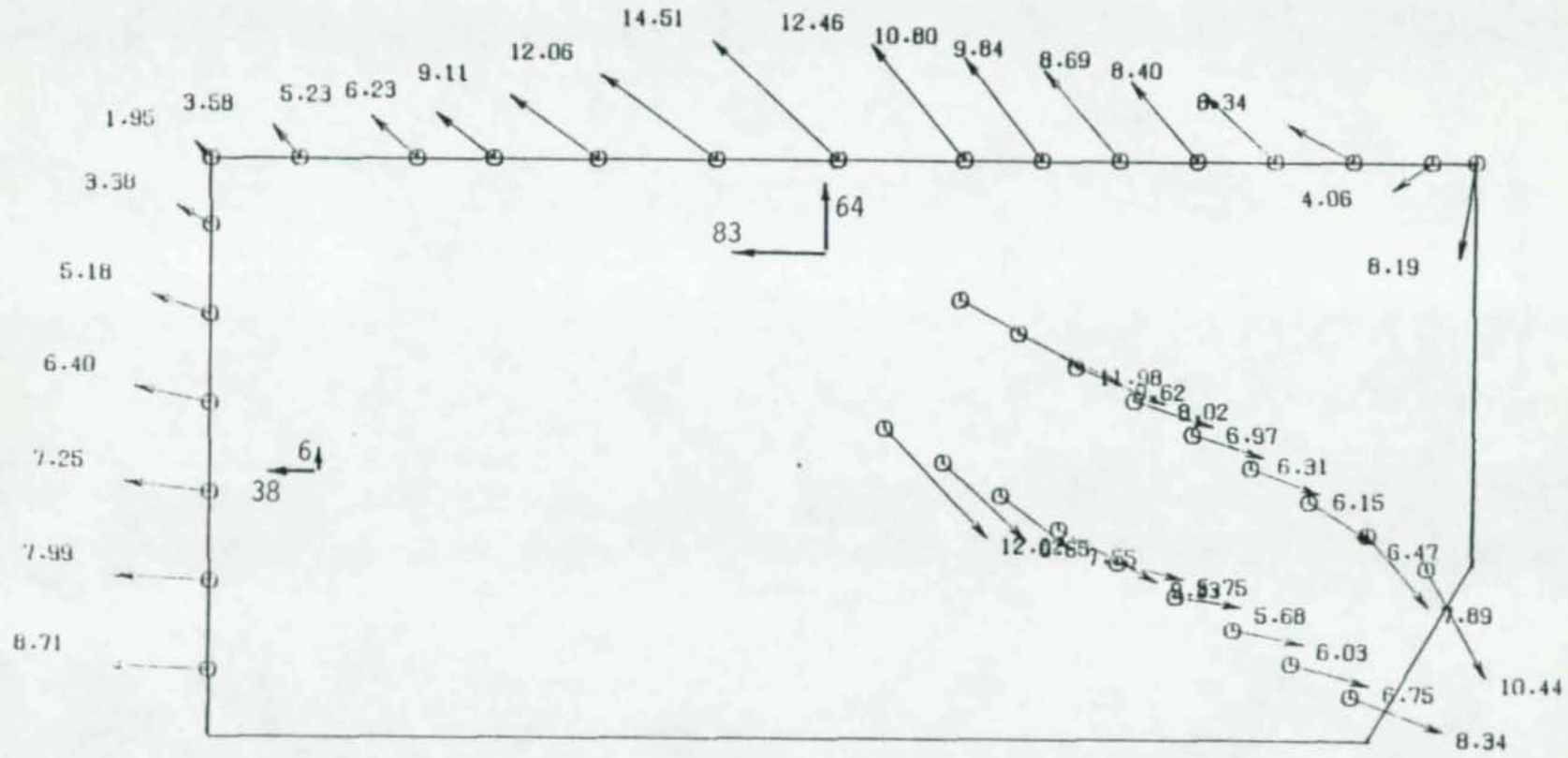


Figure A.30. Resultant Forces, 60° 1/8" Gusset, P = 140K.

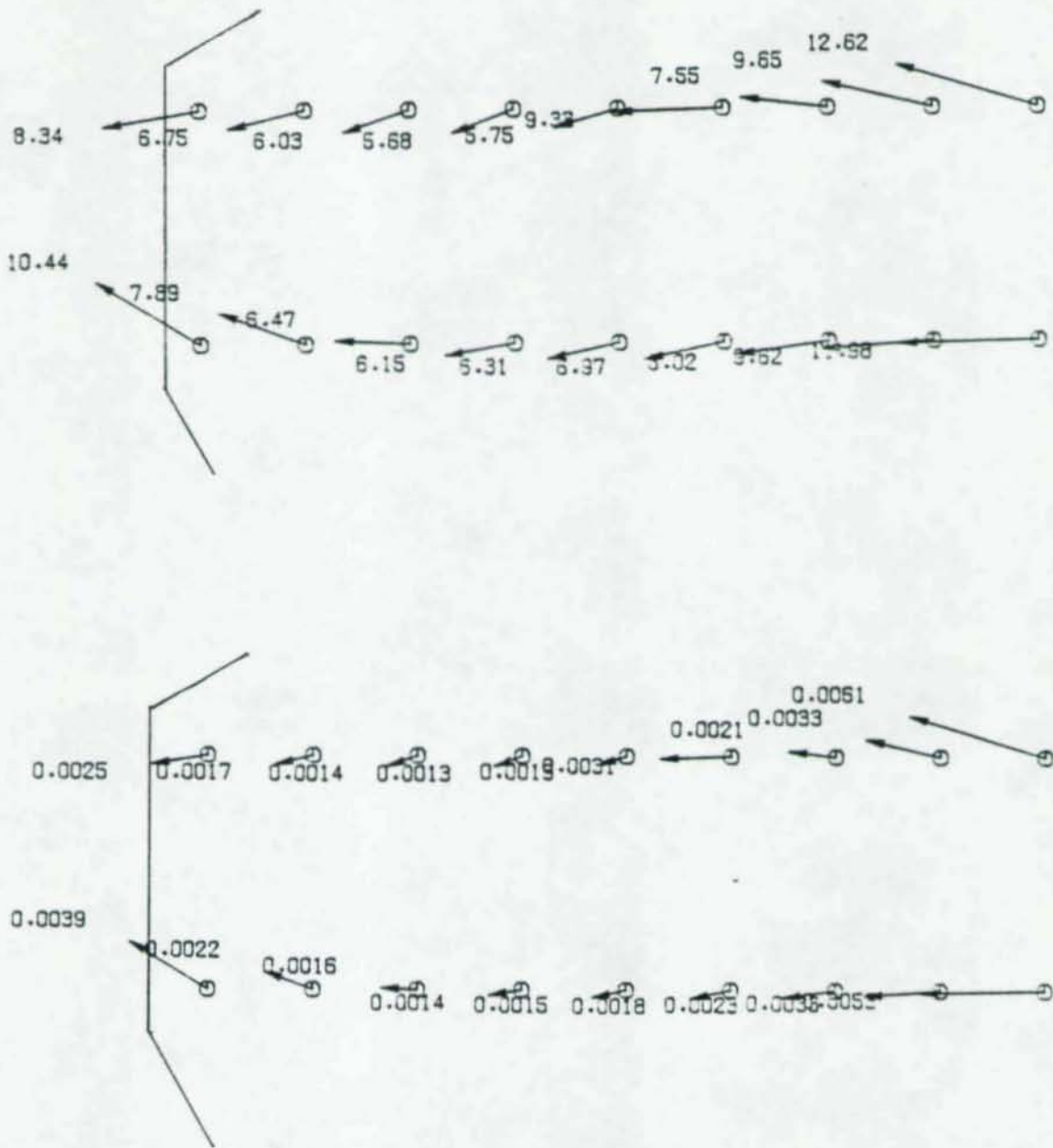


Figure A.32. Resultant Forces and Displacements 60° 1/8" Gusset Splice Plate, P = 140K.

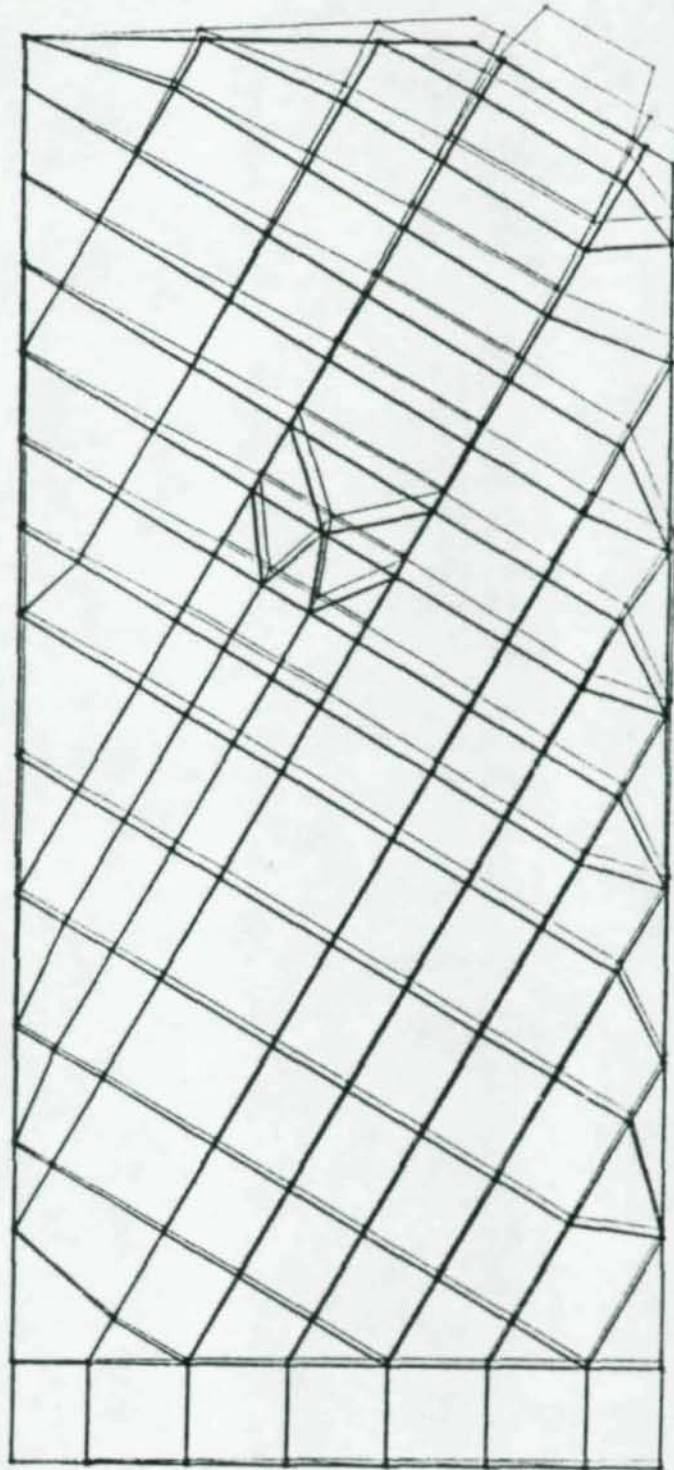


Figure A.33. 3/8" 60° Gusset Grid and Distorted Geometry.

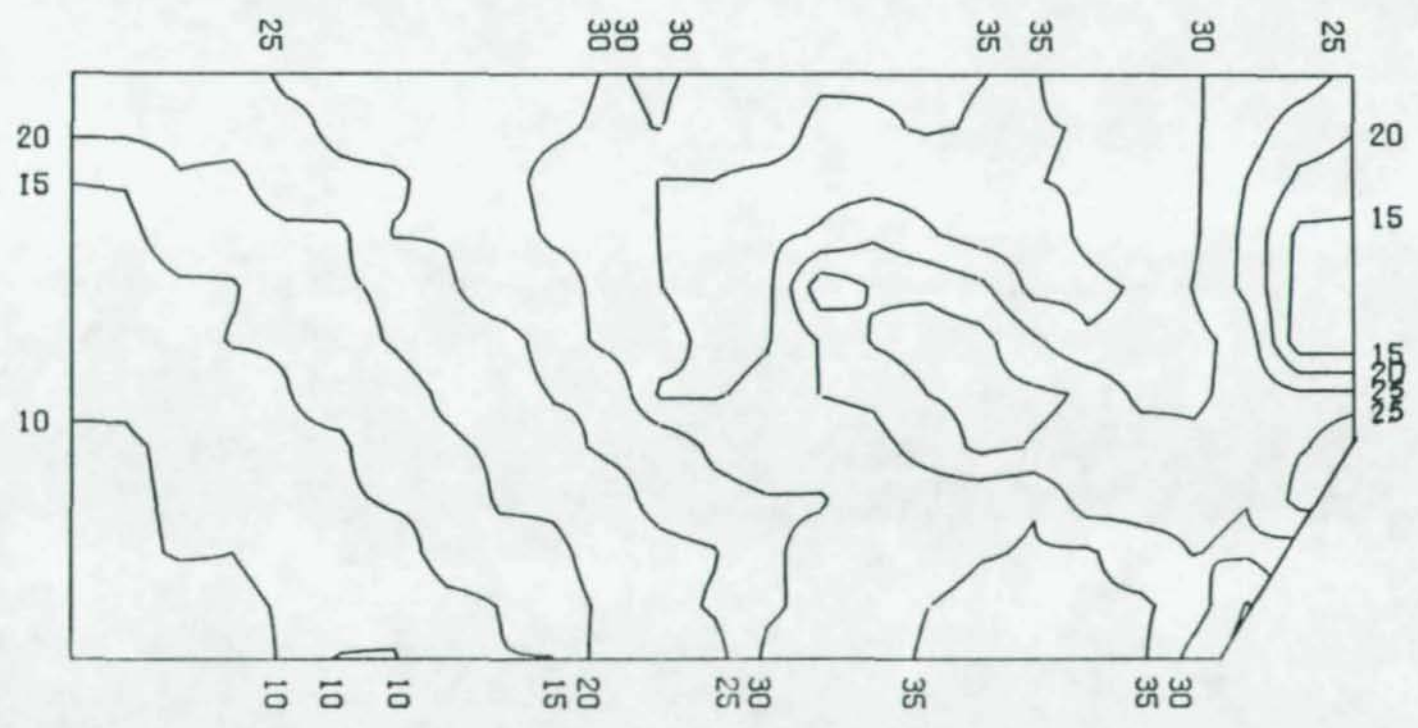
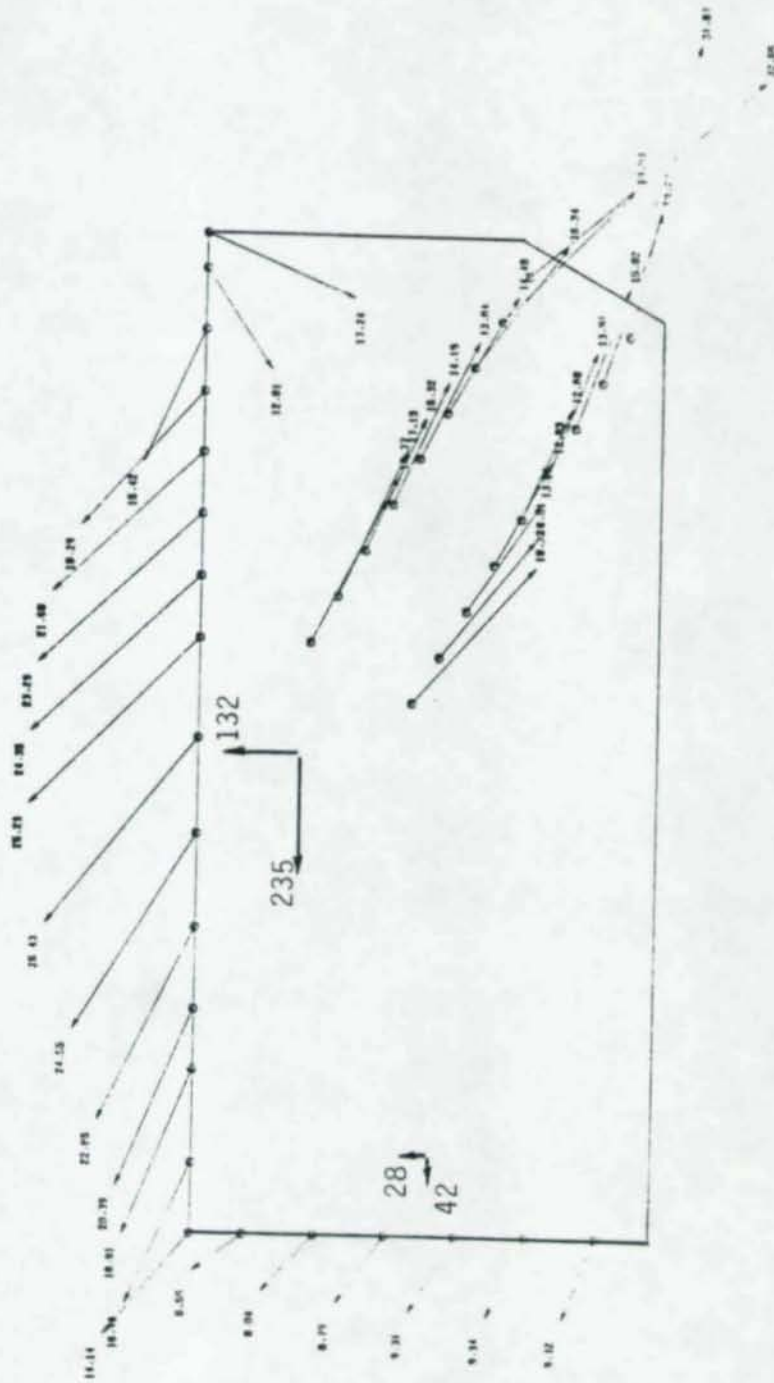


Figure A.34. Effective Stress Contour Plot 3/8" 60° Gusset, P = 320K.



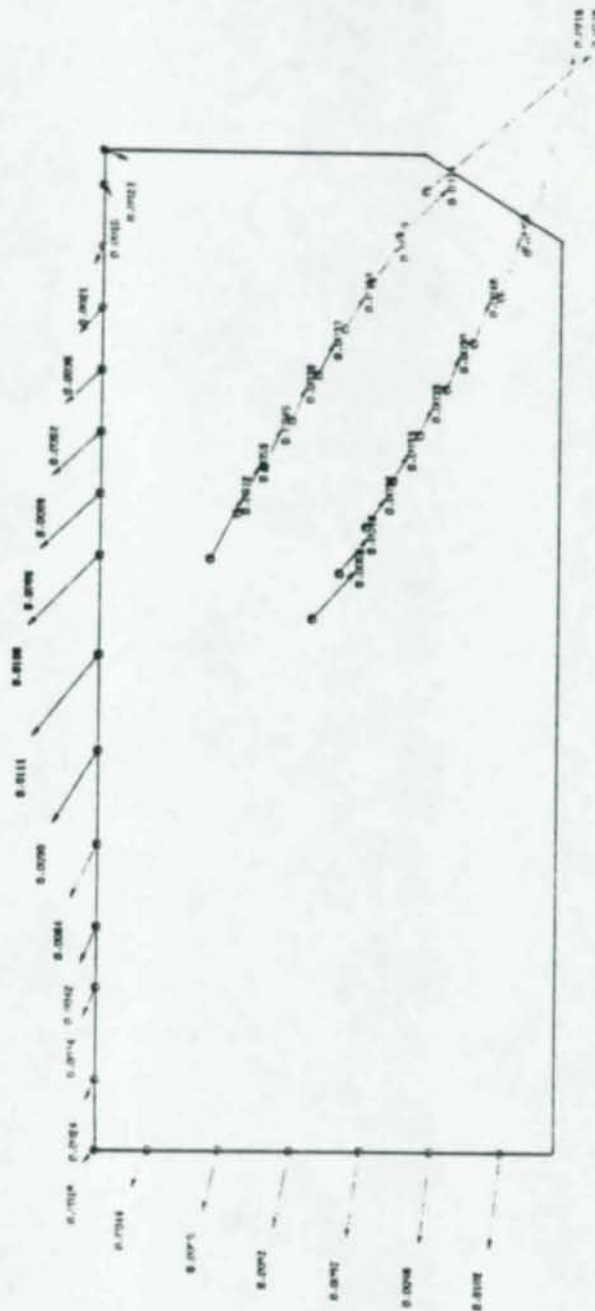


Figure A.36. Resultant Displacements, 3/8" 60° Gusset, P = 320K.

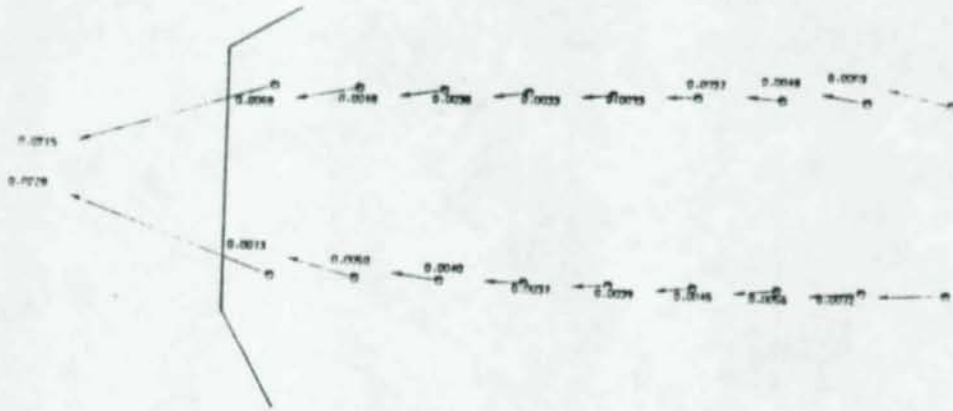
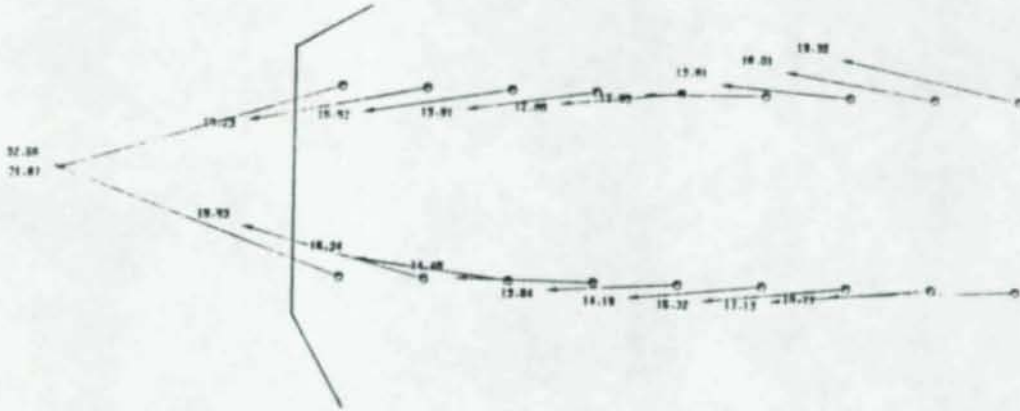


Figure A.37. Resultant Forces and Displacements, 3/8" 60° Gusset Splice Plate, P = 320K.

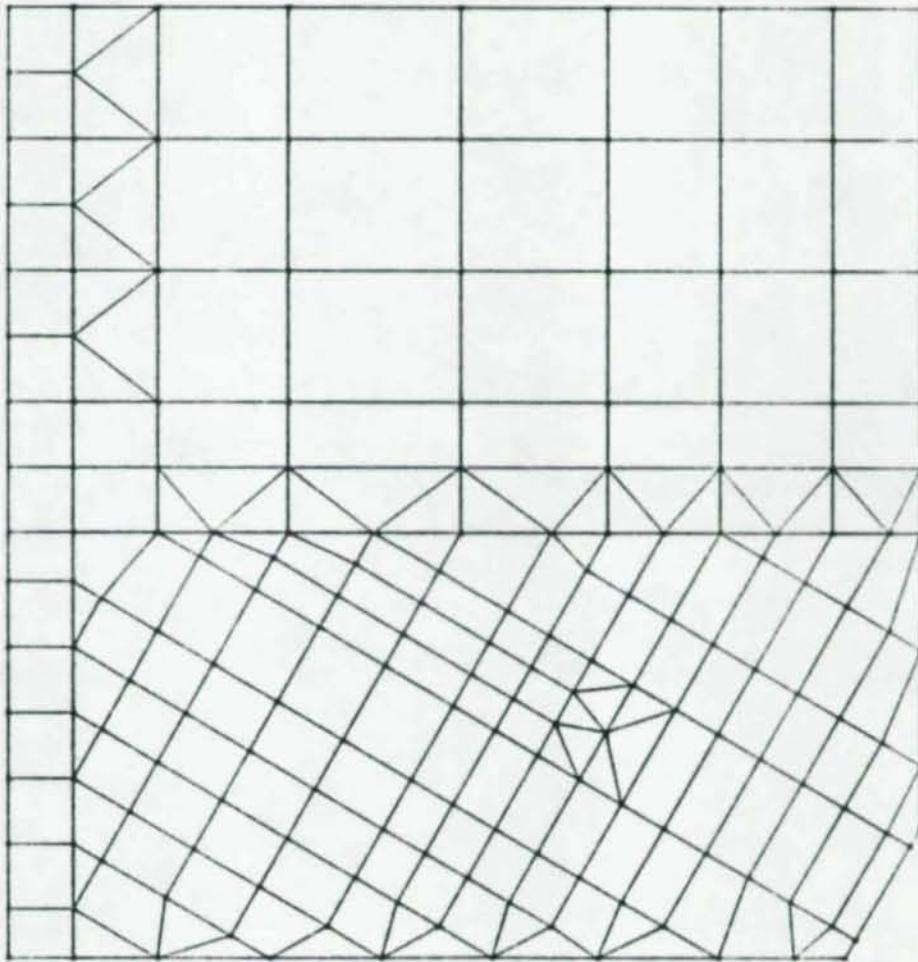


Figure A.38. Undistorted 60° Beam-Gusset Grid.

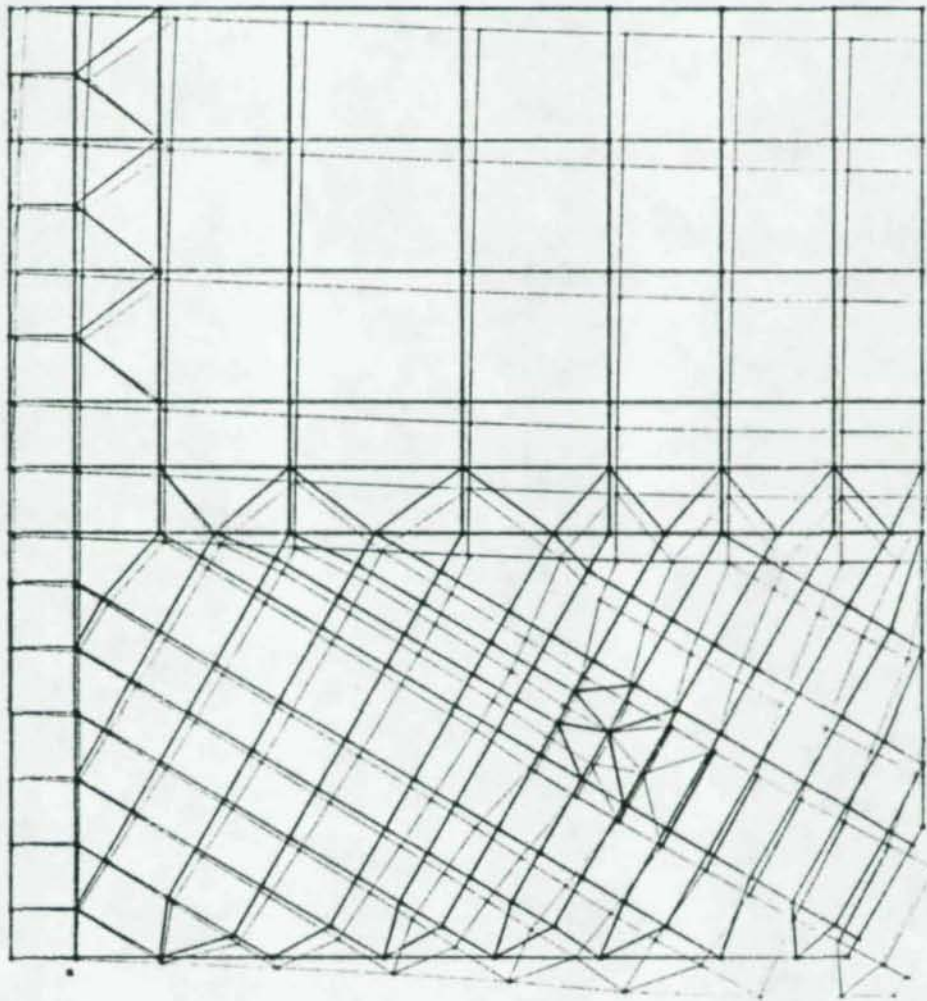


Figure A.39. $1/8''$ 60° Beam-Gusset Grid and Distorted Geometry.

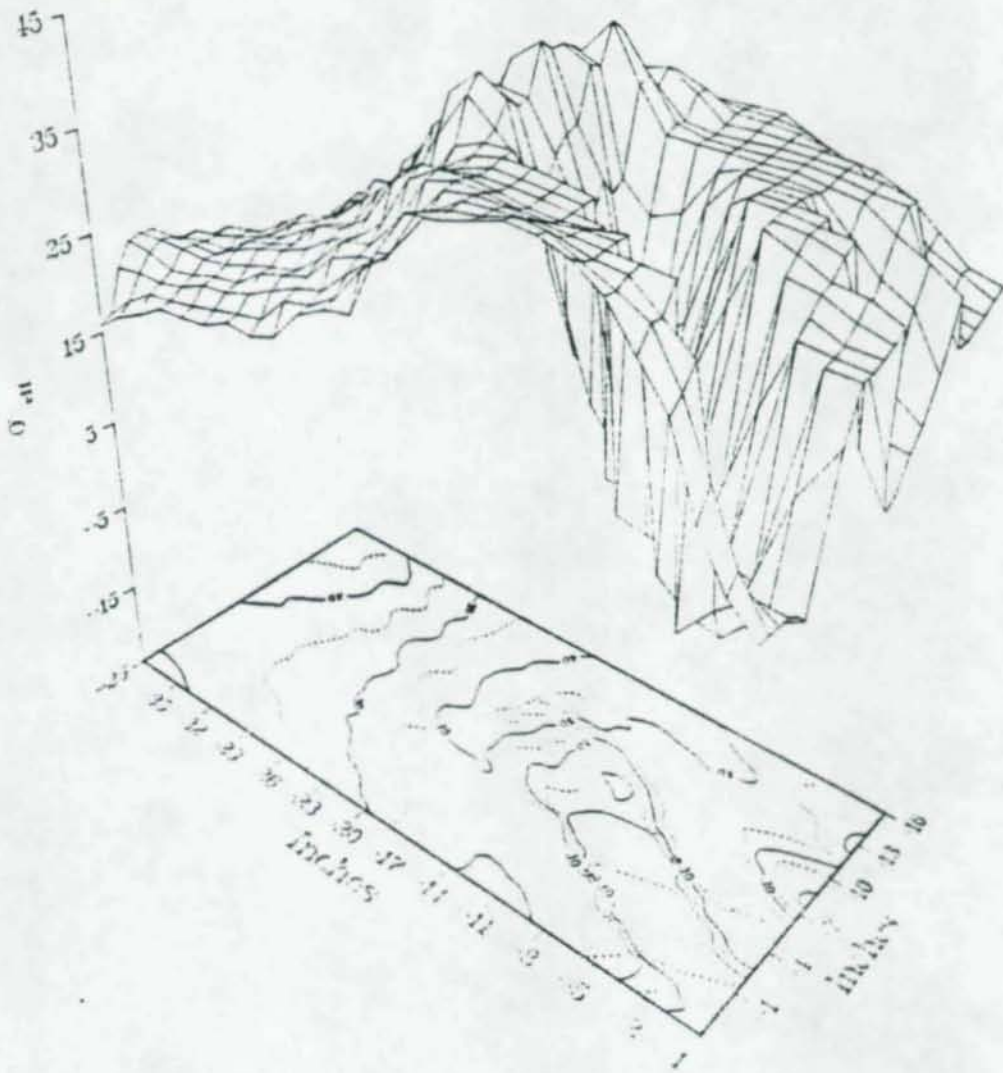


Figure A.40. 1/8" 60° Beam-Gusset Effective Stress Surface and Contour
 Plot P = 140K.

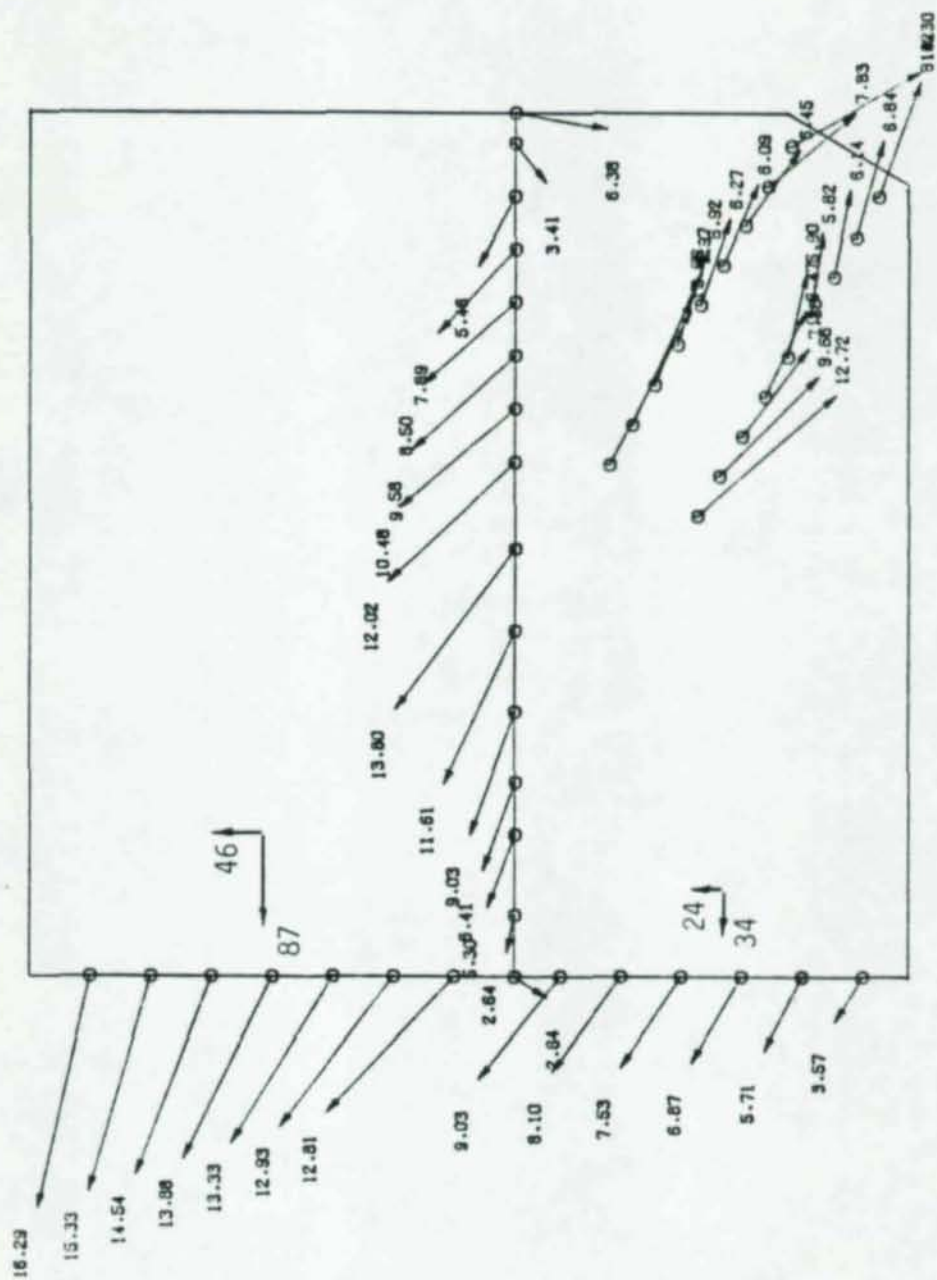


Figure A.41. Resultant Forces 1/8" 60° Beam-Gusset, P = 140K.

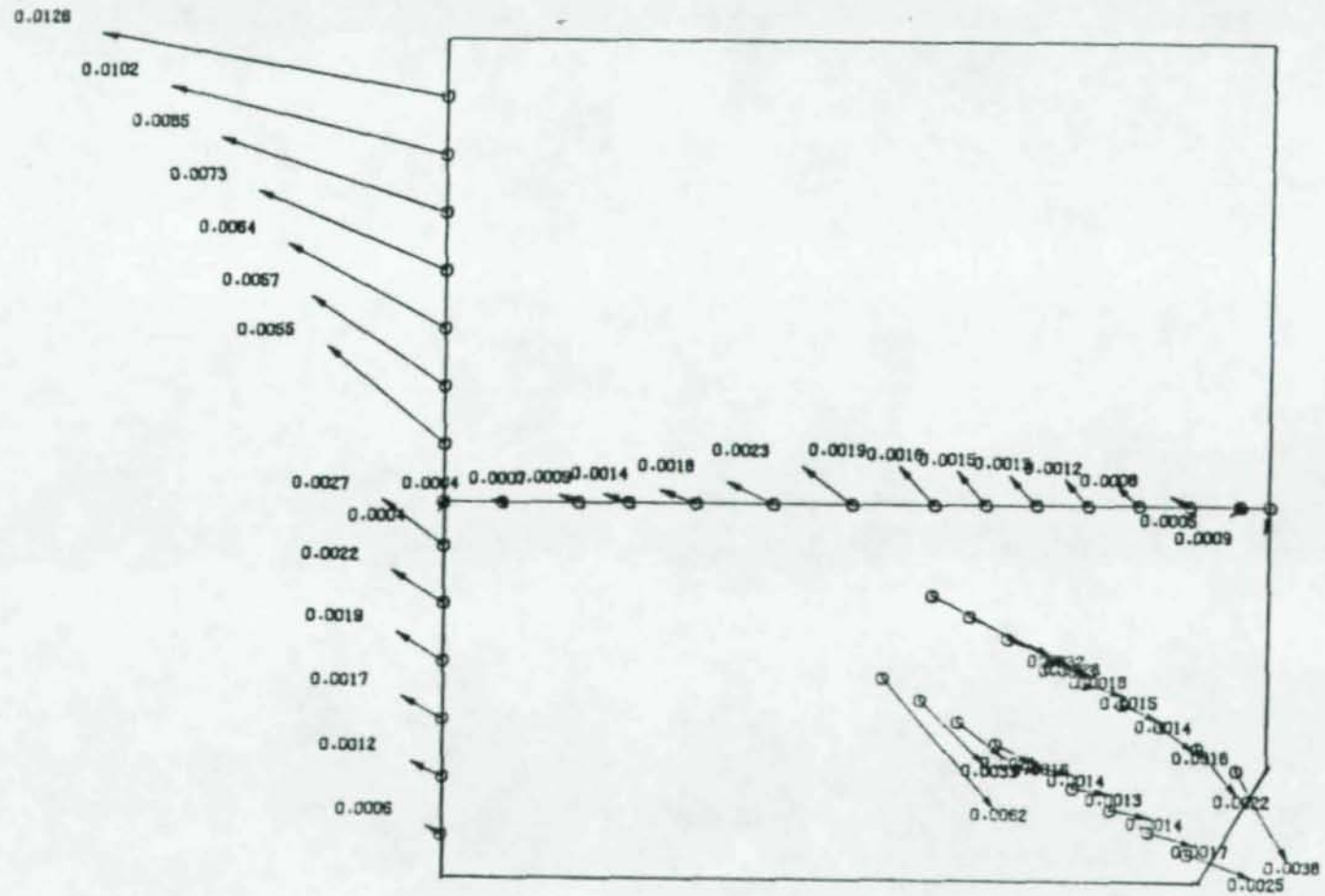


Figure A.42. Resultant Displacements, 1/8" 60° Beam-Gusset, P = 140K.

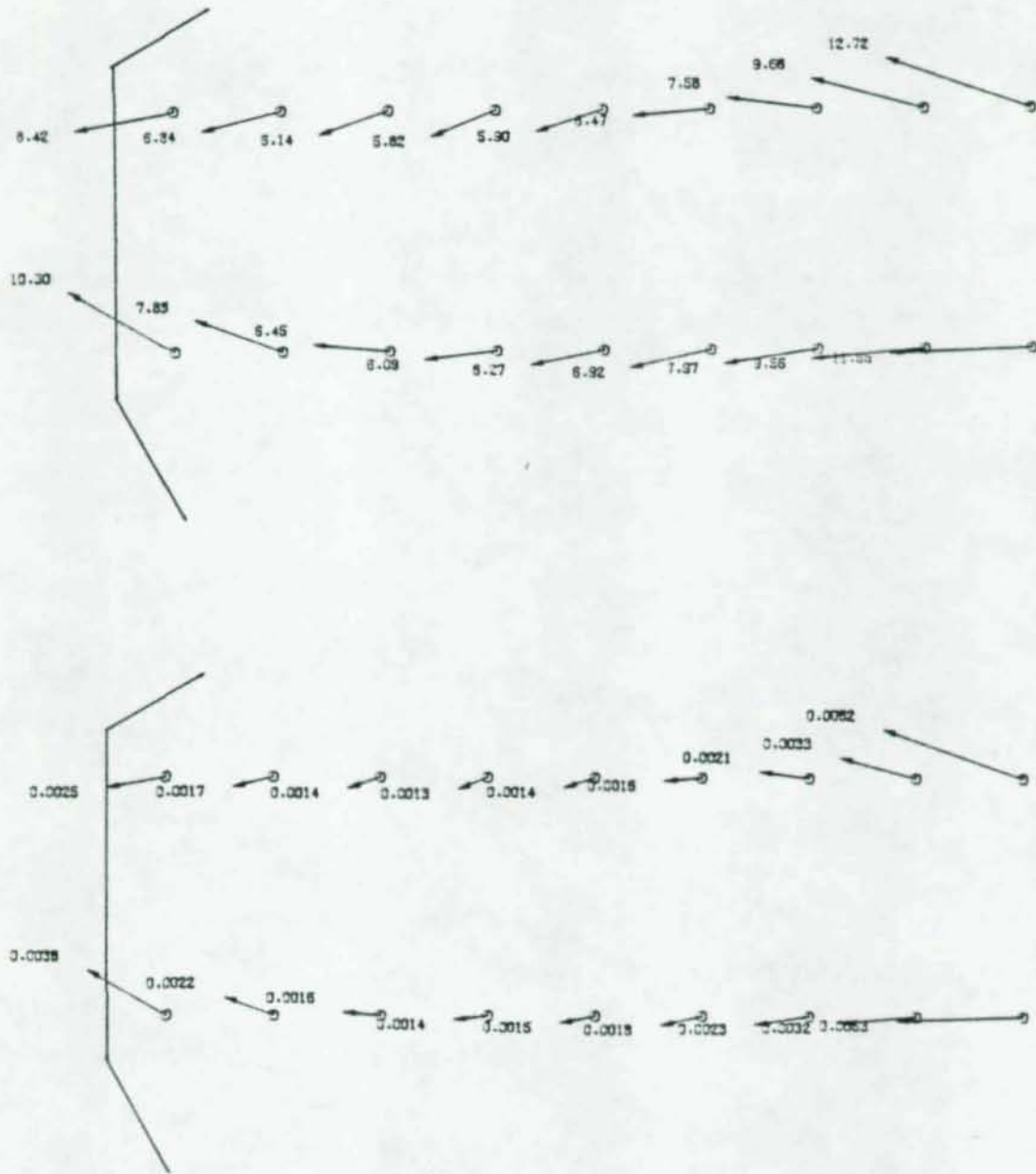


Figure A.43. Resultant Forces and Displacements, 60° 1/8" Beam-Gusset Splice Plate, P = 140K.

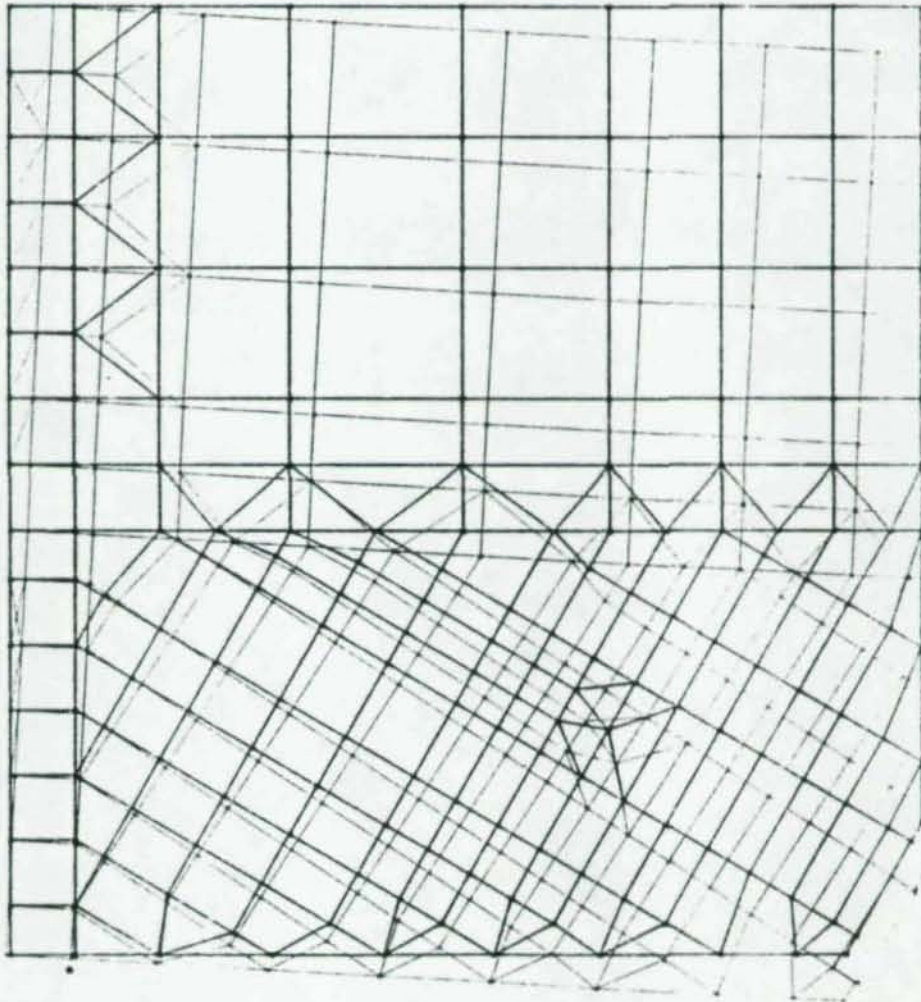


Figure A.44. $3/8''$ 60° Beam-Gusset Grid and Distorted Geometry.

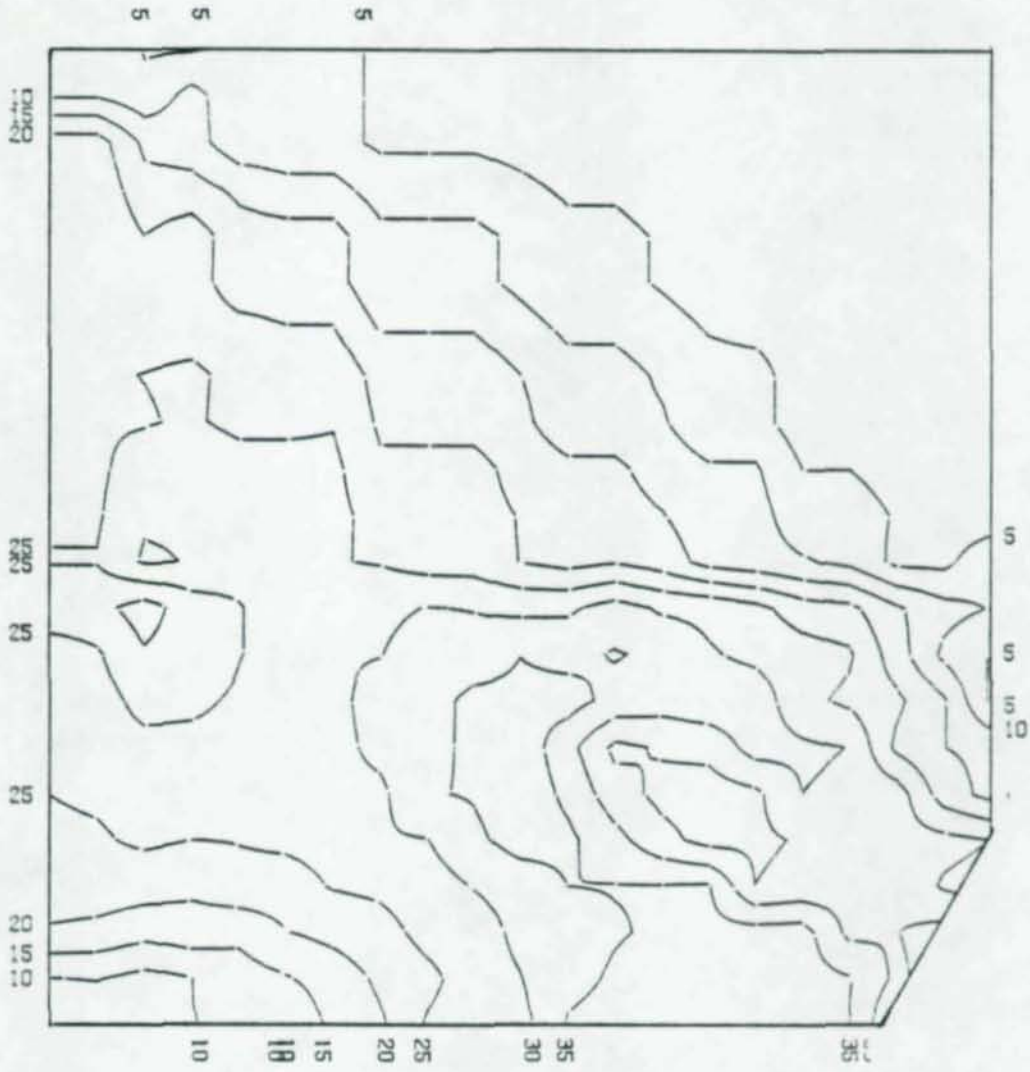


Figure A.45. Effective Stress Contour Plot, 3/8" Beam-Gusset, P = 320K.

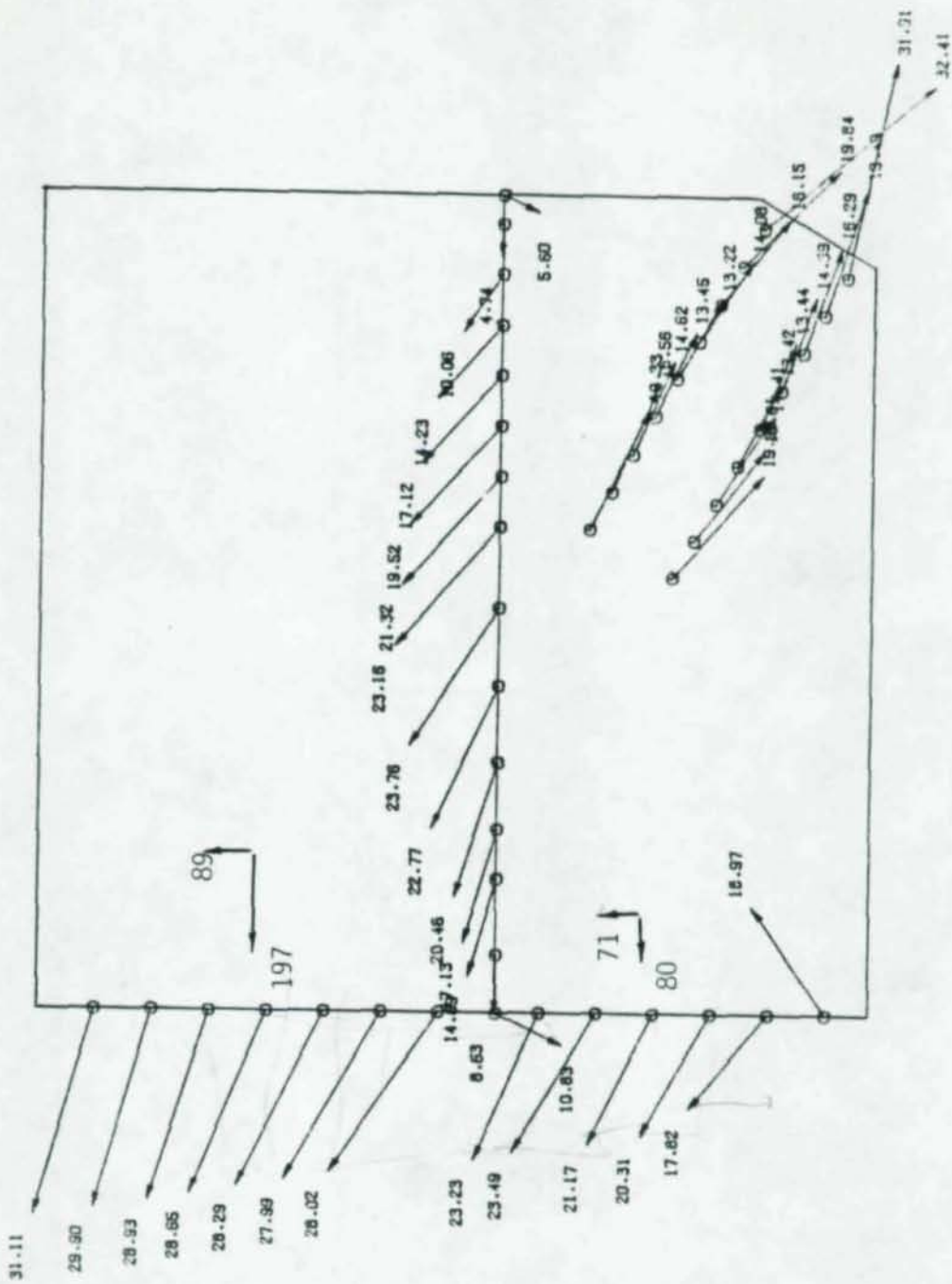


Figure A.46. Resultant Forces, 3/8" 60° Beam-Gusset, P = 320K.

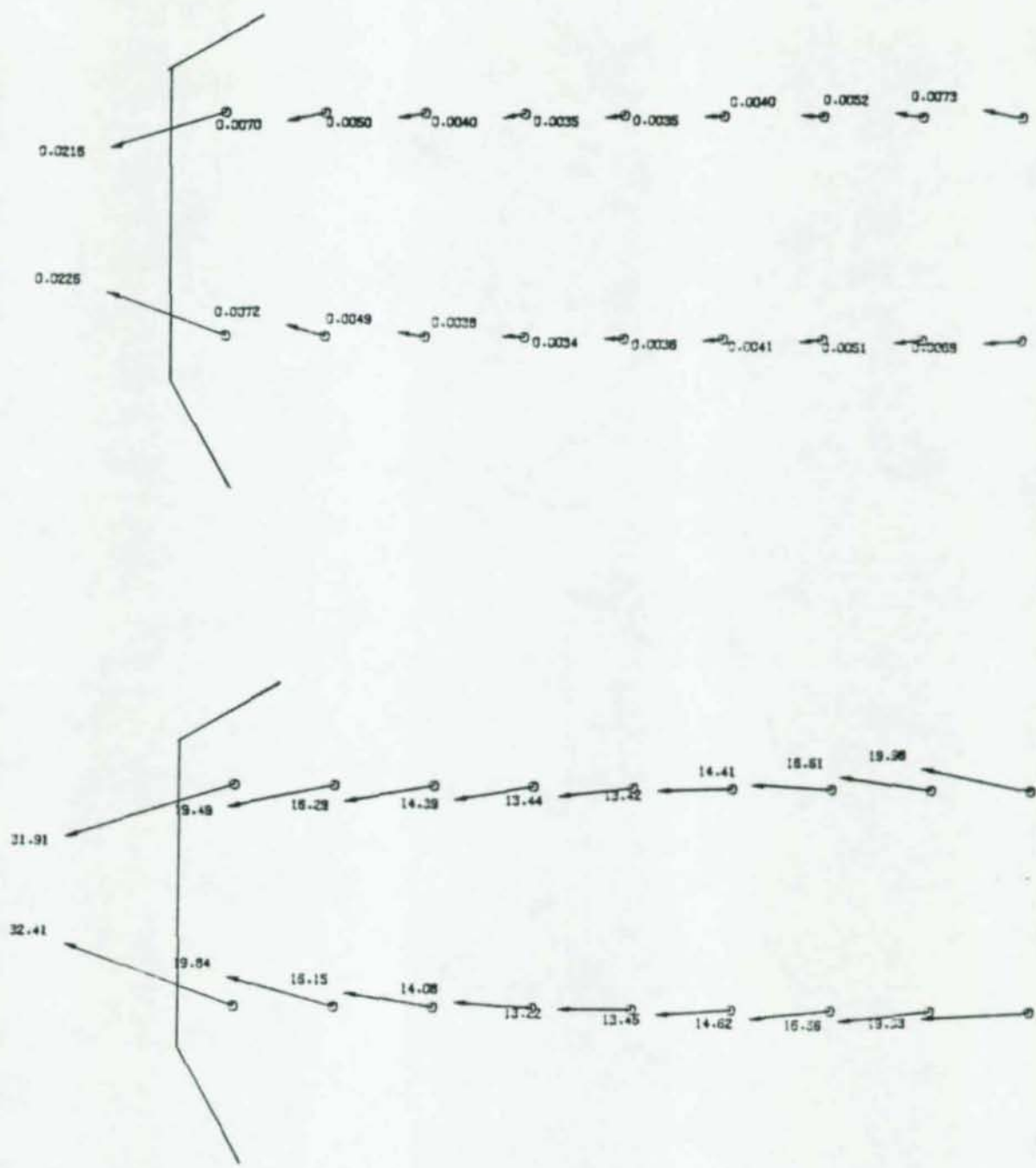


Figure A.47. Resultant Forces and Displacements 60° 3/8" Beam-Gusset Splice Plate, P = 320K.

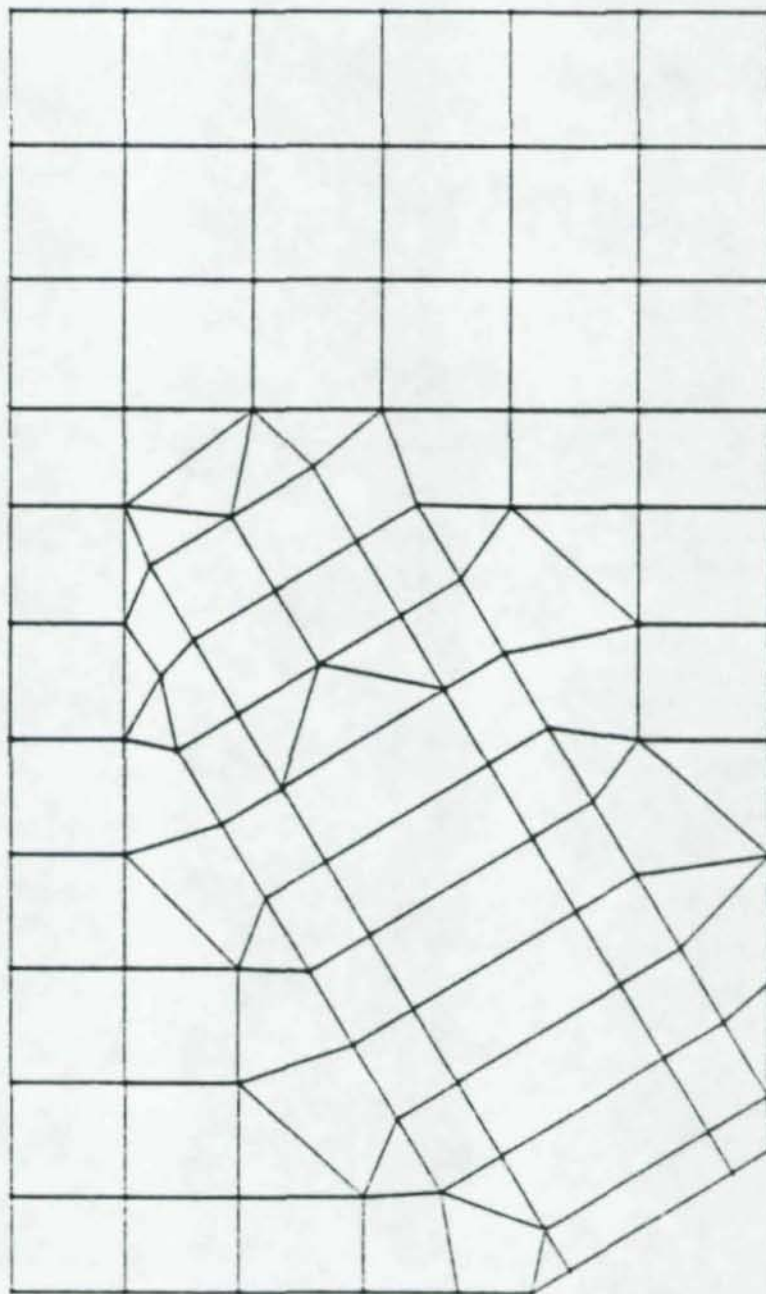


Figure A.48. 30^o Gusset Undistorted Geometry.

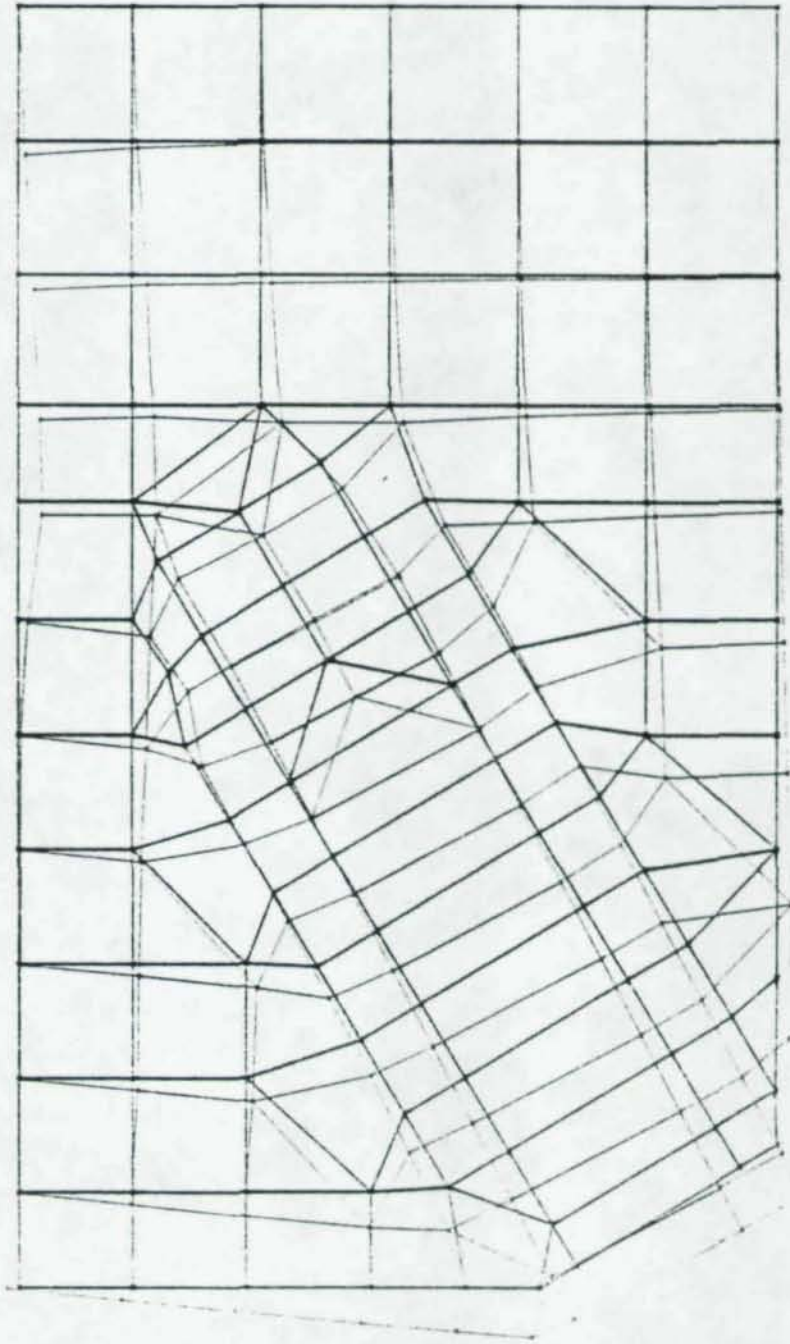


Figure A.49. $1/8''$ 30° Gusset Grid and Distorted Geometry.

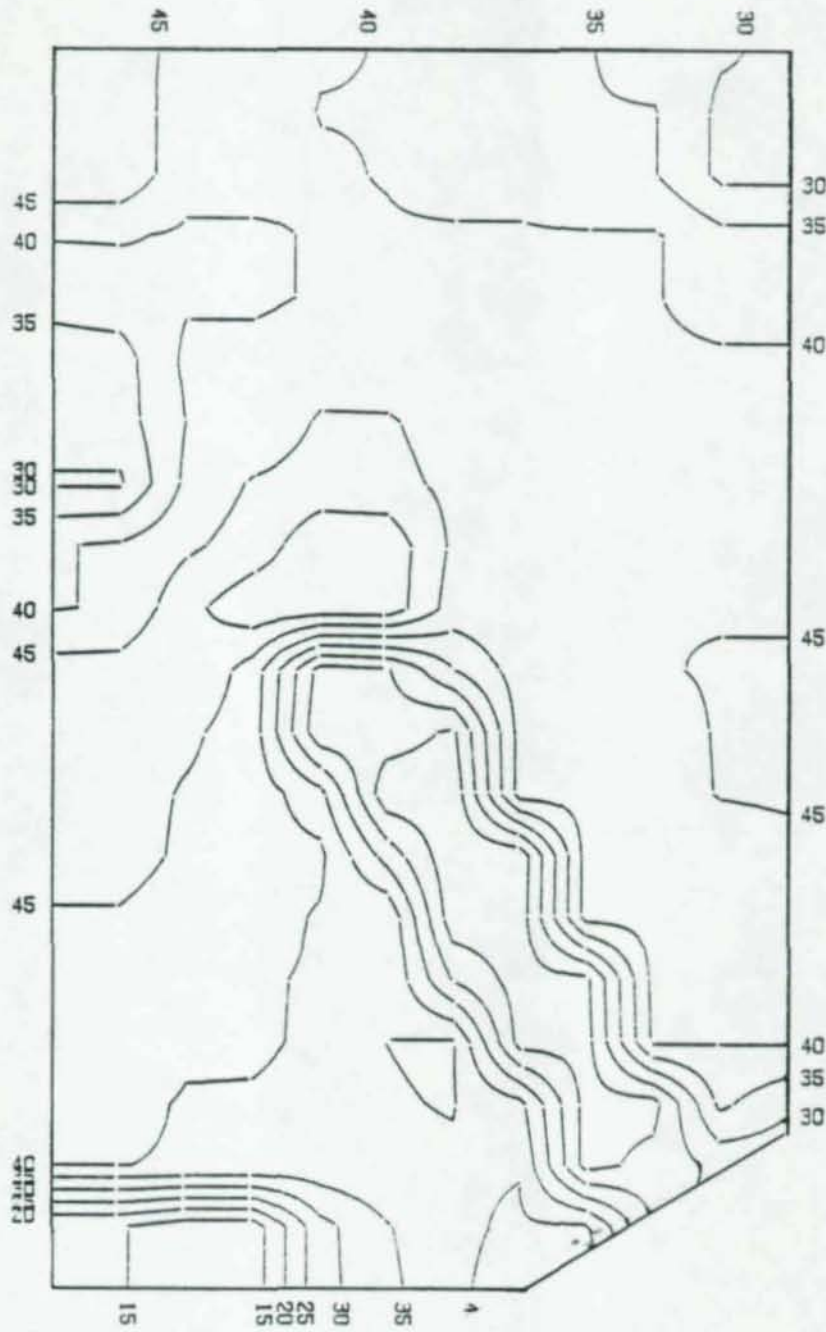


Figure A.50. Effective Stress Contour Plot 1/8" 30° Gusset, P = 158K.

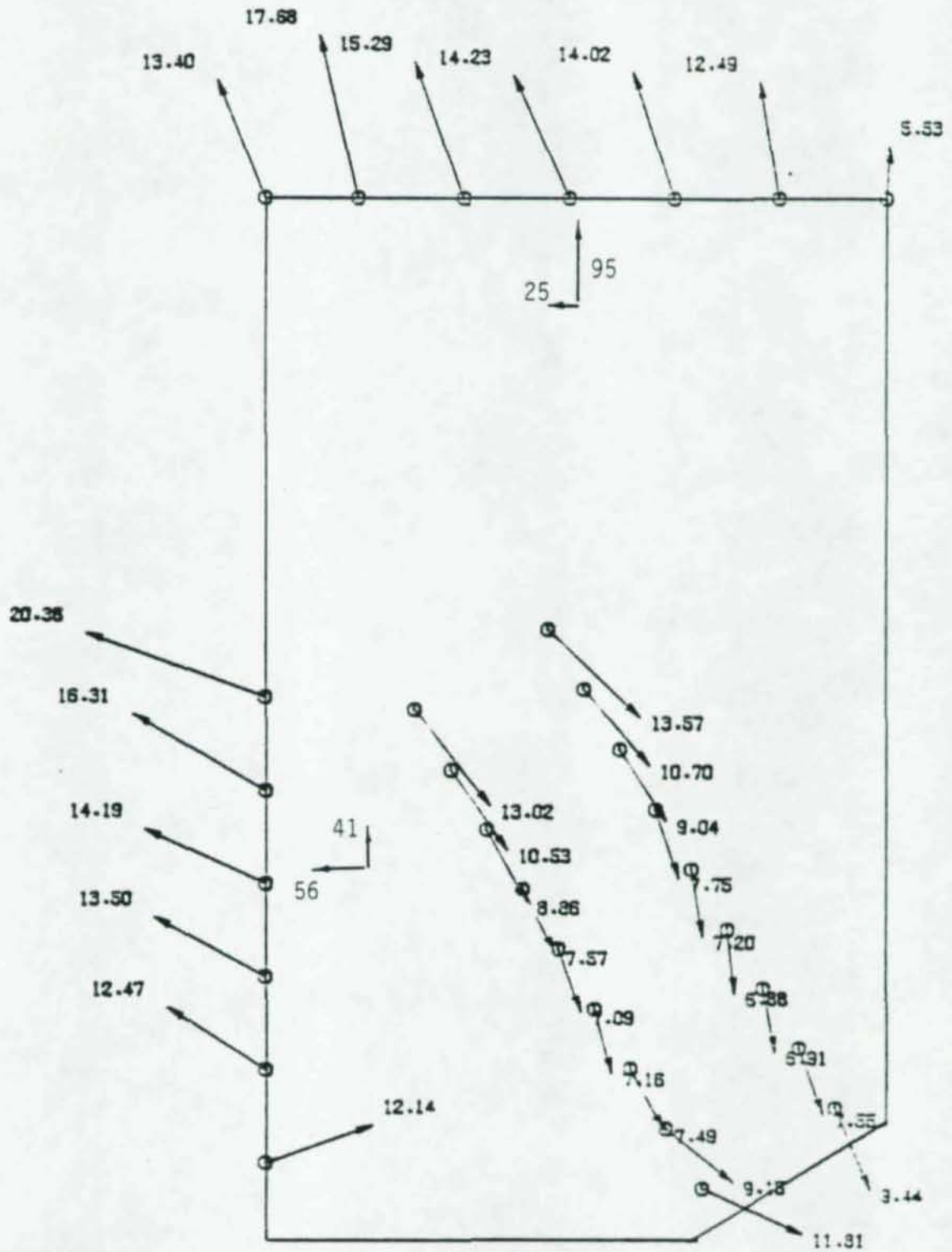


Figure A.51. Resultant Forces, 1/8" 30° Gusset, P = 158K.

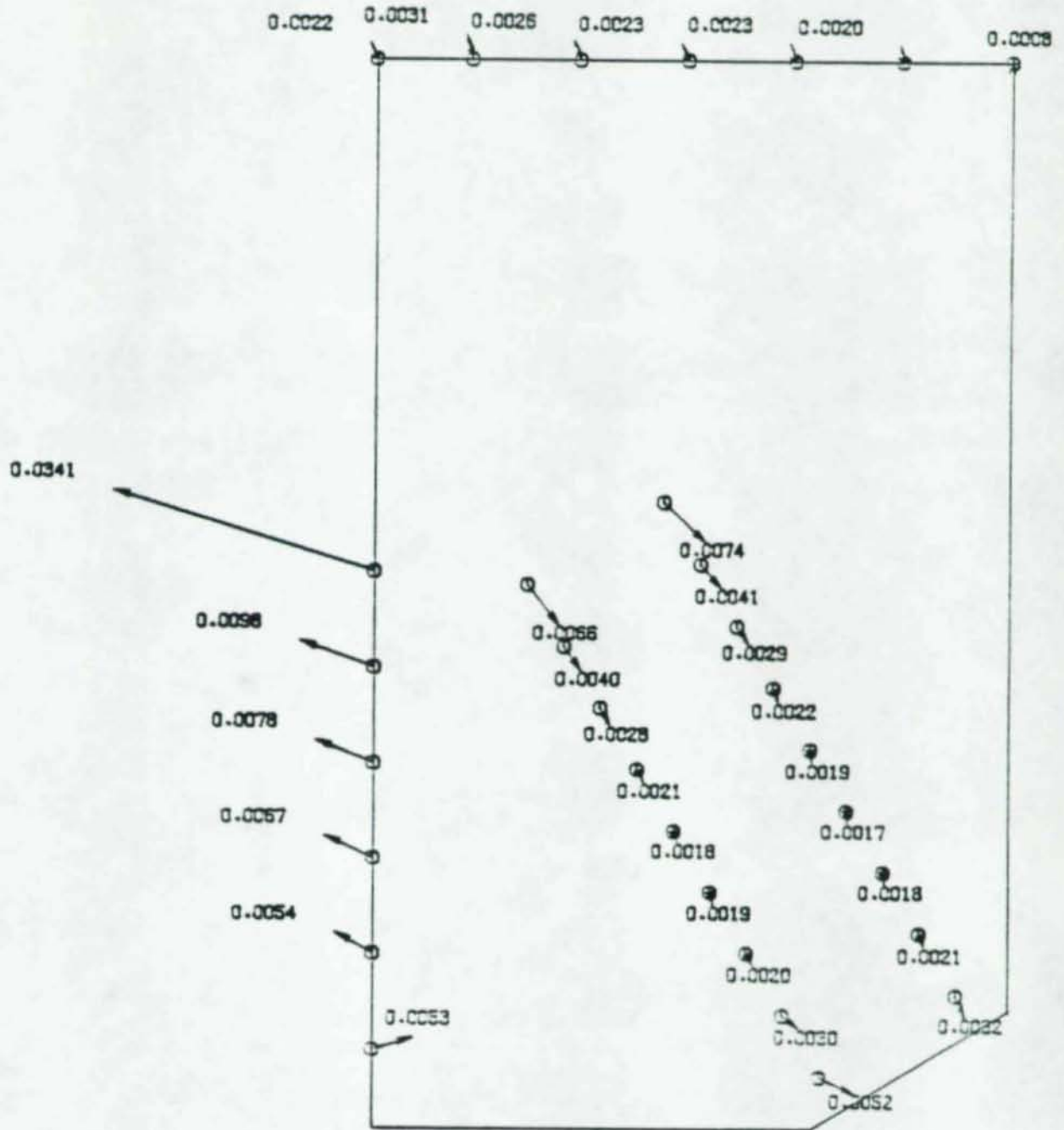


Figure A.52. Resultant Displacements, 1/8" 30° Gusset, P = 158K.

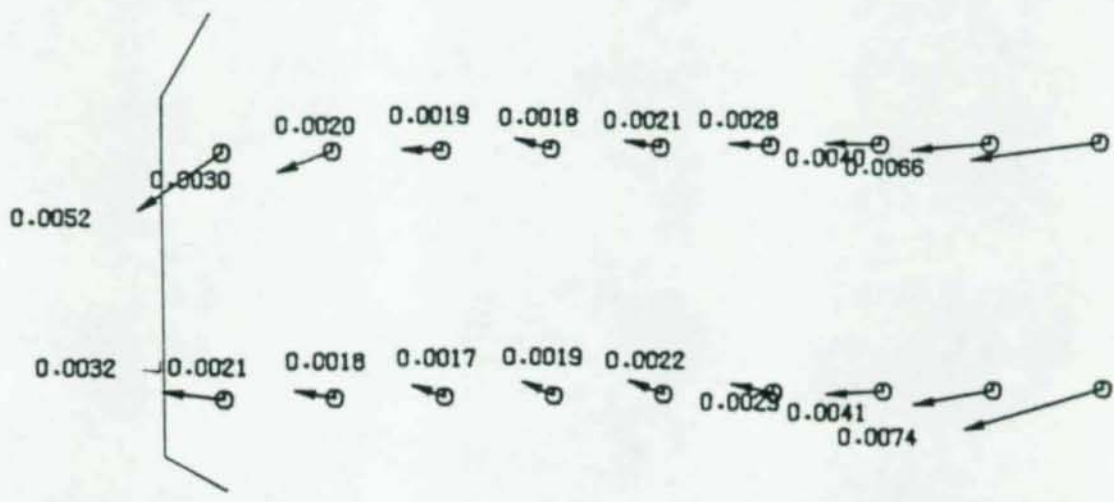
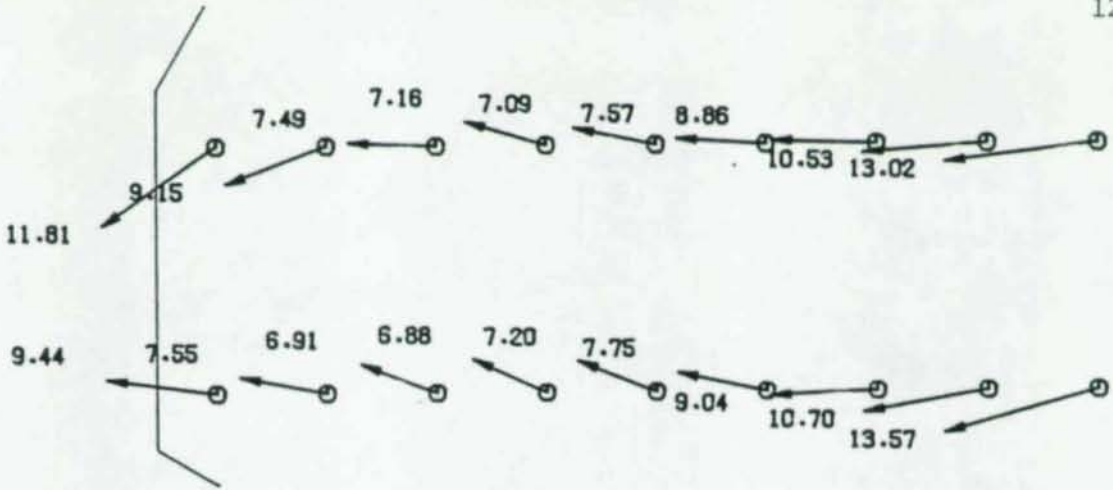


Figure A.53. Resultant Forces and Displacements 1/8" 30° Gusset Splice Plate, P = 158K.

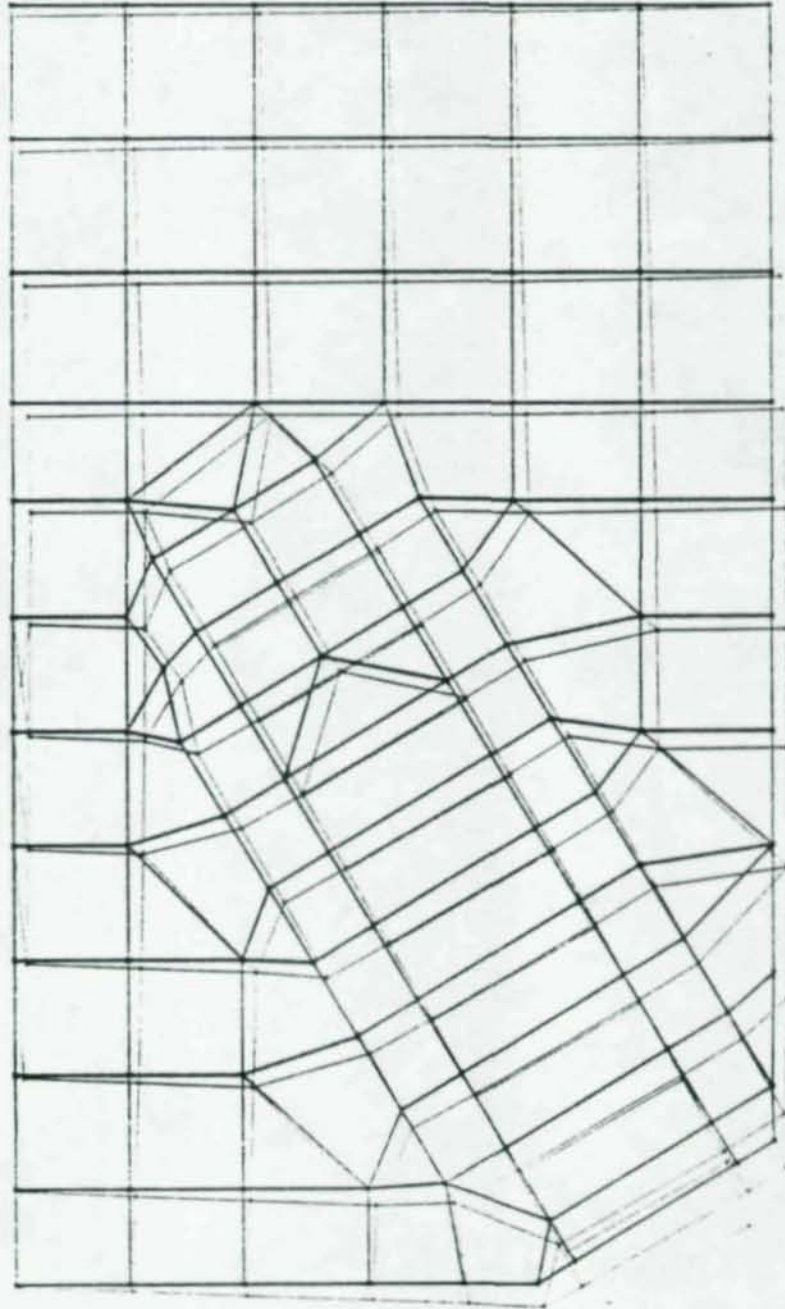


Figure A.54. 3/8" 30° Gusset Grid and Distorted Geometry.

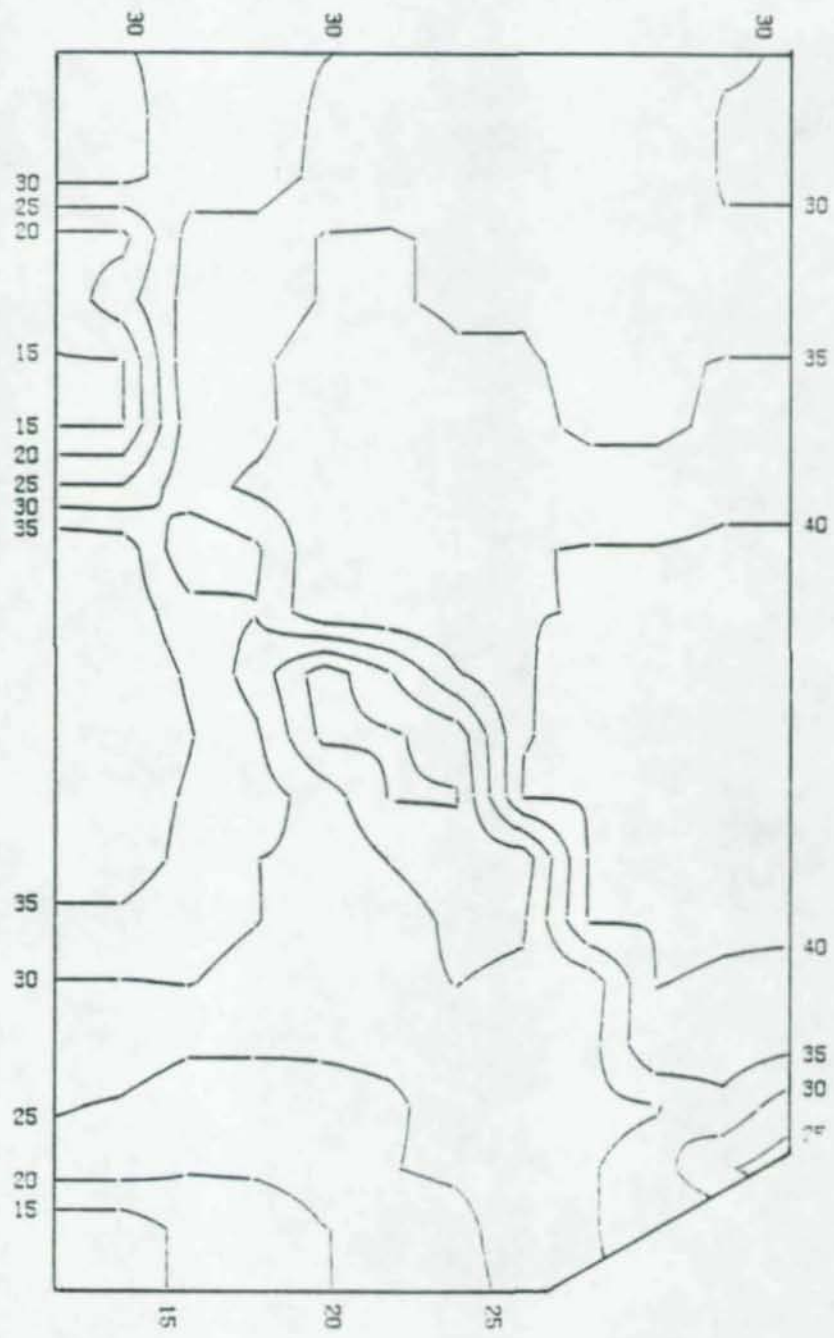


Figure A.55. Effective Stress Contour Plot, 3/8" 30° Gusset, P = 320K

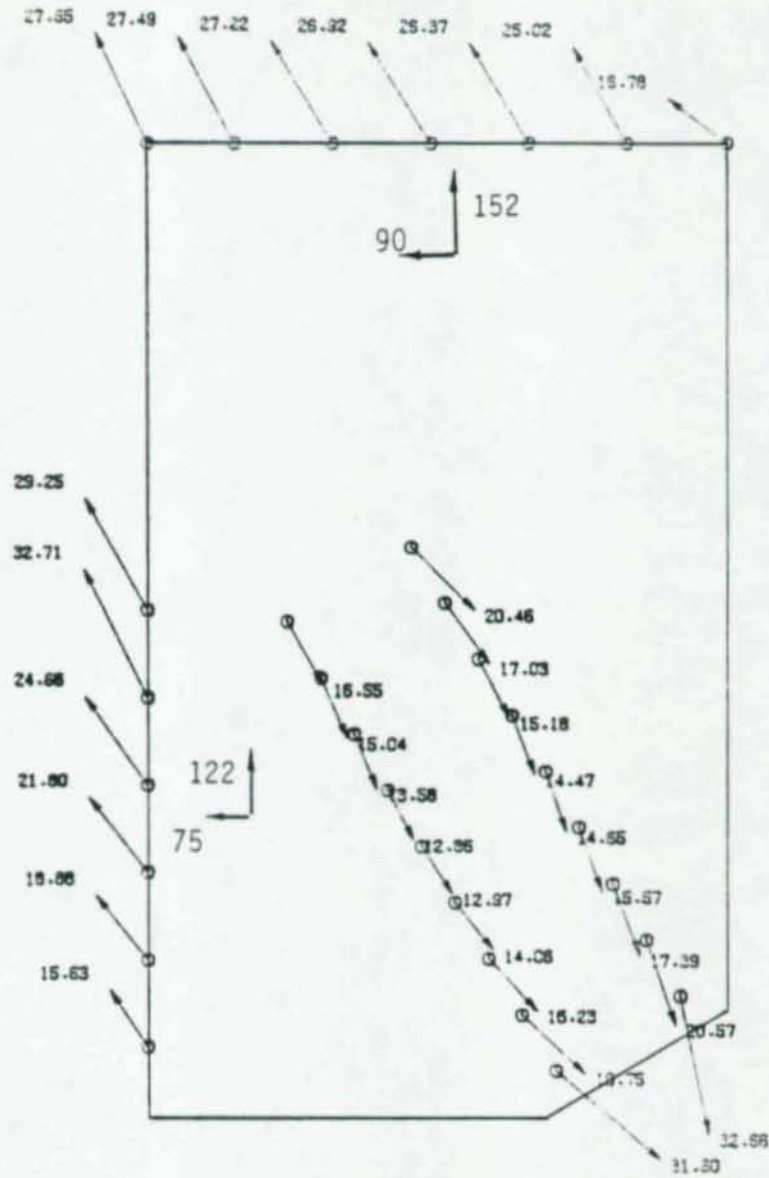


Figure A.56. Resultant Forces, 3/8" 30° Gusset, P = 320K

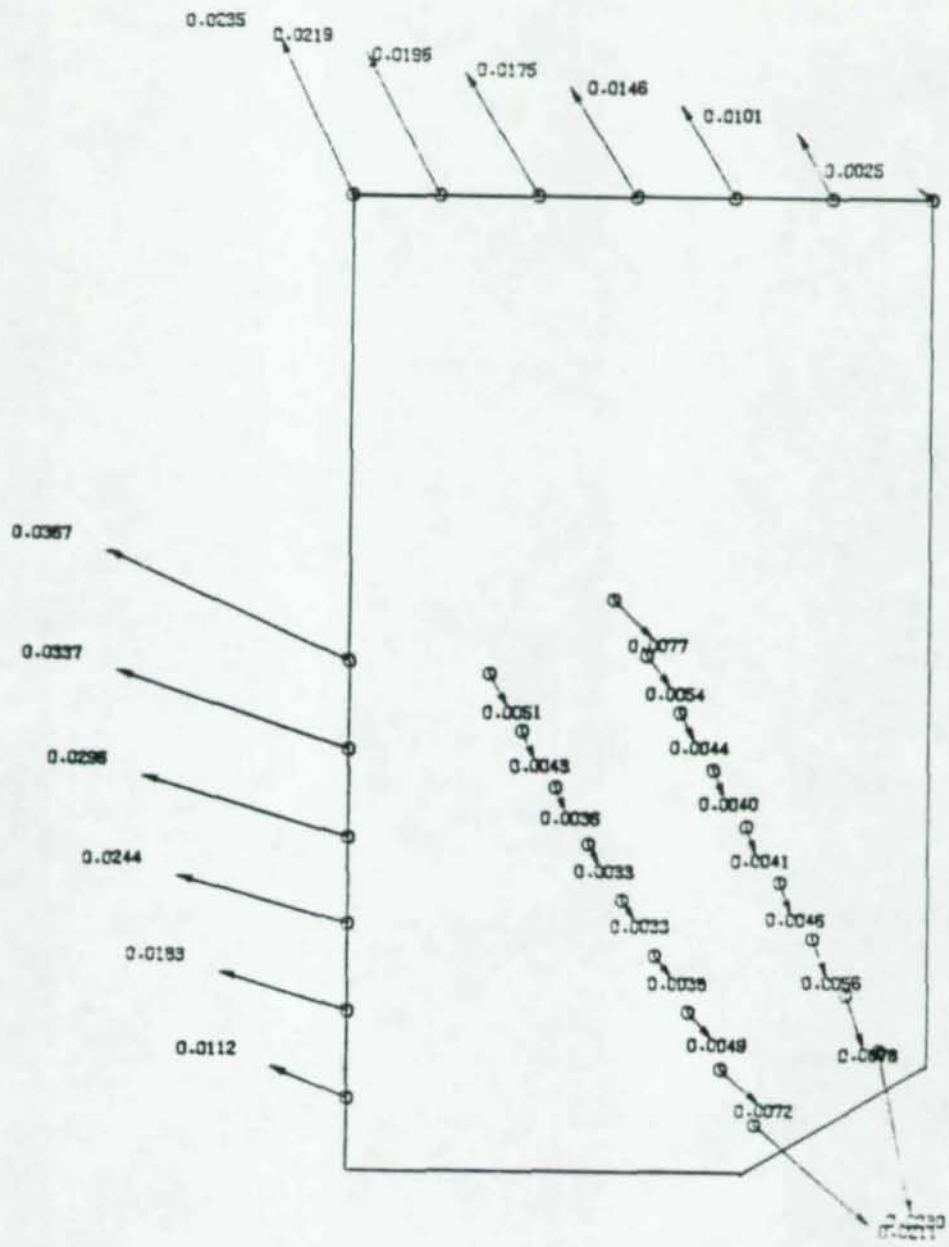


Figure A.57. Resultant Displacements, 3/8" 30° Gusset, P = 320K.

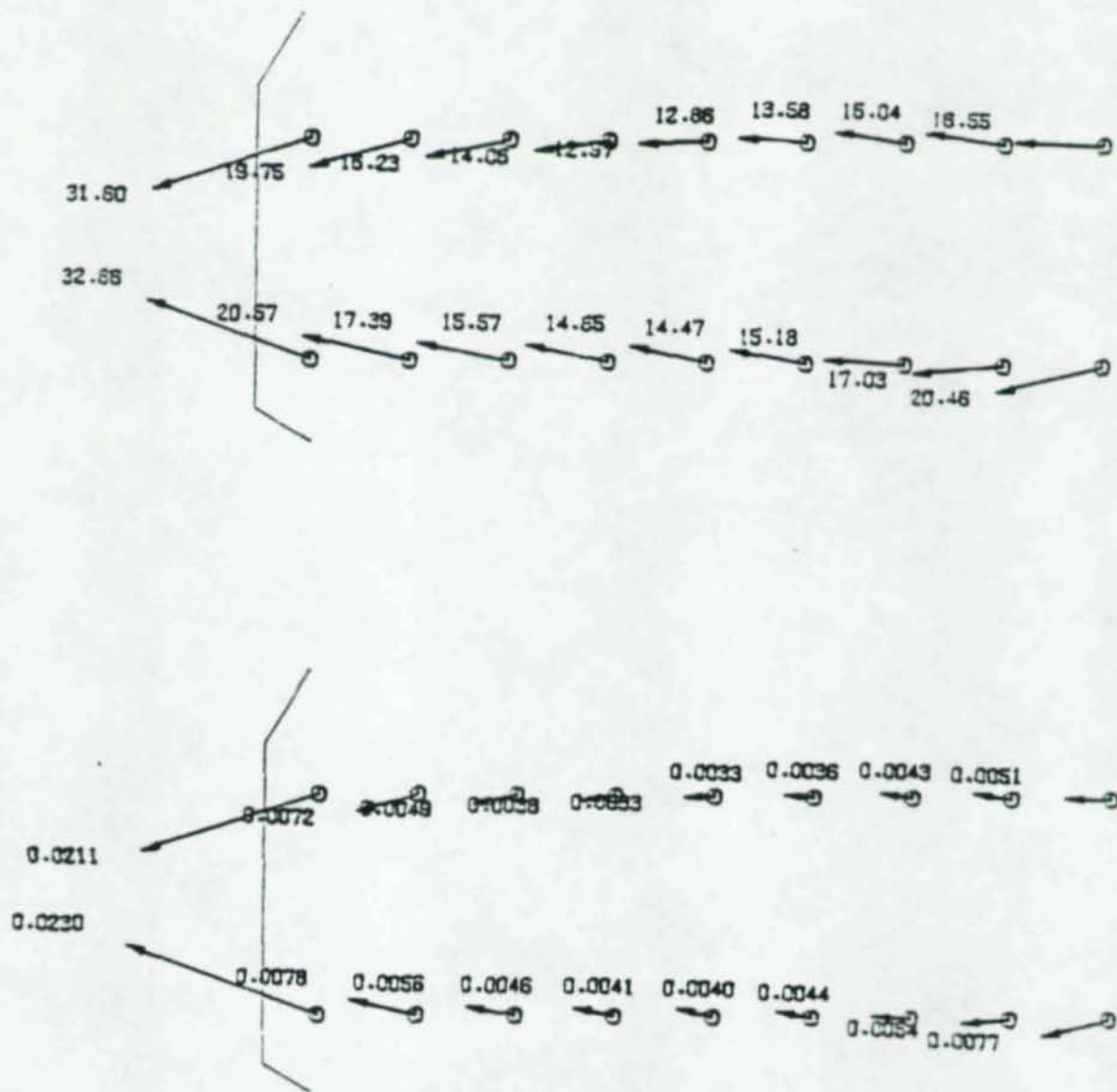


Figure A.58. Resultant Forces and Displacements, 3/8" 30° Gusset Splice Plate, P = 320K.

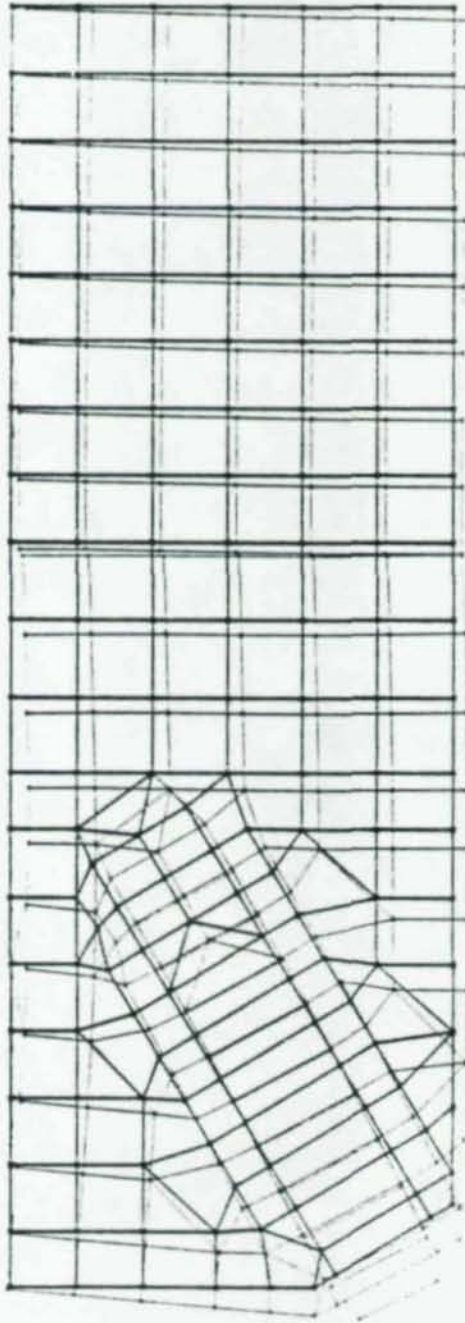


Figure A.59. 1/8" 30° Beam-Gusset Grid and Distorted Geometry.

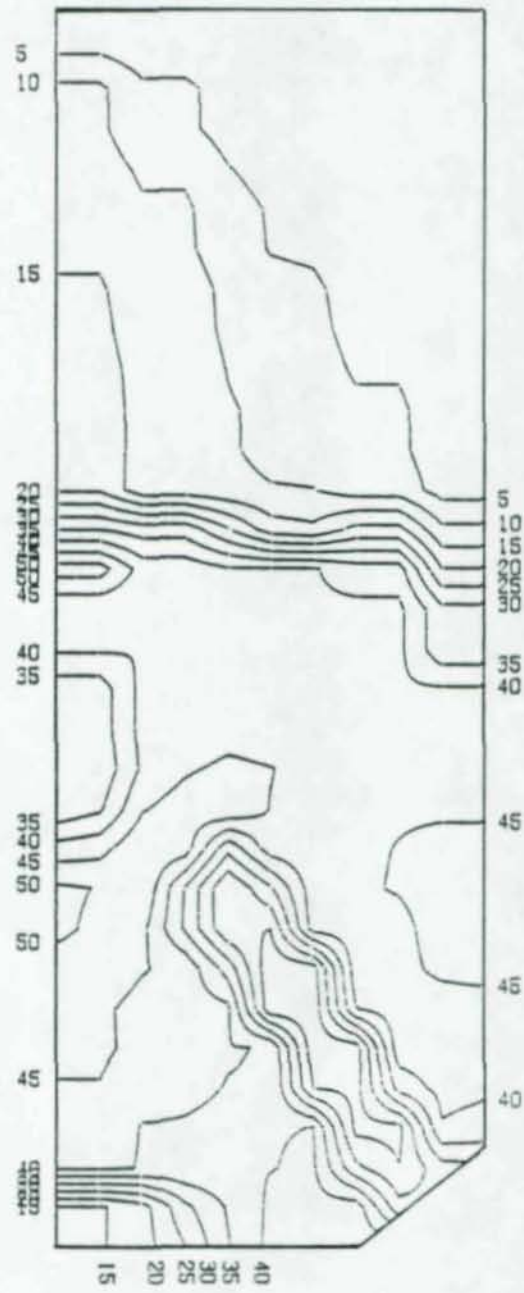


Figure A.60. Effective Stress Contour Plot, 1/8" 30° Beam-Gusset, P = 158K.

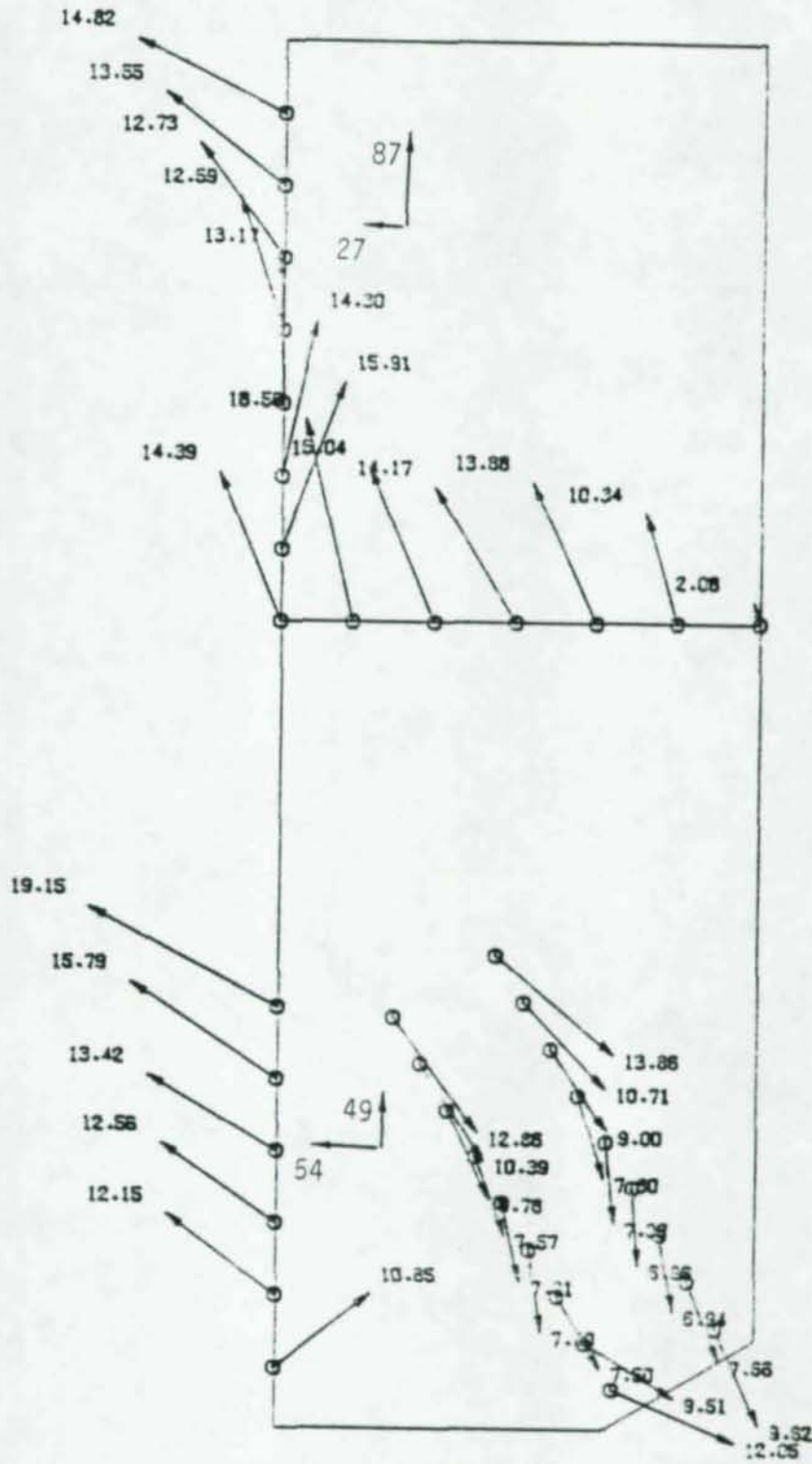


Figure A.61. Resultant Forces, 1/8" 30° Beam-Gusset, P = 158K.

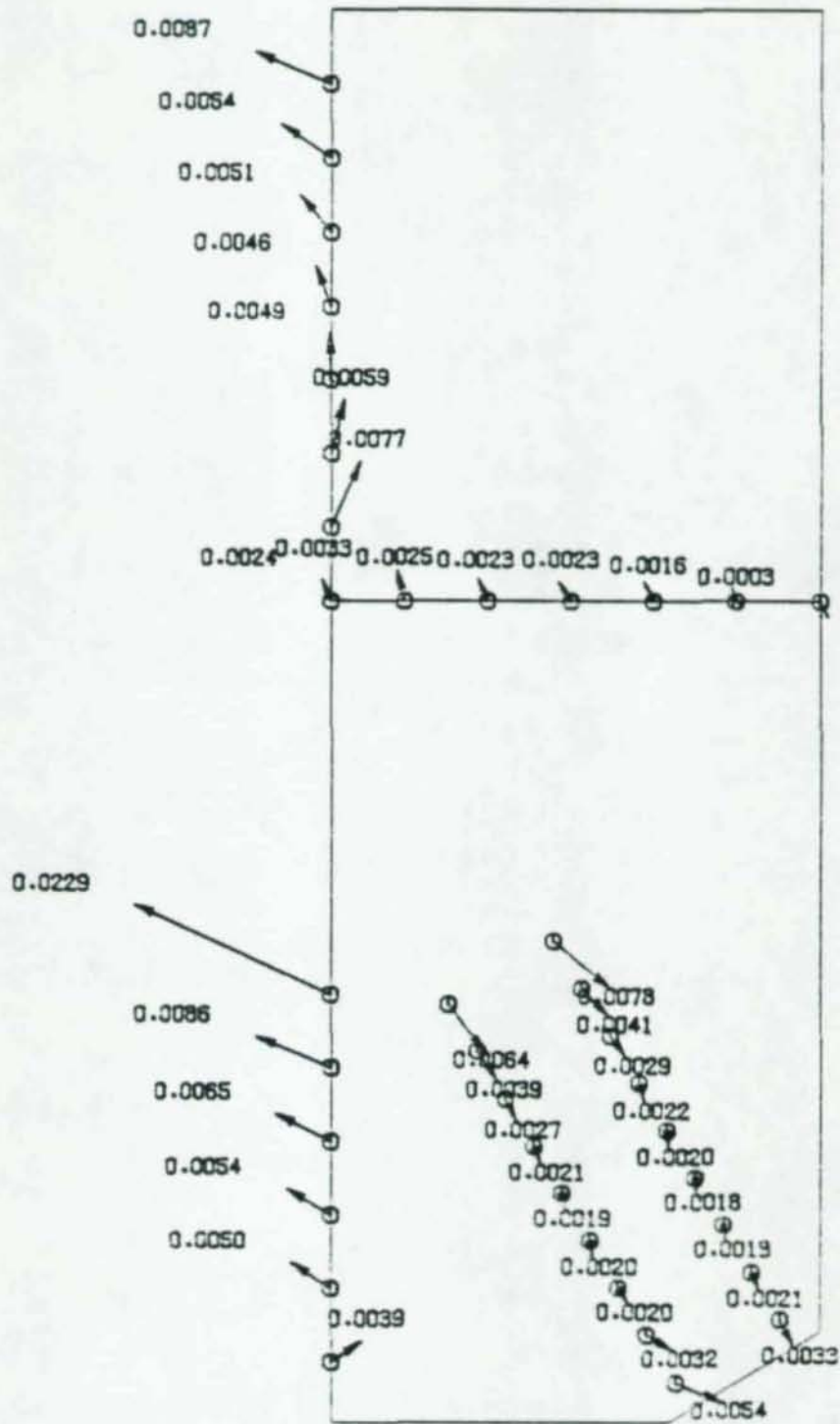


Figure A.62. Resultant Displacements 1/8" 30° Beam-Gusset. P = 158K.

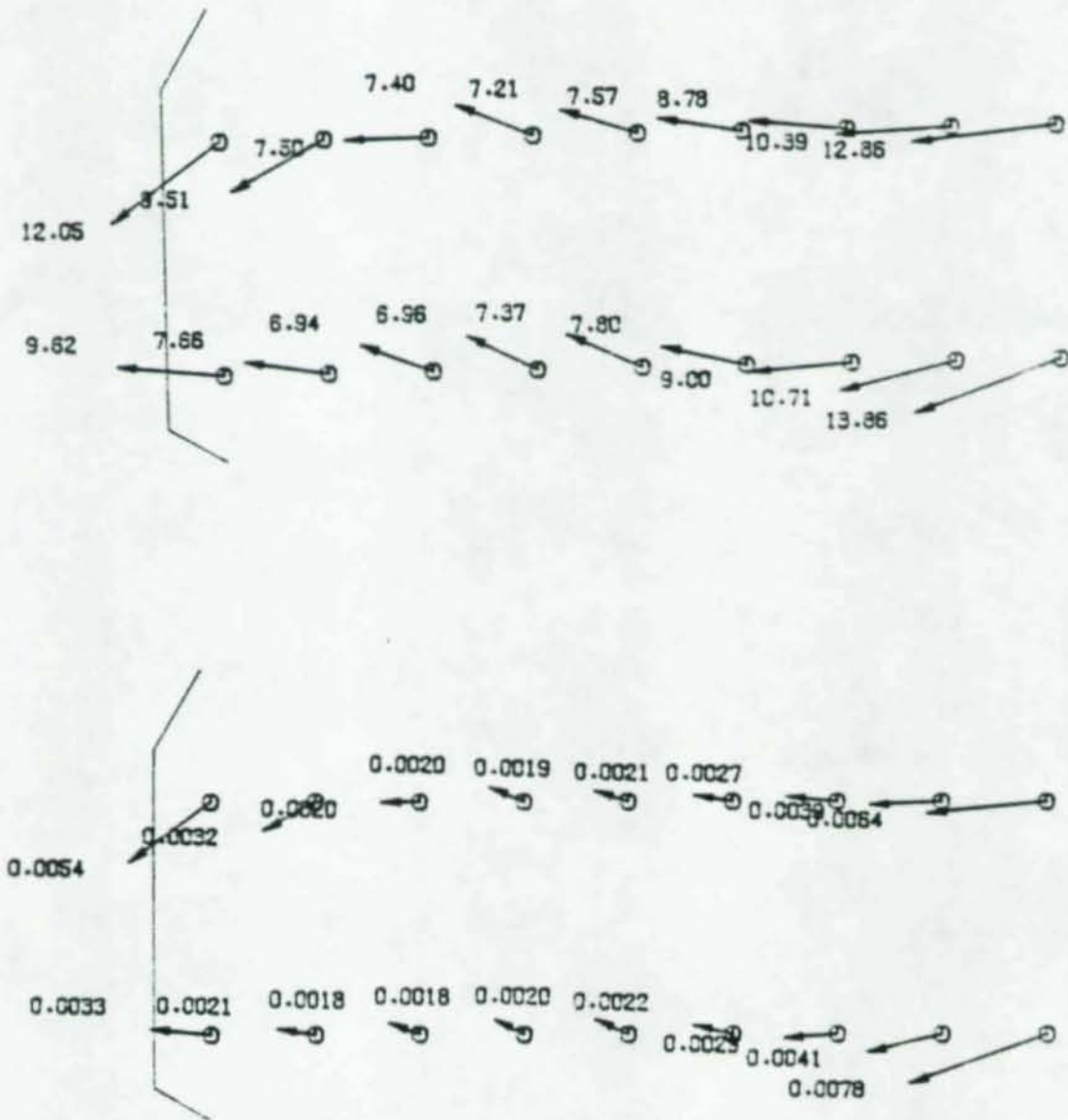


Figure A.63. Resultant Forces and Displacements 1/8" 30° Beam-Gusset Splice Plate, P = 158K.

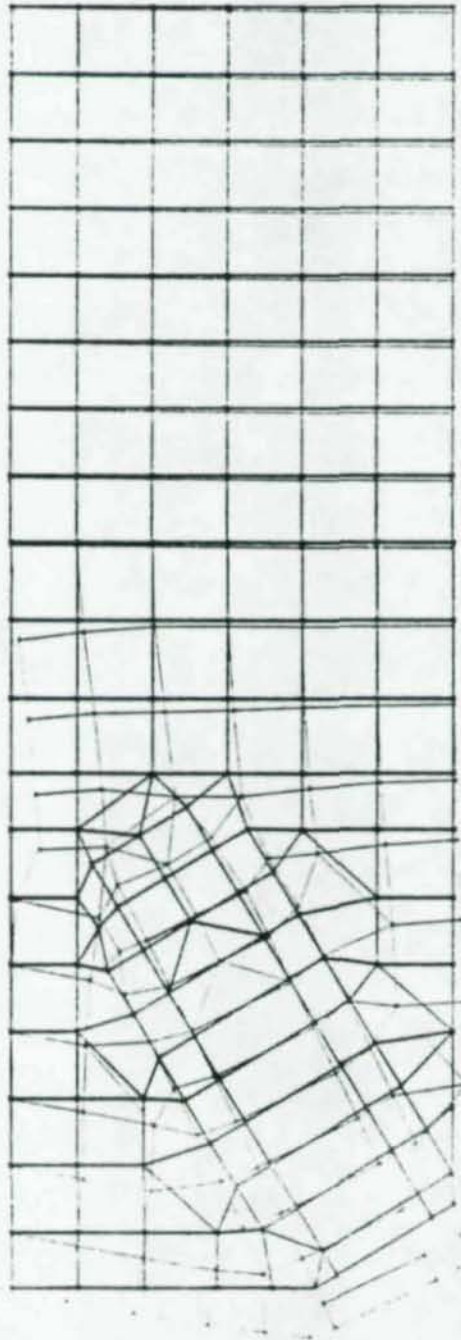


Figure A.64. 3/8" 30° Beam-Gusset Grid and Distorted Geometry.

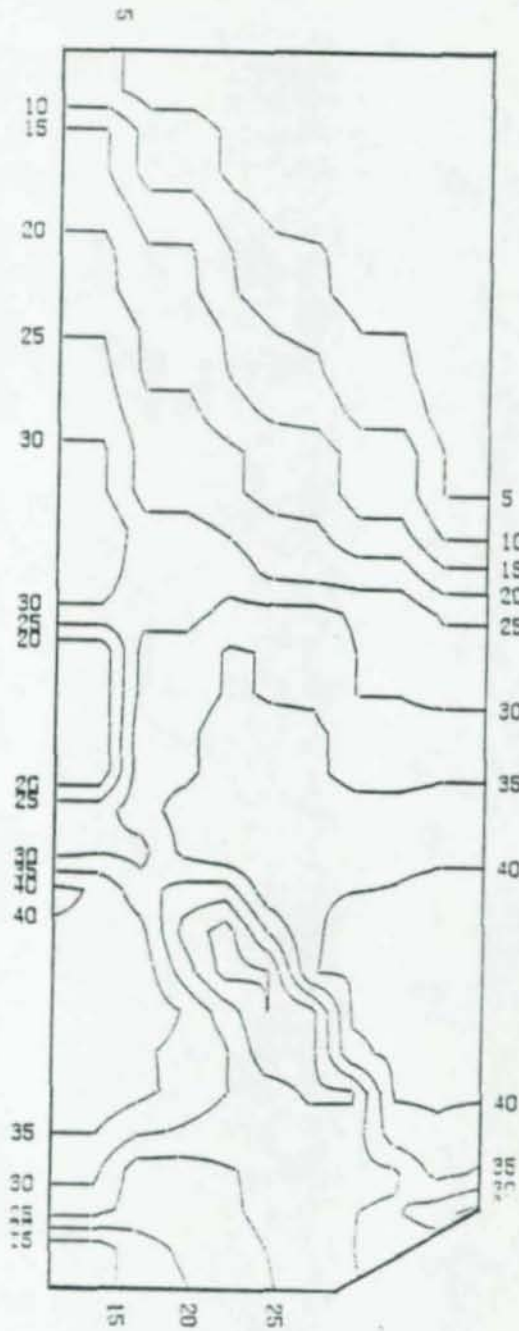


Figure A.65. Effective Stress Contour Plot, 3/8" 30° Beam-Gusset, P = 320K.

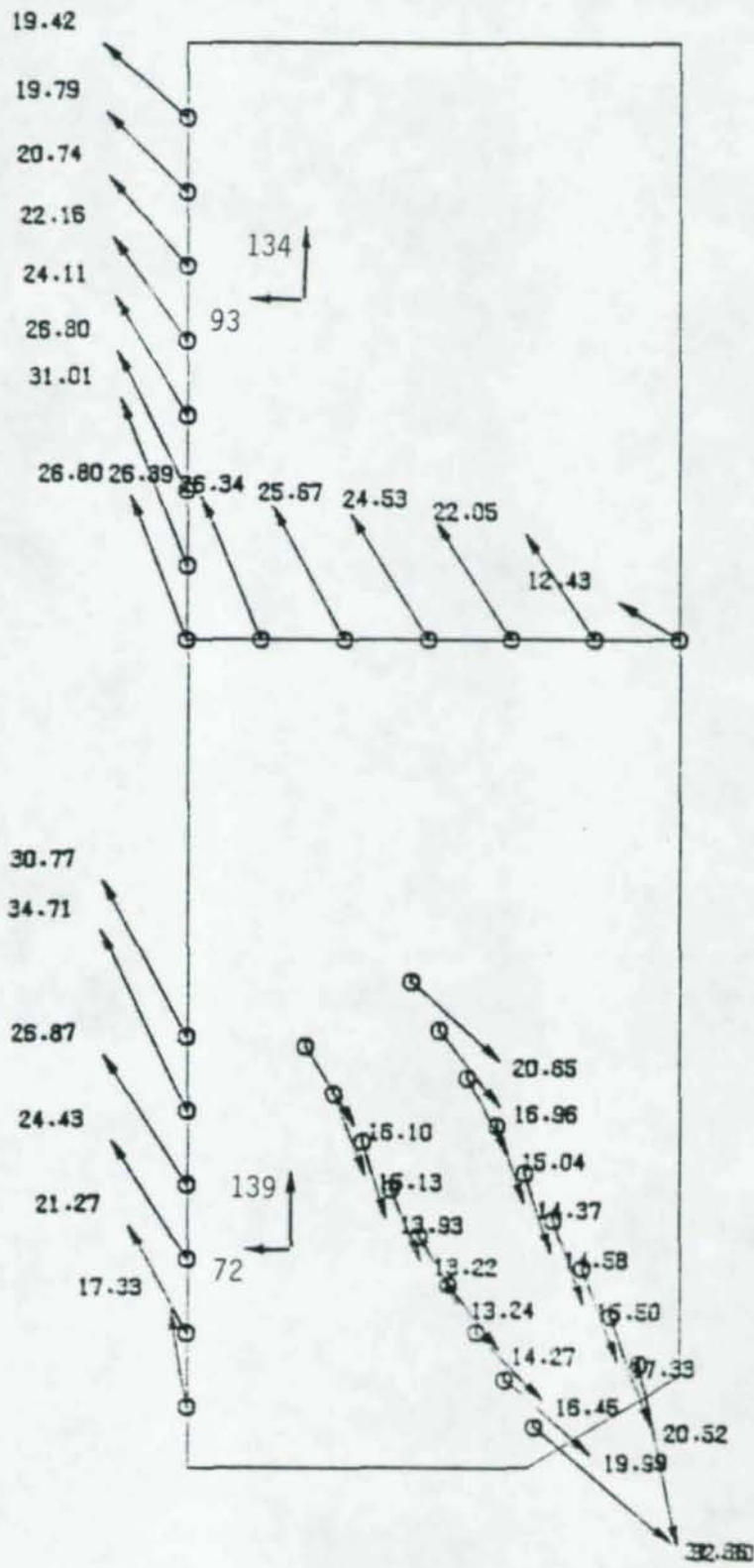


Figure A.66. Resultant Forces 3/8" 30° Beam Gusset, P = 320K.

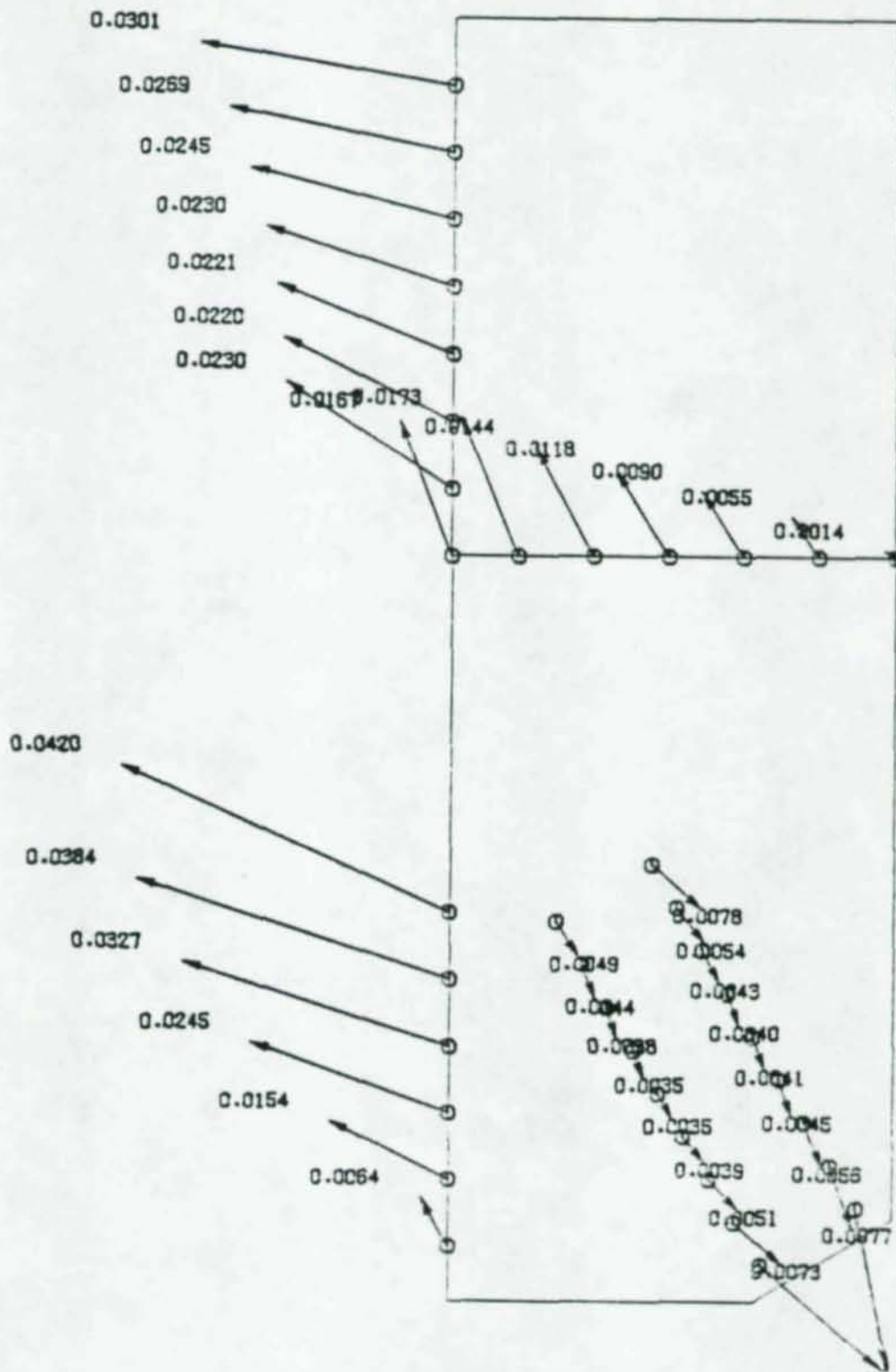


Figure A.67. Resultant Displacements 3/8" 30° Beam-Gusset, P = 320K.

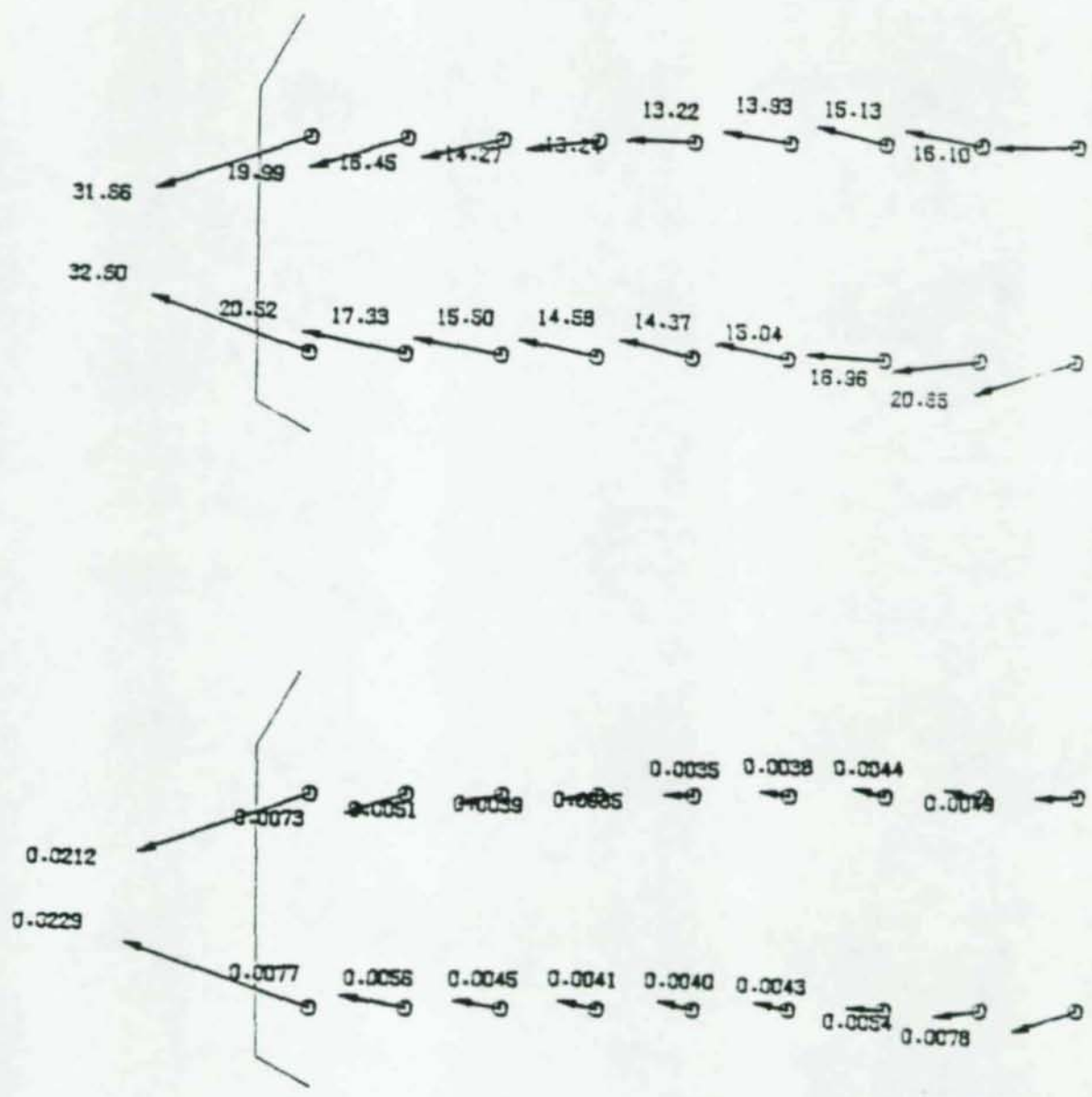


Figure A.68. Resultant Forces and Displacements 3/8" 30° Beam-Gusset, P = 320K.

REFERENCES

1. Richard, R. M., User's Manual for Nonlinear Finite Element Analysis Program INELAS Dept. of Civil Engineering, The University of Arizona, Tucson, Arizona, 1968 (Updated 1982).
2. Beaufoy, L. A. and Moharram, "Derived Moment-Angle Curves for Web-Cleat Connections," Preliminary Publication, Third Congress, International Association for Bridge and Structural Engineering, 1948.
3. Lewitt, C. W., Chesson, E., and Munse, W. H., "Restraint Characteristics of Flexible Riveted and Bolted Beam-to-Column Connections," Structural Research Series Report No. 296, University of Illinois, Urbana, Illinois, March, 1966.
4. Richard, R. M., Gillett, P. E., Kreigh, J. D., and Lewis, B. A., "The Analysis and Design of Single Plate Framing Connections," AISC Engineering Journal, No. 2, 1980.
5. Butler, L. J. and Kulak, G. L., "Strength of Fillet Welds as a Function of Load," Welding Journal Research Supplement, May, 1971.
6. Crawford, S. F. and Kulak, G. L., "Eccentrically Loaded Bolted Connections," Journal of the Structural Division, ASCE, March, 1971.
7. Manual of Steel Construction, 8th edition, by the American Institute of Steel Construction, Chicago, Illinois, 1980.
8. Bjorhovde, R. and Chakrabarti, S. K., "Tests of Full Size Gusset Plate Connections," Research Report, In Preparation, University of Arizona, Tucson, Arizona, 1983.
9. Richard, R. M. and Abbott, B. J., "A Versatile Elastic-Plastic Stress-Strain Formula," Journal of the Engineering Mechanics Division, ASCE, August, 1975.
10. Richard R. M., Hormby, D. E., "Force Distribution in Framing Connections Progress Report - May 1981 to March 1982," Department of Civil Engineering and Engineering Mechanics, February, 1982.
11. Whitmore, R. E., "Experimental Investigation of Stresses in Gusset Plates," University of Tennessee Engineering Experiment Station Bulletin, No. 16, May, 1952.

12. Birkemoe, P. C., Eubanks, R. A., and Munse, W. H., "Distribution of Stresses and Partition of Loads in Gusseted Connections," Structural Research Series Report No. 343, Department of Civil Engineering, University of Illinois, Urbana, March, 1969.
13. Vasarhelyi, D. D., "Tests of Gusset Plate Models," Journal of the Structural Division, ASCE, Vol. 97, ST2, February, 1971.
14. Davis, C. S., "Computer Analysis of the Stresses in a Gusset Plate," M.S. Thesis, Department of Civil Engineering, University of Washington, Seattle, 1967.
15. Desai, S., "Application of the Finite Element Method to the Problem of Gusseted Connections," Fritz Engineering Laboratory Report (Internal), January, 1970.
16. Struik, J.H.A., "Applications of Finite Element Analysis to Non-Linear Plane Stress Problems," Ph.D. Dissertation, Department of Civil Engineering, Lehigh University, Lehigh, Pennsylvania, 1972.
17. Birkemoe, P. C. and Gilmore, M. I., "Behavior of Bearing Critical Double Angle Beam Connections," Engineering Journal, American Institute of Steel Construction, Vol. 15, No. 4, 1978, pp. 109-115.
18. Yura, J. A., Birkemoe, P. C., and Ricles, J. M., "Beam-Web Shear Connections - An Experimental Study," Journal of the Structural Division, ASCE, Vol. 108, No. ST2, February, 1982, pp. 311-326.
19. Ricles, J. M. and Yura, J. A., "Strength of Double-Row Bolted-Web Connections," Journal of the Structural Division, ASCE, Vol. 109, No. 1, January, 1983, pp. 126-142.
20. Irish, D. J., "Strength and Behavior of Connection Elements," Masters Thesis, Department of Civil Engineering and Engineering Mechanics, University of Arizona, Tucson, Arizona, 1983.

00157

